



BIRZEIT UNIVERSITY  
FACULTY OF INFORMATION TECHNOLOGY

---

# Modeling and Control of an Elastic Ship-Mounted Crane

A THESIS  
SUBMITTED AS PARTIAL FULFILLMENT  
OF THE REQUIREMENTS

for the degree

MASTER OF SCIENTIFIC COMPUTING

By:

**Hussein M. Ahmad**

Advisors:

**Dr. Yousef M. Al-Sweiti**  
**Palestine Polytechnic University,**  
**Hebron, Palestine**

**Dr. Hassan Shibly**  
**Birzeit University,**  
**Ramallah, Palestine**

---

**February, 2010**

# Modeling and Control of an Elastic Ship-Mounted Crane

**By:**

**Hussein M. Ahmad**

**This Thesis was defended successfully on 24 February 2010 and approved by:**

**Committee Members**

**Signature**

**Prof.Dr. Karim Tahboob**

-----

**Dr. Ibrahiem Hamad**

-----

**Dr.Hasan Shibli**

-----

**Dr.Yousef Al-Sweity**

-----

---

# Dedication

*To  
my parents,  
and  
my wife*

# Acknowledgment

I am heartily thankful to my supervisors Dr.Yousef Al- Sweity and Dr. Hassan Shibli for their supervision, suggestions and continuous encouragements in every stage of my work. This thesis would not have been possible without their guidance and support from the initial to the final level which enabled me to develop a complete understanding of the thesis subject.

I am also very thankful to all people how encourages me to complete this work especially Eng. Majdi Zaloum for his great effort in helping me in Matlab programming, and the staff of the mechanical engineering department in Palestine Polytechnic University.

February, 2010

Hussein Ahmad

# Notation

$L_1, L_2$	length of the elastic boom , length of the payload .
$l$	length of the upper cable and length of the payload cable
$\beta, \delta$	angle of the boom with the horizontal and roll angle
$\rho$	the luff angle of the elastic boom.
$\alpha$	the slew angle of the elastic boom with respect to the vertical axis.
$w_i, \gamma_i$	elastic displacement and elastic rotation at node $i$ in in-plane
$v_i, \phi_i$	elastic displacement and elastic rotation at node $i$ in out-of-plane
$x_A, y_A, z_A$	the displacements of the ship due sea motion.
$\mathbf{p}$	wind forces acting directly on the payload.
$\theta, \psi$	the in-and-out-of-plane angles of the payload.
$T$	tension in $L_2$ the hosting cable
$\hat{\mathbf{p}}$	actual and estimated wind force
$m_p$	mass of the payload.
$m_e, E, I$	mass density, elastic modulus, cross section moment of area of the elastic boom
$\zeta$	local coordinate in the finite element
$\mathbf{M}_0, \mathbf{K}_0$	mass and stiffness matrices
$\mathbf{B}_1, \mathbf{B}_2$	input matrices
$\mathbf{B}_3, \mathbf{B}_4$	disturbance matrices
$\mathbf{B}_5$	wind force
$\mathbf{q}, \mathbf{z}, \hat{\mathbf{z}}$	displacement vector, state vector, and estimated state vector
$\mathbf{u}, \mathbf{y}, \mathbf{y}_m$	input, output, and measurement vectors
$\mathbf{A}, \mathbf{A}_e$	system and extended system matrices
$\mathbf{B}, \mathbf{B}_e$	input and extended input matrices
$\mathbf{E}, \mathbf{E}_e$	disturbance and extended disturbance matrices corresponding to rolling
$\mathbf{N}$	disturbance matrix corresponding to the wind force acting on the payload
$\mathbf{C}, \mathbf{C}_e$	output and extended output matrices
$\mathbf{D}, \mathbf{F}$	input and disturbance feed forward matrices.
$\mathbf{L}_1, \mathbf{L}_2, \mathbf{L}_e$	observer gain components and extended observer gain matrix
$\lambda_i$	$i^{th}$ eigenvalue
$\mathbf{e}, \mathbf{J}$	error vector and input matrix for the error equation of the observer
$\mathbf{Q}, \mathbf{Q}_e$	weight matrix of the states and the estimated states for the optimal design
$\mathbf{R}, \mathbf{R}_e$	weight matrix of the inputs and the measurements for the optimal design
$\mathbf{P}$	solution of Ricatti equation
$\mathbf{u}, \mathbf{K}_f$	input vector and gain of the optimal controller

# List of Figures

Figure 1.1: Picture of a ship-mounted crane at sea.	1
Figure 1.2: Al-Sweiti crane configuration with Maryland Rigging .	3
Figure 1.3: Modified ship- mounted crane structure.	5
Figure 2.1: Modified crane configuration.	7
Figure 2.2: Payload configuration .	8
Figure 2.3: Tension and wind forces configuration.	9
Figure 2.4: Free body diagram of the elastic boom ( $AB$ ).	12
Figure 2.5: Geometry of a single boom element.	13
Figure 2.6: Single finite element .	15
Figure 3.1: The effect of $\Delta x_{0A}$ on the crane .	36
Figure 3.2: The effect of $\Delta y_{0A}$ on the crane .	37
Figure 3.3: The effect of $\Delta z_{0A}$ on the crane .	37
Figure 3.4: The effect of $\Delta \delta_{0A}$ on the crane .	38
Figure 3.5: The effect of initial condition of $\Delta \varphi$ on the crane.	39
Figure 3.6: The effect of initial condition of $\Delta \theta$ on the crane.	39
Figure 3.7: The effect of initial conditions of $\Delta \theta$ and $\Delta \varphi$ on the crane .	40
Figure 3.8: Structure of the extendable Observer design.	43
Figure 3.9: The actual and the estimated signals of the wind forces.	45
Figure 3.10: The actual and estimated signals of $[\Delta \omega_5 \quad \Delta \vartheta_5]$ .	46
Figure 3.11: The actual and estimated signals of $[\Delta \dot{\omega}_5 \quad \Delta \dot{\vartheta}_5]$ .	47
Figure 3.12: The actual and the estimated signals of the wind forces under the effect of the initial conditions of original system.	48
Figure 3.13: Operating regions of the crane.	49
Figure 3.14: Block diagram of the control system	52
Figure 3.15: Operating regions ( $R_i$ ), $i = 1, \dots, 108$ .	54
Figure 3.16 : The plotting of $(\lambda_1, \lambda_2, \lambda_3)$ for $R_1$ , the design point is the center point of the region.	55

Figure 3.17: the local coordinates of region $R_1$ .	56
Figure 3.18 : The plotting of $(\lambda_1, \lambda_2, \lambda_3)$ for $R_1$ , after the updating of gains for each operating point.	58
Figure 3.19: Constant cable length, constant luff and slew angles with $\theta = \psi = \frac{\pi}{5}$ rad as initial conditions Control is turned ON at $t=10$ sec.	60
Figure 3.20: Variable cable length, constant luff and slew angles with $\theta = \psi = \frac{\pi}{5}$ rad as initial conditions Control is turned ON at $t=5$ sec.	60
Figure 3.21: Variable cable length, variable luff angle and constant slew angles with $\theta = \psi = \frac{\pi}{5}$ rad as initial conditions. Control is turned ON at $t=5$ sec .	61
Figure 3.22: Variable cable length, variable luff angle and variable slew angles with $\theta = \psi = \frac{\pi}{5}$ rad as initial conditions. Control is turned ON at $t=5$ sec.	61
Figure 3.23: Constant cable length, constant luff and slew angles with sinusoidal rolling at the average value of the first eigenfrequency. Control is turned ON at $t=5$ sec.	62
Figure 3.24: : Variable cable length, variable luff and slew angles with sinusoidal rolling at the average value of the first eigenfrequency. Control is turned ON at $t=5$ sec.	62
Figure 3.25: Variable cable length, variable luff and slew angles with sinusoidal rolling at the average value of the first eigenfrequency and $\theta = \psi = \frac{\pi}{5}$ rad as initial conditions. Control is turned ON at $t=5$ sec.	63

Figure 3.26: Variable cable length, variable luff and slew angles with sinusoidal rolling at the average value of the first eigenfrequency and sinusoidal wind forces . Control is turned ON at $t=5$ sec.	63
Figure 3.27: Chaotic rolling displacement.	64
Figure 3.28: The responses for chaotic rolling of the ship . Control is turned ON at $t=5$ sec.	65
Figure 3.29: Constant cable length, constant luff and slew angles with sinusoidal rolling at the average value of the first eigenfrequency. Control is turned ON at $t=5$ sec. $m_p = 50kg$ .	65



# Abstract

Modeling and control of 3D-elastic ship-mounted cranes with a circular cross section elastic boom had been developed. The developed model contains three kinematic inputs (the luff and slew angles of the boom together with the length of the payload hosting cable) to control the elastic vibrations of the boom and the pendulation of the payload. Two kinds of disturbances are considered; the sea waves which act on the ship and the wind force which act directly on the payload. The developed nonlinear model of the crane is expanded about the current operating point which varies with the luff and slew angles and the length of the payload cable using Taylor series. The result is a linear time-variant model for the crane under consideration.

Simulation results for the linearized model show that the disturbances considered cause the payload to oscillate in the in-plane and in the out-of-plane . Consequently, the linear model is used to design the control system of the crane. The coefficient matrices of this linear model are calculated at the current (instantaneous) operating point, which varies with the luff and slew angles and the length of the payload cable, therefore, a variable-model problem is created and accordingly a variable-gain observer and a variable-gain controller are designed to cover the operation of the crane for all possible operating points in the working space of the crane.

The switching between these gains takes place automatically according to the output of a region finder, which uses the measurements of the luff and slew angles and the length of the payload cable to detect the current operating region. Extended-observer is used to estimate the states and unknown disturbances; this guarantees that the estimated states converge to their true values even though a nonzero disturbance force acts on the payload. The controller uses the estimated states and the measured pendulation distances of the elastic boom in both in-plane and out-of-plane, and the measured in-plane and out-of-plane pendulation angles of the payload cable to create the required damping and to reduce the effect of the disturbances on the ship. Stability and performance robustness of the system are ensured for the total working space and

also for the expected range of the payload mass. Simulation results show that the observer can estimate the states and the disturbances very well and the controller can reduce the payload pendulations significantly.

# Table of Contents

**Notation**

**List of figures**

**Abstract**

<b>1</b>	<b>Introduction</b>	<b>1</b>
1.1	Motivation	2
1.2	Organization of the thesis	4
<b>2</b>	<b>Model development</b>	<b>6</b>
2.1	Assumptions	6
2.2	Kinematics of the payload	7
2.3	Kinetics of the payload	8
2.4	Kinematics of the elastic boom	11
2.5	Dynamic of the elastic part of the boom	12
2.6	Derivation of the operating point	26
2.7	Expanding the model about the current equilibrium point	28
<b>3</b>	<b>Control system design</b>	<b>34</b>
3.1	Introduction	34
3.2	State space representation	34
3.3	Simulation results	36
3.4	State and disturbance estimation	40
3.5	Controller design	49
3.5.1	Optimal state feedback control	50
3.6	Robustness	52
3.7	Simulation results	58
<b>4</b>	<b>Summary, conclusions, and recommendations</b>	<b>66</b>
4.1	Summary and conclusions	66
4.2	Recommendations	68
	<b>References</b>	<b>69</b>
	<b>Appendix A</b> Matlab code	<b>71</b>
	<b>Appendix B</b> Simulation diagram	<b>81</b>
	<b>Appendix C</b> Derivation of Payload equations	<b>82</b>

# 1 Introduction

## 1.1 Motivation

The crane can be considered as one of the most important tools used to transfer loads and cargo from one ship to another. As shown in Fig. 1.1 cranes have very strong structures in order to be able to lift heavy objects on their working space.

When cargo ships can not dock directly at port, ship-mounted cranes are used to lift and transfer cargo from these large ships to lighter port-going vessels. During this process, any sea motions can result in wave induced crane pendulations making the operation of the ship-mounted cranes unsafe especially whenever the waves are sufficiently high to produce large displacements of the payload.

At ports where such conditions (sea motions) exist for extended periods of time, this constraint on the flow of cargo shipping results in significant delays and cost overruns. Several control mechanisms have been proposed to suppress unsafe pendulations and enable the operation of ship-mounted cranes at high seas.



Figure 1.1: Picture of a ship-mounted crane at sea[6].

Boom cranes are modeled as spherical pendulum. It is found that when a lightly damped spherical pendulum is subjected to a simple harmonic planar displacement at the suspension point, nonplanar motions of the pendulum could be

excited due to the nonlinear interaction between in-plane and out-of-plane modes. Chin and Nayfeh (1996, 2001) [1] studied ship-mounted crane dynamics in two cases of harmonic base excitations at the boom tip: the case of primary resonance and the case of principal parametric resonance. They found out that, while the parametric excitation exhibits principal resonance in neighborhood of twice the natural frequency of the system, the response is always periodic and planar with arbitrary plane of oscillations. On the other hand, direct excitations produce complex dynamics when the excitation frequency approaches the natural frequency of the system (primary resonance). They also found out that a strictly planar excitation could produce in-plane and out-of-plane pendulations and that response may exhibit sudden jumps, modulation of the response amplitudes and phases and chaos.

Yuan and Ott (1997) [2] proposed a rigging to ship-mounted cranes, which is referred to as the “Maryland Rigging” system . A passive control effort is applied to the planar payload pendulations by applying a brake system to the upper cable as it passes over the pulley. They derived a planar model of this rigging and utilized it to investigate the response of the system to periodic and chaotic roll motions. Their simulation results showed that the payload response builds up significantly when the dominant frequency of the chaotic motion approaches the natural frequency of the lower pendulum. The pulley was then used as a brake to apply a constant and continuous dry friction. Simulation results showed that a constant friction force up to 10% of the payload weight can reduce planar payload pendulations significantly even in the neighborhood of the natural frequency of the system.

Kimiaghalam (1999) [3] proposed a fuzzy logic control approach to dampen the pendulations in a Maryland rigged crane by changing the length of the upper cable to eliminate and dampen payload pendulations; however, its performance is inferior to that of the passive controller.

Dadone and Landingham (1999) [4] used a fuzzy logic interference engine to stabilize the in-plane motions of the payload by determining the level of dry friction in the pulley based on the positions and velocities of the pulley and payload. Simultaneously, the pulley velocity and acceleration are used to feedback changes in the pulley cable to eliminate vertical oscillations of the pulley. Simulation results

showed fast damping of the payload motions, however the friction level (control effort) in the pulley was much higher than that employed by Yuan (1997). Further, although changes in the length of the pulley cable absorbed the pulley vertical oscillations, they introduced horizontal oscillations in the positions of both the pulley and payload.

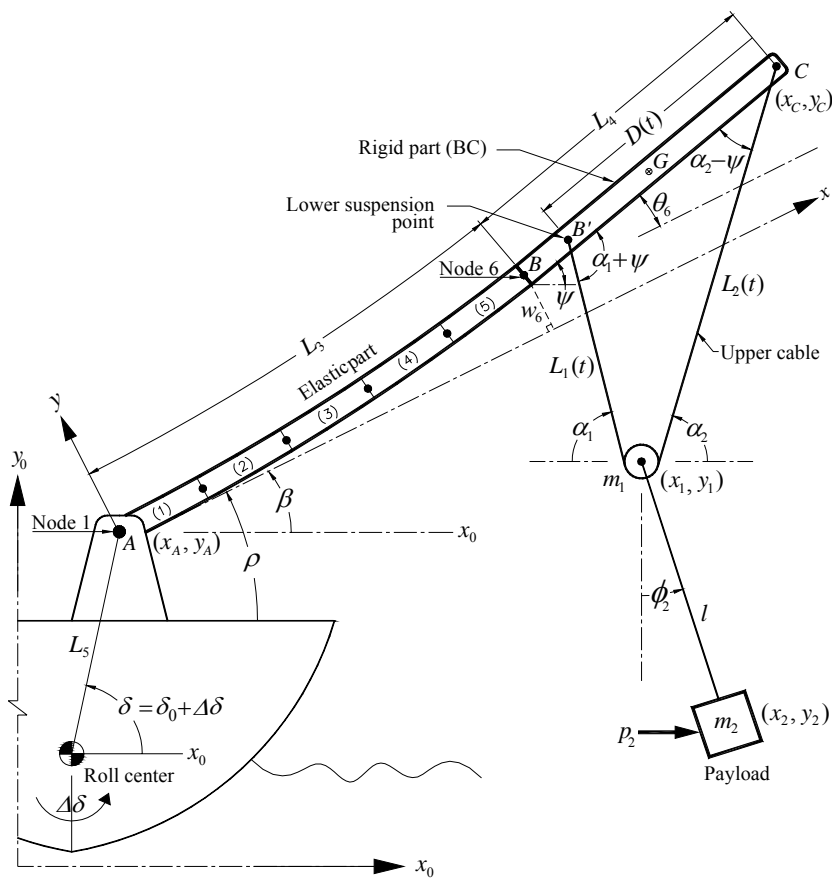


Figure 1.2: Al-Sweiti crane configuration with Maryland Rigging [6].

Kimiagharam (2000) [5], proposed another control system to reduce the excursions of the equilibrium point of the pulley due to ship rolling by keeping the position of the pulley directed above the payload. Simulation results showed that the proposed control strategy is effective and fast in damping payload pendulations. However, the control system assume full authority over the lengths of both segments of the upper cable, and hence the pulley position. This assumption violates the pulley's equilibrium equation.

Al-Sweiti (2006) [6,7] considered the Maryland Rigging crane with elastic boom system as shown in Fig. 1.2. The boom luff angle, the length of the upper cable, and the position of its lower suspension point were employed as inputs to control the planar vibrations of the elastic boom and the planar pendulation of the payload.

The disturbances acting on the crane are the rolling action of the ship due to sea motions in addition to the wind force acting directly on the payload. The dynamic of the crane is described by a multi-model problem depending on the current values of the cable length and boom luff angle.

Accordingly a variable-gain observer and a variable-gain controller were designed. The controller used the estimated states and the measured roll angle to create the required damping and to compensate for the rolling motion of the ship. Simulation and experimental results showed that the expressed control strategy performs very well and has a significant effect in suppressing the planar vibrations by 95% for different operating conditions and payload masses.

This work focuses on modeling and control of three dimensional ship-mounted crane with an elastic boom (see Figure 1.3). The goal is to dampen the planar and the nonplanar elastic vibrations of the boom and the in-plane and out-of-plane payload pendulations induced from sea wave motions causing the ship to roll and move in the 3D dimension and the air forces acting directly on the load due to the air .

## 1.2 Organization of the thesis

The thesis consists of four chapters; Chapter 1 is a literature reviews, Chapter 2 the development of the mathematical model of the elastic boom and payload, the nonlinear terms are separated using Taylor series expansion and the model is examined by simulations to investigate the effect of the disturbances on the overall response for different operating conditions.

In Chapter 3, the state space representation of the crane is obtained. A variable-gain extended-Observer is designed to reconstruct the states and approximate the unknown disturbances during the cargo transfer process, and a variable gain state controller is designed to suppress the vibration. Chapter 4 summarizes the results and conclusions with some recommendations which may be useful for future studies.

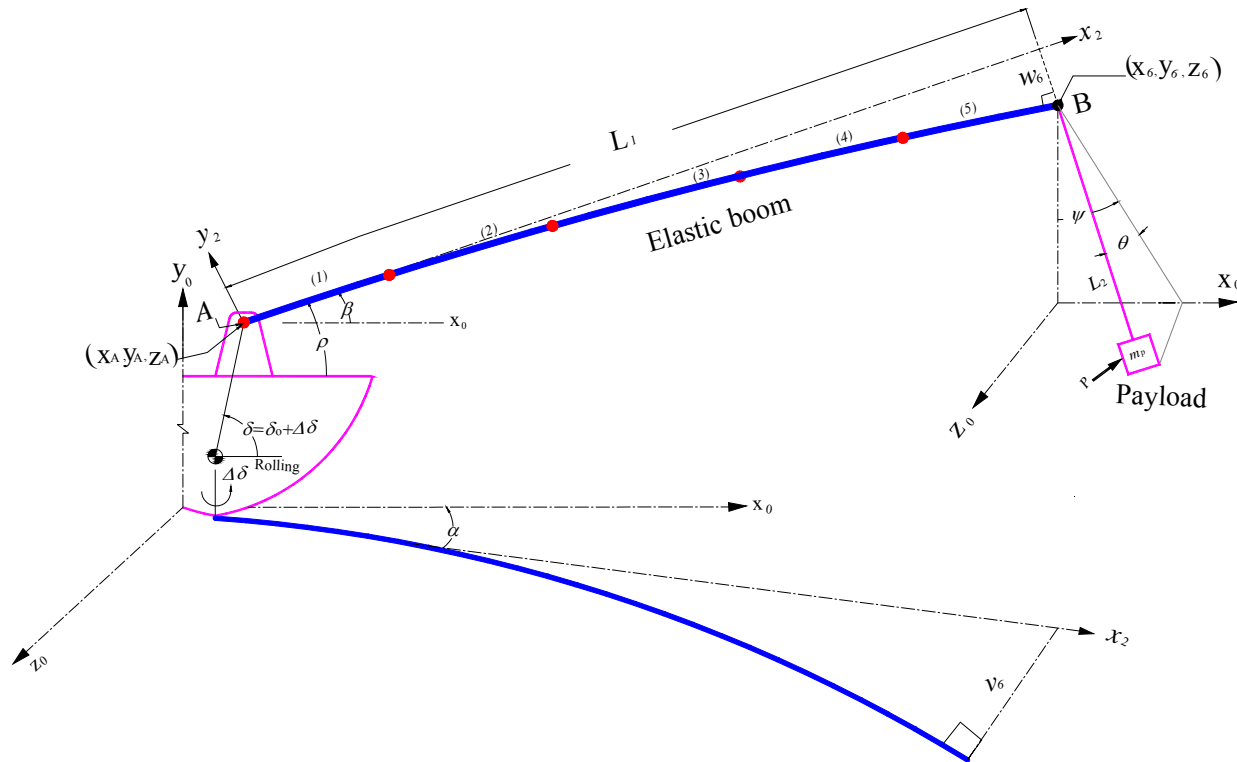


Figure 1.3: Modified ship-mounted crane structure.



## 2 Model development

In this chapter we will develop the mathematical model of the 3D-elastic ship-mounted crane based on the configuration shown in Fig. 1.3. The elastic boom is modeled using the finite element method. The dynamics of the payload is modeled using Lagrange equation of energy. Three inputs are assigned to control the planar and nonplanar vibrations of the elastic boom and payload due to excitations either from the sea wave motion in  $x_0, y_0$  and  $z_0$  directions or the wind forces acting directly on the payload, in the same directions as the wave motion.

### 2.1 Assumptions

In deriving the mathematical model of the 3D-crane, the following assumptions are considered:

- The elastic boom ( $AB$ ) is divided into five finite elements from ( $i = 1, 2 \dots 5$ ), thus six nodes are considered.
- The cross section of the elastic boom is circular.
- The mass of cable  $L_2$  is neglected and its length varies with time.
- The elongation of the cables and the structural damping of the boom are neglected.
- The slew angle  $\alpha$ , represents the rotation of the elastic boom with respect to the  $y_0$  axis's.
- The angle  $\beta$  represents the orientation of the boom axis with respect to the horizontal. It is equal to the sum of the roll angle  $\Delta\delta$  and the luff angle  $\rho$   $\beta = \rho + \Delta\delta$ .
- The disturbances acting on the crane are the rolling action of the ship  $\delta$  and  $x_A, y_A$  and  $z_A$  displacement of the ship caused by the sea motion in addition to the wind force  $\mathbf{P}$  in the direction of  $(x_0, y_0, z_0)$  acting directly on the payload; this force may appear due to a strong wind or a direct impact force which may happen by accident during the operation of the crane.
- $\theta$  and  $\psi$  represent the in-plane and the out-of-plane motion of the payload respectively as shown in figure 2.1 and figure 2.2.

- $\alpha$ ,  $\rho$  and  $L_2$  are considered the control inputs to suppress the vibrations of the payload and the elastic boom.

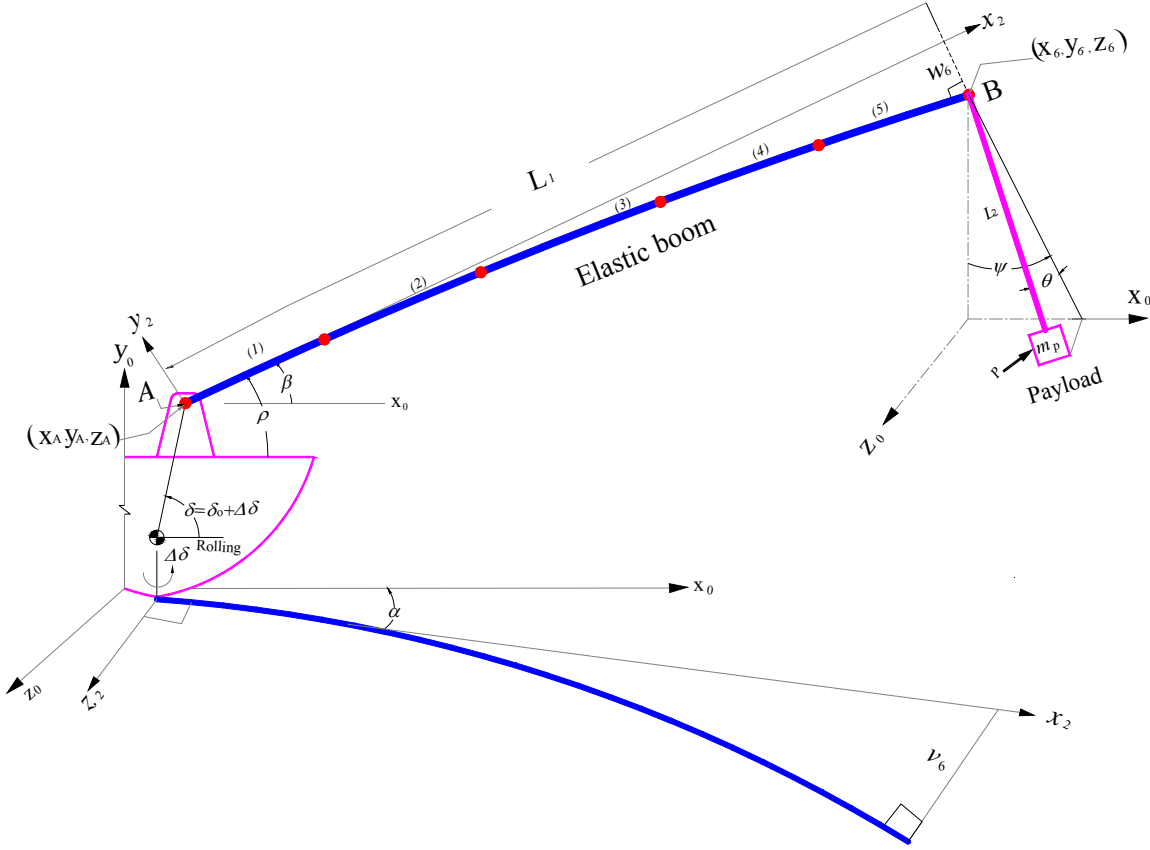


Figure 2.1: Modified crane configuration.

## 2.2 Kinematics of the payload

Assume that the position of the tip of the boom where the payload cable is attached is expressed by the coordinates  $(X_6, Y_6, Z_6)$  as shown in Fig.2.2, therefore, the global position of the payload is expressed by the coordinates  $(X_p, Y_p, Z_p)$  such that:

$$X_p = X_6 + L_2 \cos \theta \sin \psi \quad (2.1)$$

$$Y_p = Y_6 - L_2 \cos \theta \cos \psi \quad (2.2)$$

$$Z_p = Z_6 + L_2 \sin \theta \quad (2.3)$$

The velocity components of the payload can be expressed as:

$$\dot{X}_p = \dot{X}_6 + \dot{L}_2 \cos \theta \sin \psi - L_2 \dot{\theta} \sin \theta \sin \psi + L_2 \dot{\psi} \cos \theta \cos \psi \quad (2.4)$$

$$\dot{Y}_p = \dot{Y}_6 - \dot{L}_2 \cos \theta \cos \psi + L_2 \dot{\theta} \sin \theta \cos \psi + L_2 \dot{\psi} \cos \theta \sin \psi \quad (2.5)$$

$$\dot{Z}_p = \dot{Z}_6 + \dot{L}_2 \sin \theta + L_2 \dot{\theta} \cos \theta \quad (2.6)$$

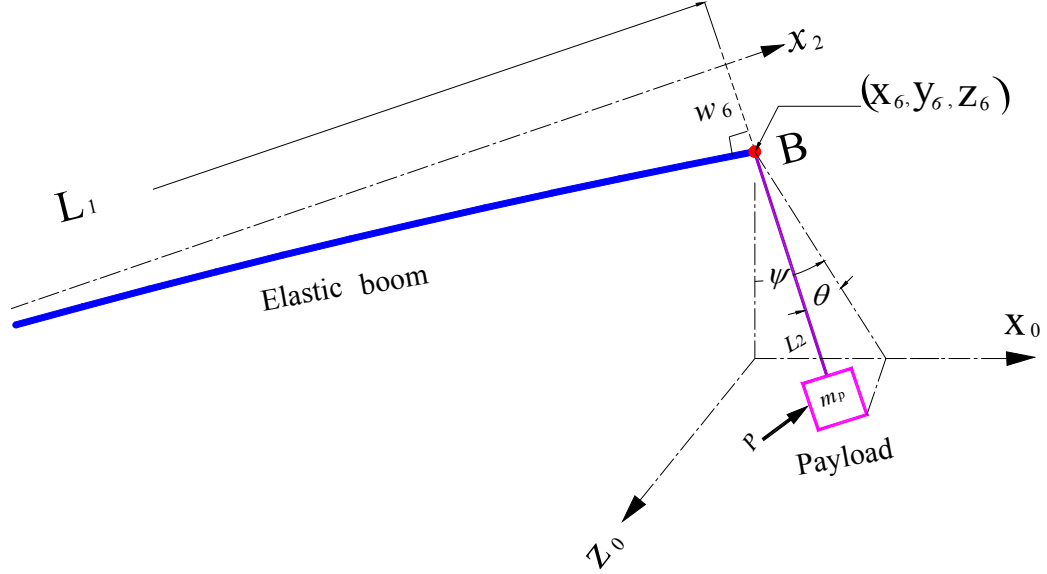


Figure 2.2: Payload configuration.

### 2.3 Kinetics of the payload

The generalized forces corresponding to the generalized coordinates  $(\theta, \psi, L_2)$  are shown in Fig. 2.3; They can be expressed as:

$$F_x = p_x - T \cos \theta \sin \psi \quad (2.7)$$

$$F_y = p_y + T \cos \theta \cos \psi \quad (2.8)$$

$$F_z = p_z - T \sin \theta \quad (2.9)$$

Where:

$T$  : represents the tension in the cable  $L_2$ .

$(p_x, p_y, p_z)$  : the 3D-dimensional component of wind force.

The kinetic and the potential energies of the payload is given by Eq.(2.10) and Eq. (2.11) respectively:

$$K_E = (1/2) m_p (\dot{X}_p^2 + \dot{Y}_p^2 + \dot{Z}_p^2) \quad (2.10)$$

$$U = m_p g Y_p \quad (2.11)$$

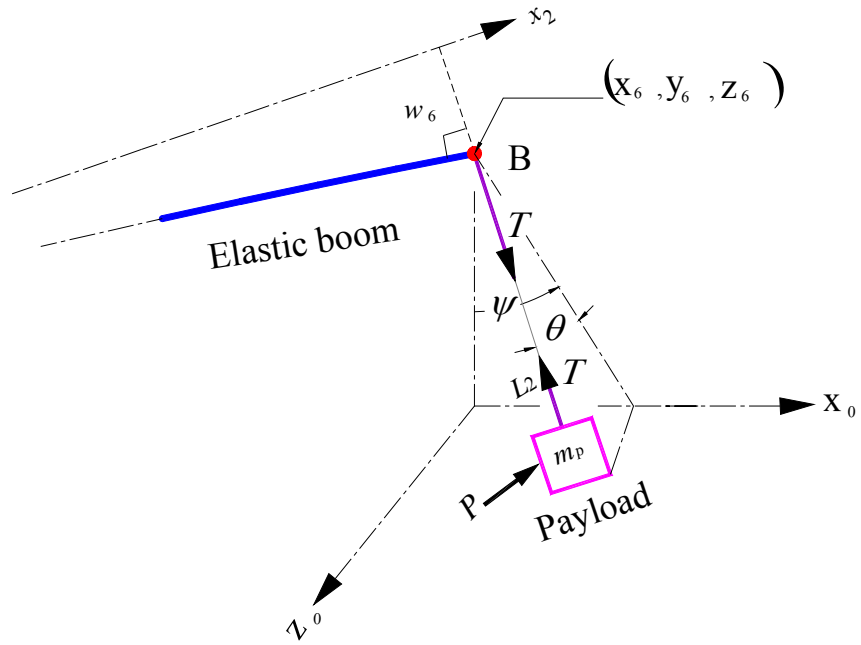


Figure 2.3: Tension and wind forces configuration.

Thus the Lagrange equation can be expressed as

$$\begin{aligned} L &= K_E - U \\ &= (1/2) m_p (\dot{X}_p^2 + \dot{Y}_p^2 + \dot{Z}_p^2 - 2gY_p) \end{aligned} \quad (2.12)$$

The equations of motion of the payload take the following form (see derivation in Appendix C):

$$\frac{d}{dt} \left( \frac{\partial L}{\partial \dot{\theta}} \right) - \frac{\partial L}{\partial \theta} = F_x \frac{\partial X_p}{\partial \theta} + F_y \frac{\partial Y_p}{\partial \theta} + F_z \frac{\partial Z_p}{\partial \theta} \quad (2.13)$$

$$\frac{d}{dt} \left( \frac{\partial L}{\partial \dot{\psi}} \right) - \frac{\partial L}{\partial \psi} = F_X \frac{\partial X_p}{\partial \psi} + F_Y \frac{\partial Y_p}{\partial \psi} + F_Z \frac{\partial Z_p}{\partial \psi} \quad (2.14)$$

$$\frac{d}{dt} \left( \frac{\partial L}{\partial \dot{L}_2} \right) - \frac{\partial L}{\partial L_2} = F_X \frac{\partial X_p}{\partial L_2} + F_Y \frac{\partial Y_p}{\partial L_2} + F_Z \frac{\partial Z_p}{\partial L_2} \quad (2.15)$$

Substituting equations (2.2, 4, 5, 6) into equation (2.12), and after the evaluation of equations (2.13, 14, 15) then the nonlinear differential equations of the payload motion can be expressed as follows:

$$\begin{aligned} & \ddot{X}_6 (-L_2 \sin \theta \sin \psi) + \ddot{Y}_6 (L_2 \sin \theta \cos \psi) + \ddot{Z}_6 (L_2 \cos \theta) + \ddot{\theta} L_2^2 + 2\dot{\theta} \dot{L}_2 L_2 \\ & + \dot{\psi}^2 (L_2^2 \sin \theta \cos \theta) \\ & + g L_2 \sin \theta \cos \psi \\ & = (1/m_p) [-P_x L_2 \sin \theta \sin \psi \\ & + p_y L_2 \sin \theta \cos \psi + p_z L_2 \cos \theta] \end{aligned} \quad (2.16)$$

$$\begin{aligned} & \ddot{X}_6 (L_2 \cos \theta \cos \psi) + \ddot{Y}_6 (L_2 \cos \theta \sin \psi) + \ddot{\psi} L_2^2 \cos^2 \theta + 2\dot{\psi} \dot{L}_2 L_2 \cos^2 \theta \\ & - \dot{\psi} \dot{\theta} (2L_2 \sin \theta \cos \theta \sin^2 \psi) + \dot{\theta}^2 (L_2^2 \cos^2 \theta \cos \psi \sin \psi) \\ & + \dot{\psi}^2 (L_2^2 \cos^2 \theta \cos \psi \sin \psi) \\ & + g L_2 \cos \theta \sin \psi \\ & = (1/m_p) [p_x L_2 \cos \theta \cos \psi + p_y L_2 \cos \theta \sin \psi] \end{aligned} \quad (2.17)$$

$$\begin{aligned} & \ddot{X}_6 (\cos \theta \sin \psi) + \ddot{Y}_6 (-\cos \theta \cos \psi) + \ddot{Z}_6 \sin \theta + \ddot{L}_2 - \dot{\theta}^2 L_2^2 \\ & - \dot{\psi}^2 (L_2 \cos^2 \theta) \\ & - g \cos \theta \cos \psi \\ & = (1/m) [p_x \cos \theta \sin \psi - p_y \cos \theta \cos \psi + p_z \sin \theta - T] \end{aligned} \quad (2.18)$$

According to equation 2.18 the tension  $T$  in the hosting cable can be expressed as follows:

$$\begin{aligned} T = -m_p & \left[ \ddot{X}_6 (\cos \theta \sin \psi) + \ddot{Y}_6 (-\cos \theta \cos \psi) + \ddot{Z}_6 \sin \theta + \ddot{L}_2 - \dot{\theta}^2 L_2^2 \right. \\ & \left. - \dot{\psi}^2 (L_2 \cos^2 \theta) - g \cos \theta \cos \psi \right] \\ & + [p_x \cos \theta \sin \psi - p_y \cos \theta \cos \psi + p_z \sin \theta] \end{aligned} \quad (2.19)$$

In order to find the position of the tip of the elastic boom  $B(X_6, Y_6, Z_6)$  relative to the spherical joint  $A(x_0, y_0, z_0) = (x_A, y_A, z_A)$  connecting the lower end of the boom to the ship, the axis transformation method is used, considering that the boom  $AB$  rotates around  $y_0$  axis in clockwise direction with angle  $\alpha$  and around  $z_0$  axis in counter clockwise with angle  $\beta$  shown in Fig. 2.4, thus the obtained vectors are as follows :

$$X_6 = x_{0A} + L_1 \cos \alpha \cos \beta - w_6 \cos \alpha \sin \beta - v_6 \sin \alpha \quad (2.20)$$

$$Y_6 = y_{0A} + L_1 \sin \beta + w_6 \cos \beta$$

$$Z_6 = z_{0A} + L_1 \sin \alpha \cos \beta - w_6 \sin \alpha \sin \beta + v_6 \cos \alpha$$

And the second derivative of  $(X_6, Y_6, Z_6)$  with respect to time are:

$$\begin{aligned} \ddot{X}_6 = & \ddot{x}_{0A} + \ddot{\alpha}(-L_1 \sin \alpha \cos \beta + w_6 \sin \alpha \sin \beta - v_6 \cos \alpha) \\ & + \ddot{\beta}(-L_1 \cos \alpha \sin \beta - w_6 \cos \alpha \cos \beta) \\ & + \ddot{w}_6(-\cos \alpha \sin \beta) + \ddot{v}_6(-\sin \alpha) \\ & + \dot{\alpha}\dot{\beta}(2L_1 \sin \alpha \sin \beta + 2w_6 \sin \alpha \cos \beta) \\ & + \dot{w}_6\dot{\alpha}(2 \sin \alpha \sin \beta) + \dot{w}_6\dot{\beta}(-2 \cos \alpha \cos \beta) \\ & + \dot{v}_6\dot{\alpha}(-2 \sin \alpha \cos \alpha) \\ & + \dot{\alpha}^2(w_6 \cos \alpha \sin \beta + v_6 \sin \alpha - L_1 \cos \alpha \cos \beta) \\ & + \dot{\beta}^2(-L_1 \cos \alpha \cos \beta + w_6 \cos \alpha \sin \beta) \end{aligned} \quad (2.21)$$

$$\begin{aligned} \ddot{Y}_6 = & \ddot{y}_{0A} + \ddot{\beta}(L_1 \cos \beta - w_6 \sin \beta) + \ddot{w}_6(\cos \beta) + \dot{w}_6\dot{\beta}(-2 \sin \beta) \\ & + \dot{\beta}^2(-L_1 \sin \beta - w_6 \cos \beta) \end{aligned} \quad (2.22)$$

$$\begin{aligned} \ddot{Z}_6 = & \ddot{z}_{0A} + \ddot{\alpha}(L_1 \cos \alpha \cos \beta - w_6 \cos \alpha \sin \beta - v_6 \sin \alpha) \\ & + \ddot{\beta}(-L_1 \sin \alpha \sin \beta - w_6 \sin \alpha \cos \beta) + \ddot{w}_6(-\sin \alpha \sin \beta) \\ & + \ddot{v}_6(\cos \alpha) + \dot{\alpha}\dot{\beta}(-2L_1 \cos \alpha \sin \beta - 2w_6 \cos \alpha \cos \beta) \\ & + \dot{w}_6\dot{\alpha}(-2 \cos \alpha \sin \beta) + \dot{w}_6\dot{\beta}(-2 \sin \alpha \cos \beta) \\ & + \dot{v}_6\dot{\alpha}(-2 \sin \alpha) \\ & + \dot{\alpha}^2(-L_1 \sin \alpha \cos \beta + w_6 \sin \alpha \sin \beta - w_6 \cos \alpha) \\ & + \dot{\beta}^2(-L_1 \sin \alpha \cos \beta + w_6 \sin \alpha \sin \beta) \end{aligned} \quad (2.23)$$

## 2.4 Kinematics of the elastic boom

In order to derive the equations of motion for the 3D-elastic boom ( $AB$ ) using the finite element model shown in Fig. 2.4. First: we need to find the absolute lateral accelerations of the point  $B$  relative to point  $A$  which has an acceleration in the three dimension space denoted by  $\ddot{x}_{0A}, \ddot{y}_{0A}, \ddot{z}_{0A}$ .

From Fig. 2.4 it can be concluded that point  $B$  has two absolute lateral accelerations in the vertical plane  $x_2y_2$  and in the out-of-plane  $x_2z_2$  denoted by  $a_{y_2}, a_{z_2}$  respectively. Thus by utilizing the following equations :

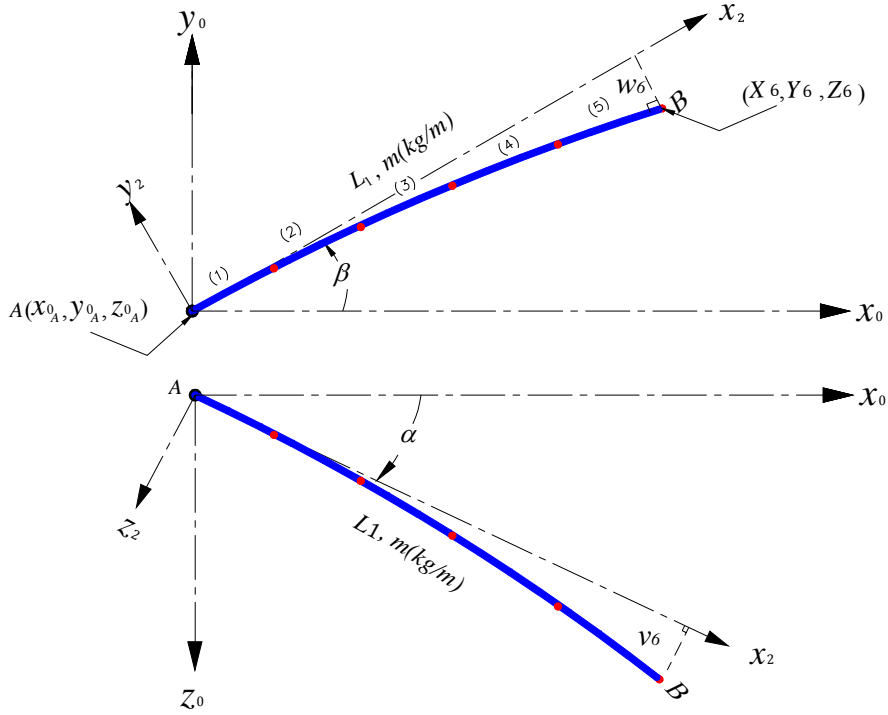


Figure 2.4: Free body diagram of the elastic boom (AB).

$$a_{By_2} = a_{Ay_2} + a_{B/A} \quad (2.24)$$

$$a_{Bz_2} = a_{Az_2} + a_{B/A} \quad (2.25)$$

We can derive the absolute lateral accelerations for any of the elements of the elastic boom (AB) as:

$$\ddot{a}_{y_2} = \ddot{y}_{0A} \cos \beta - \ddot{z}_{0A} \sin \alpha \sin \beta - \ddot{x}_{0A} \cos \alpha \sin \beta + x_2 \ddot{\beta} + \ddot{w} \quad (2.26)$$

$$\ddot{a}_{z_2} = \ddot{z}_{0A} \cos \alpha - \ddot{x}_{0A} \sin \alpha + x_2 \cos \beta \ddot{\alpha} + \ddot{v} \quad (2.27)$$

Where  $w, v$  denotes the local deflection of the boom in  $x_2 y_2$  and  $x_2 z_2$  planes respectively .

## 2.5 Dynamics of the elastic part of the boom

For deriving the finite element model of the elastic part (AB), the effects of rotary inertia, transverse shear deformation, and the axial force are neglected. Accordingly, with reference to the single element shown in Fig. 2.5, the equation of motion in  $x_2 y_2$  plane can be written as

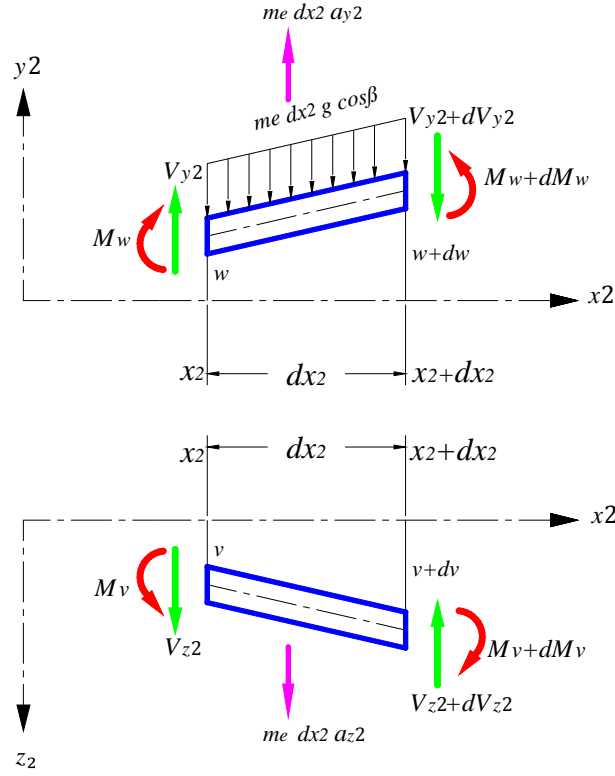


Figure 2.5: Geometry of a single boom element, all axial force components are neglected.

$$\frac{\partial V_{y_2}}{\partial x_2} + m_e a_{y_2} = -m_e g \cos \beta \quad (2.28)$$

and in  $x_2 z_2$  plane the equation of motion is

$$\frac{\partial V_{z_2}}{\partial x_2} + m_e a_{z_2} = 0 \quad (2.29)$$

where  $m_e$  denotes the mass per unit length of the boom and  $a_{y_2}$ ,  $a_{z_2}$  represent the absolute lateral accelerations of the element located at  $x_2$ ,

Substituting Eq. (2.26) into Eq. (2.28) and utilizing the relation

$$V_{y_2} = \frac{\partial}{\partial x_2} \left( EI \frac{\partial^2 w}{\partial x_2^2} \right) \quad (2.30)$$



yield

$$\frac{\partial^2}{\partial x_2^2} \left( EI \frac{\partial^2 w}{\partial x_2^2} \right) + m_e \frac{\partial^2 w}{\partial t^2} = p_{y_2}(x_2, t) \quad (2.31)$$

where

$$p_{y_2}(x_2, t) = -m_e \ddot{\beta} x_2 - m_e \cos \beta (g + \ddot{y}_{0_A}) + m_e (\ddot{z}_{0_A} \sin \alpha \cos \beta + \ddot{x}_{0_A} \cos \alpha \sin \beta) \quad (2.32)$$

represents the distributed lateral load acting on the part  $AB$  in  $x_2 y_2$  plane.

Substituting Eq. (2.27) into Eq. (2.29) and utilizing the relation

$$V_{z_2} = \frac{\partial}{\partial x_2} \left( EI \frac{\partial^2 v}{\partial x_2^2} \right) \quad (2.33)$$

yield

$$\frac{\partial^2}{\partial x_2^2} \left( EI \frac{\partial^2 v}{\partial x_2^2} \right) + m_e \frac{\partial^2 v}{\partial t^2} = p_{z_2}(x_2, t) \quad (2.34)$$

where

$$p_{z_2}(x_2, t) = -m_e x_2 \cos \beta \ddot{\alpha} - m_e (\ddot{z}_{0_A} \cos \alpha - \ddot{x}_{0_A} \sin \alpha) \quad (2.35)$$

represents the distributed lateral load acting on the part  $AB$  in  $x_2 z_2$  plane.

The free body diagram of a single finite element of length  $l$  is shown in Fig. 2.6, the transverse displacement  $w(\zeta)$  can be related to the node variables ( $w_i, \gamma_i, w_{i+1}, \gamma_{i+1}$ ) in  $x_2 y_2$  plane, and  $v(\zeta)$  can be related to the node variables ( $v_i, \phi_i, v_{i+1}, \phi_{i+1}$ ) in  $x_2 z_2$  plane, through four cubic interpolation functions, such that:

$$w(\zeta) = \mathbf{N}_{y_2}^T \boldsymbol{\vartheta}_{y_2} \quad (2.36)$$

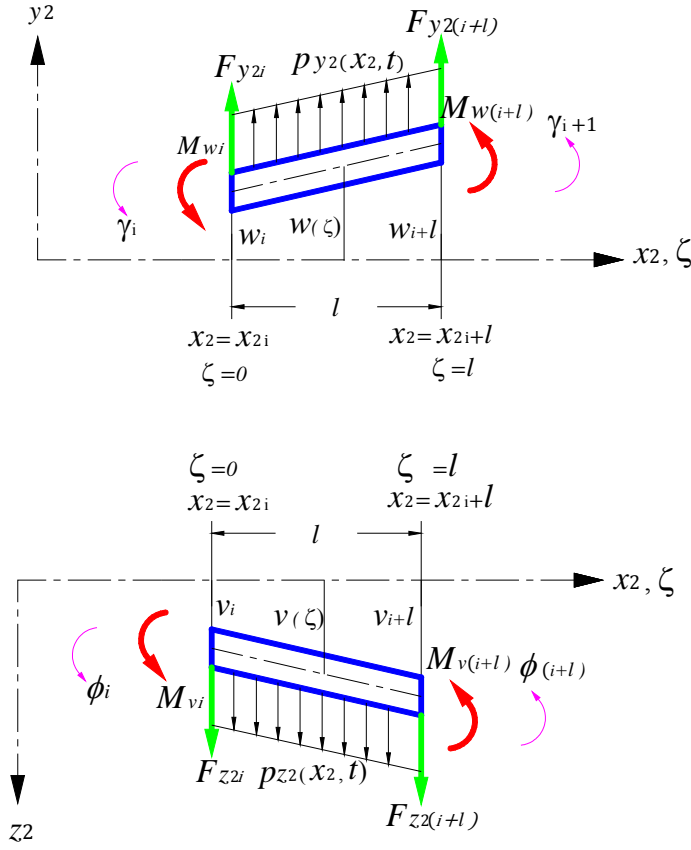


Figure 2.6: Single finite element.

where

$$\boldsymbol{\vartheta}_{y_2} = [w_i, \gamma_i, w_{i+1}, \gamma_{i+1}]^T \quad (2.37)$$

is the node variables vector of order  $4 \times 1$  in  $x_2 y_2$  plane, and

$$\mathbf{N}_{y_2} = \begin{bmatrix} 1 - 3(\zeta/l)^2 + 2(\zeta/l)^3 \\ (\zeta^3/l^2) - 2(\zeta^2/l) + \zeta \\ -2(\zeta/l)^3 + 3(\zeta/l)^2 \\ (\zeta^3/l^2) - (\zeta^2/l) \end{bmatrix} \quad (2.38)$$

is the cubic interpolation shape functions vector of order  $4 \times 1$  [8] in  $x_2 y_2$  plane which is a typical method for the discretization of elastic continua.

In the same manner we can derive the shape functions of element  $i$  in  $x_2z_2$  as follows:

$$v(\zeta) = \mathbf{N}_{z_2}^T \boldsymbol{\vartheta}_{z_2} \quad (2.39)$$

where

$$\boldsymbol{\vartheta}_{z_2} = [v_i, \phi_i, v_{i+1}, \phi_{i+1}]^T \quad (2.40)$$

is the node variables vector of order  $4 \times 1$  in  $x_2z_2$  plane, and

$$\mathbf{N}_{z_2} = \begin{bmatrix} 1 - 3(\zeta/l)^2 + 2(\zeta/l)^3 \\ (\zeta^3/l^2) - 2(\zeta^2/l) + \zeta \\ -2(\zeta/l)^3 + 3(\zeta/l)^2 \\ (\zeta^3/l^2) - (\zeta^2/l) \end{bmatrix} \quad (2.41)$$

is the cubic interpolation shape functions vector of order  $4 \times 1$  [8] in  $x_2z_2$  plane

The element mass and stiffness matrices in  $x_2y_2$  plane for element  $i$  are defined respectively as:

$$\mathbf{M}_{y_2} = \int_0^l m_e \mathbf{N}_{y_2} \mathbf{N}_{y_2}^T d\zeta \quad (2.42)$$

$$= \frac{m_e l}{420} \begin{bmatrix} 156 & 22l & 54 & -13l \\ 22l & 4l^2 & 13l & -3l^2 \\ 54 & 13l & 156 & -22l \\ -13l & -3l^2 & -22l & 4l^2 \end{bmatrix} \quad (2.43)$$

$$\mathbf{K}_{y_2} = \int_0^l E I \ddot{\mathbf{N}}_{y_2} \ddot{\mathbf{N}}_{y_2}^T d\zeta \quad (2.44)$$

$$= \frac{EI}{l^3} \begin{bmatrix} 12 & 6l & -12 & 6l \\ 6l & 4l^2 & -6l & 2l^2 \\ -12 & -6l & 12 & -6l \\ 6l & 2l^2 & -6l & 4l^2 \end{bmatrix} \quad (2.45)$$

where  $\ddot{\mathbf{N}}_{y_2}$  denotes the second derivative of  $\mathbf{N}_{y_2}$  with respect to the local coordinate  $\zeta$ .

In the same manner we can derive the mass and stiffness matrices of element  $i$  in  $x_2z_2$  plane and they are as follows:

$$\mathbf{M}_{z_2} = \int_0^l m_e \mathbf{N}_{z_2} \mathbf{N}_{z_2}^T d\zeta \quad (2.46)$$

$$= \frac{m_e l}{420} \begin{bmatrix} 156 & 22l & 54 & -13l \\ 22l & 4l^2 & 13l & -3l^2 \\ 54 & 13l & 156 & -22l \\ -13l & -3l^2 & -22l & 4l^2 \end{bmatrix} \quad (2.47)$$

$$\mathbf{K}_{z_2} = \int_0^l E I \ddot{\mathbf{N}}_{z_2} \ddot{\mathbf{N}}_{z_2}^T d\zeta \quad (2.48)$$

$$= \frac{EI}{l^3} \begin{bmatrix} 12 & 6l & -12 & 6l \\ 6l & 4l^2 & -6l & 2l^2 \\ -12 & -6l & 12 & -6l \\ 6l & 2l^2 & -6l & 4l^2 \end{bmatrix} \quad (2.49)$$

Therefore the local mass and stiffness matrices for the element  $i$  in both  $x_2y_2$  and  $x_2z_2$  planes can be expressed respectively as:

$$\mathbf{M}_t = \frac{m_e l}{420} \begin{bmatrix} w_i & v_i & \gamma_i & \phi_i & w_{i+1} & v_{i+1} & \gamma_{i+1} & \phi_{i+1} \\ 156 & 0 & 22l & 0 & 54 & 0 & -13l & 0 \\ 0 & 156 & 0 & 22l & 0 & 54 & 0 & -13l \\ 22l & 0 & 4l^2 & 0 & 13l & 0 & -3l^2 & 0 \\ 0 & 22l & 0 & 4l^2 & 0 & 13l & 0 & -3l^2 \\ 54 & 0 & 13l & 0 & 156 & 0 & -22l & 0 \\ 0 & 54 & 0 & 13l & 0 & 156 & 0 & -22l \\ -13l & 0 & -3l^2 & 0 & -22l & 0 & 4l^2 & 0 \\ 0 & -13l & 0 & -3l^2 & 0 & -22l & 0 & 4l^2 \end{bmatrix} \begin{matrix} w_i \\ v_i \\ \gamma_i \\ \phi_i \\ w_{i+1} \\ v_{i+1} \\ \gamma_{i+1} \\ \phi_{i+1} \end{matrix} \quad (2.50)$$

$$\mathbf{K}_t = \frac{EI}{l^3} \begin{bmatrix}
12 & 0 & 6l & 0 & -12 & 0 & 6l & 0 \\
0 & 12 & 0 & 6l & 0 & -12 & 0 & 6l \\
6l & 0 & 4l^2 & 0 & -6l & 0 & 2l^2 & 0 \\
0 & 6l & 0 & 4l^2 & 0 & -6l & 0 & 2l^2 \\
-12 & 0 & -6l & 0 & 12 & 0 & -6l & 0 \\
0 & -12 & 0 & -6l & 0 & 12 & 0 & -6l \\
6l & 0 & 2l^2 & 0 & -6l & 0 & 4l^2 & 0 \\
0 & 6l & 0 & 2l^2 & 0 & -6l & 0 & 4l^2
\end{bmatrix} \begin{matrix} w_i \\ v_i \\ \gamma_i \\ \phi_i \\ w_{i+1} \\ v_{i+1} \\ \gamma_{i+1} \\ \phi_{i+1} \end{matrix} \quad (2.51)$$

Also, the element force vector in  $x_2y_2$  plane (acting on the nodes  $i$  and  $i + 1$ ) which are  $\left[ F_{y_{2i}}, M_{w_i}, F_{y_{2i+1}}, M_{w_{i+1}} \right]^T$  can be also expressed as :

$$\mathbf{f}_{y_2} = \int_0^l p_{y_2}(x_2, t) \mathbf{N}_{y_2} d\zeta \quad (2.52)$$

Since  $p_{y_2}(x_2, t)$  varies linearly with the position  $x_2$  of the element, each element has a different force vector whose magnitude depends on the location of the element along the boom. Therefore, to calculate the integration in the right hand side of Eq. (2.52), equation (2.32) is rewritten as:

$$p_{y_2}(x_2, t) = -m_e \ddot{\beta}(x_{2i} + \zeta) - f_{0y_2} \quad (2.53)$$

with

$$f_{0y_2} = m_e \cos \beta (g + \ddot{y}_{0A}) - m_e (\ddot{z}_{0A} \sin \alpha \cos \beta + \ddot{x}_{0A} \cos \alpha \sin \beta) \quad (2.54)$$

where  $0 \leq \zeta \leq l$  is the local longitudinal axis of the element, and  $x_{2i}$  locates the element under consideration with respect to point A as shown in Fig. 2.6. Inserting Eq. (2.53) into Eq. (2.52) and carrying out the integration yield:

$$\mathbf{f}_{y_2} = \frac{-l}{20} \begin{bmatrix} 10f_{0y_2} + m_e \ddot{\beta}(10x_{2i} + 3l) \\ \frac{5}{3}lf_{0y_2} + \frac{m_e l \ddot{\beta}}{3}(5x_{2i} + 2l) \\ 10f_{0y_2} + m_e \ddot{\beta}(10x_{2i} + 7l) \\ -\frac{5}{3}lf_{0y_2} - \frac{m_e l \ddot{\beta}}{3}(5x_{2i} + 3l) \end{bmatrix} \quad (2.55)$$

the element force vector in  $x_2 z_2$  plane (acting on the nodes  $i$  and  $i + 1$ ) which are  $[F_{z_{2i}}, M_{vi}, F_{z_{2i+1}}, M_{v_{i+1}}]^T$  can be also expressed as

$$\mathbf{f}_{z_2} = \int_0^l p_{z_2}(x_2, t) \mathbf{N}_{z_2} d\zeta \quad (2.56)$$

where

$$p_{z_2}(x_2, t) = -m_e \ddot{\alpha}(x_{2i} \cos \beta + \zeta) - f_{0z_2} \quad (2.57)$$

with

$$f_{0z_2} = m_e (\ddot{z}_{0A} \cos \alpha - \ddot{x}_{0A} \sin \alpha) \quad (2.58)$$

After inserting Eq. (2.57) into Eq. (2.56) and evaluating the integration the force vector in  $x_2 z_2$  plane becomes:

$$\mathbf{f}_{z_2} = \frac{-l}{20} \begin{bmatrix} 10f_{0z_2} + m_e \ddot{\alpha}(10x_{2i} \cos \beta + 3l) \\ \frac{5}{3}lf_{0z_2} + \frac{m_e l \ddot{\alpha}}{3}(5x_{2i} \cos \beta + 2l) \\ 10f_{0z_2} + m_e \ddot{\alpha}(10x_{2i} \cos \beta + 7l) \\ -\frac{5}{3}lf_{0z_2} - \frac{m_e l \ddot{\alpha}}{3}(5x_{2i} \cos \beta + 3l) \end{bmatrix} \quad (2.59)$$

Therefore the total local force vector has a dimension  $8 \times 1$  for the element  $i$  in both  $x_2 y_2$  and  $x_2 z_2$  planes is as follows :

$$\mathbf{f}_t = \frac{-l}{20} \begin{bmatrix} 10f_{0y_2} + m_e \ddot{\beta}(10x_{2i} + 3l) \\ 10f_{0z_2} + m_e \ddot{\alpha}(10x_{2i} \cos \beta + 3l) \\ \frac{5}{3}lf_{0y_2} + \frac{m_e l \ddot{\beta}}{3}(5x_{2i} + 2l) \\ \frac{5}{3}lf_{0z_2} + \frac{m_e l \ddot{\alpha}}{3}(5x_{2i} \cos \beta + 2l) \\ 10f_{0y_2} + m_e \ddot{\beta}(10x_{2i} + 7l) \\ 10f_{0z_2} + m_e \ddot{\alpha}(10x_{2i} \cos \beta + 7l) \\ -\frac{5}{3}lf_{0y_2} - \frac{m_e l \ddot{\beta}}{3}(5x_{2i} + 3l) \\ -\frac{5}{3}lf_{0z_2} - \frac{m_e l \ddot{\alpha}}{3}(5x_{2i} \cos \beta + 3l) \end{bmatrix} \begin{bmatrix} F_{y_{2i}} \\ F_{z_{2i}} \\ M_{wi} \\ M_{vi} \\ F_{y_{2i+1}} \\ F_{z_{2i+1}} \\ M_{w_{i+1}} \\ M_{v_{i+1}} \end{bmatrix} \quad (2.60)$$

By dividing the boom into five elements ( $i = 1, \dots, 5$ ), the mass matrix, the symmetric stiffness matrix, and the nodal force vector for the complete boom ( $AB$ ) can be easily constructed by the assembling process [8] such that :

$$[\bar{\mathbf{M}}] = \sum_{i=1}^5 [\mathbf{M}_t] \quad (2.61)$$

$$[\bar{\mathbf{K}}] = \sum_{i=1}^5 [\mathbf{K}_t] \quad (2.62)$$

$$[\bar{\mathbf{F}}] = \sum_{i=1}^5 [\mathbf{f}_t] \quad (2.63)$$

where :

$\bar{\mathbf{M}}, \bar{\mathbf{K}}, \bar{\mathbf{F}}$  represent the symmetric mass matrix, symmetric stiffness matrix and the nodal force vector respectively for the complete elastic boom ( $AB$ ).

After utilizing the equations (2.61), (2.62) and (2.63) the following expression for the matrices were found :

[illegible]

[illegible]



$$\bar{F} = \frac{-l}{20} \begin{bmatrix} F_{y_{21}} & (10f_{0y_2} + 3lm_e\ddot{\beta}) \\ F_{z_{21}} & (10f_{0z_2} + 3lm_e\ddot{\alpha}) \\ M_{\omega_1} & \left(\frac{5}{3}lf_{0y_2} + \frac{2l^2m_e\ddot{\beta}}{3}\right) \\ M_{\vartheta_1} & \left(\frac{5}{3}lf_{0z_2} + \frac{2l^2m_e\ddot{\alpha}}{3}\right) \\ F_{y_{22}} & (20f_{0y_2} + 20lm_e\ddot{\beta}) \\ F_{z_{22}} & (20f_{0z_2} + m_e\ddot{\alpha}l(10\cos\beta + 10)) \\ M_{\omega_2} & \frac{4m_el^2\ddot{\beta}}{3} \\ M_{\vartheta_2} & \frac{l^2m_e\ddot{\alpha}}{3}(5\cos\beta - 1) \\ F_{y_{23}} & (20f_{0y_2} + 40lm_e\ddot{\beta}) \\ F_{z_{23}} & (20f_{0z_2} + m_e\ddot{\alpha}l(30\cos\beta + 10)) \\ M_{\omega_3} & \frac{4m_el^2\ddot{\beta}}{3} \\ M_{\vartheta_3} & \frac{l^2m_e\ddot{\alpha}}{3}(5\cos\beta - 1) \\ F_{y_{24}} & (20f_{0y_2} + 60lm_e\ddot{\beta}) \\ F_{z_{24}} & (20f_{0z_2} + m_e\ddot{\alpha}l(50\cos\beta + 10)) \\ M_{\omega_4} & \frac{4m_el^2\ddot{\beta}}{3} \\ M_{\vartheta_4} & \frac{l^2m_e\ddot{\alpha}}{3}(5\cos\beta - 1) \\ F_{y_{25}} & (20f_{0y_2} + 80lm_e\ddot{\beta}) \\ F_{z_{25}} & (20f_{0z_2} + m_e\ddot{\alpha}l(70\cos\beta + 10)) \\ M_{\omega_5} & \frac{4m_el^2\ddot{\beta}}{3} \\ M_{\vartheta_5} & \frac{l^2m_e\ddot{\alpha}}{3}(5\cos\beta - 1) \\ F_{y_{26}} & T_{y2} \\ F_{z_{26}} & T_{z2} \\ M_{\omega_6} & 0 \\ M_{\vartheta_6} & 0 \end{bmatrix} \quad (2.66)$$

Now, the equations of motion that governs the elastic vibrations are presented by:

$$\bar{M}\ddot{\boldsymbol{\vartheta}} + \bar{K}\boldsymbol{\vartheta} = \bar{F} \quad (2.67)$$

where  $\bar{\mathbf{M}}$  and  $\bar{\mathbf{K}}$  denote the  $24 \times 24$  constant mass and stiffness matrices respectively,  $\bar{\mathbf{F}}$  denotes the  $24 \times 1$  nodal force vector and

$$\boldsymbol{\vartheta} = [w_1 \ v_1 \ \gamma_1 \ \phi_1 \ \dots \ w_6 \ v_6 \ \gamma_6 \ \phi_6]^T \quad (2.68)$$

is the  $24 \times 1$  nodal displacement vector with  $w_i$  and  $\gamma_i$  representing the nodal translational and rotational displacements respectively at node  $i$  with respect to the  $x_2$ -axis of the boom in  $x_2y_2$  plane, and with  $v_i$  and  $\phi_i$  representing the nodal translational and rotational displacements at node  $i$  with respect to the  $x_2$ -axis of the boom in  $x_2z_2$  plane.

It is very important to be noted that, in the total node vector  $\bar{\mathbf{F}}$  at node 6 (Eq. 2.66) the tension in the cable  $L_2$  is the only external force which acts on that node with both tension components  $T_{y2}$  and  $T_{z2}$ , and all the reaction forces and moments are equal zero. But before adding the tension to the force vector, the components of the tension in  $x_2y_2$  and  $x_2z_2$  planes should be determined.

Using the principle of axis transformation method. The following equations are obtained for these components:

$$T_{y2} = T(-\cos \theta \sin \psi \sin \beta \cos \alpha - \cos \theta \cos \psi \cos \beta - \sin \theta \sin \alpha \sin \beta) \quad (2.69)$$

$$T_{z2} = T(-\cos \theta \sin \psi \sin \alpha + \sin \theta \cos \alpha) \quad (2.70)$$

where:

$T_{y2}$ ,  $T_{z2}$  are the components of the tension in both  $x_2y_2$  - and  $x_2z_2$  -planes respectively.

Because the boom is clamped at point A, the translational and rotational displacements of the elastic boom at node 1 must be zero, so  $w_1 = 0$ ,  $v_1 = 0$ ,  $\gamma_1 = 0$  and  $\phi_1 = 0$ ,

then the order of mass and stiffness matrices ( $\bar{\mathbf{M}}, \bar{\mathbf{K}}$ ) reduced to  $20 \times 20$  and the force vector ( $\bar{\mathbf{F}}$ ) order reduced to  $20 \times 1$ . Thus, the reduced displacement vector  $\boldsymbol{\vartheta}$  will be represented as follows:

$$\boldsymbol{\vartheta} = [w_2 \quad v_2 \quad \gamma_2 \quad \phi_2 \quad \dots \quad w_6 \quad v_6 \quad \gamma_6 \quad \phi_6]^T \quad (2.71)$$

and the system mass and stiffness matrices respectively will be reduced to the following:

$$\bar{\mathbf{M}} = \frac{m_e l}{420} \begin{bmatrix} 312 & 0 & 0 & 0 & 54 & 0 & -13l & 0 & 0 & 0 & 0 & 0 & 0 & 0 & 0 & 0 & 0 & 0 & 0 & 0 \\ 0 & 312 & 0 & 0 & 0 & 54 & 0 & -13l & 0 & 0 & 0 & 0 & 0 & 0 & 0 & 0 & 0 & 0 & 0 & 0 \\ 0 & 0 & 8l^2 & 0 & 13l & 0 & -3l^2 & 0 & 0 & 0 & 0 & 0 & 0 & 0 & 0 & 0 & 0 & 0 & 0 & 0 \\ 0 & 0 & 0 & 8l^2 & 0 & 13l & 0 & -3l^2 & 0 & 0 & 0 & 0 & 0 & 0 & 0 & 0 & 0 & 0 & 0 & 0 \\ 54 & 0 & 13l & 0 & 312 & 0 & 0 & 0 & 54 & 0 & -13l & 0 & 0 & 0 & 0 & 0 & 0 & 0 & 0 & 0 \\ 0 & 54 & 0 & 13l & 0 & 312 & 0 & 0 & 0 & 54 & 0 & -13l & 0 & 0 & 0 & 0 & 0 & 0 & 0 & 0 \\ -13l & 0 & -3l^2 & 0 & 0 & 0 & 8l^2 & 0 & 13l & 0 & -3l^2 & 0 & 0 & 0 & 0 & 0 & 0 & 0 & 0 & 0 \\ 0 & -13l & 0 & -3l^2 & 0 & 0 & 0 & 8l^2 & 0 & 13l & 0 & -3l^2 & 0 & 0 & 0 & 0 & 0 & 0 & 0 & 0 \\ 0 & 0 & 0 & 0 & 54 & 0 & 13l & 0 & 312 & 0 & 0 & 0 & 54 & 0 & -13l & 0 & 0 & 0 & 0 & 0 \\ 0 & 0 & 0 & 0 & 0 & 54 & 0 & 13l & 0 & 312 & 0 & 0 & 0 & 54 & 0 & -13l & 0 & 0 & 0 & 0 \\ 0 & 0 & 0 & 0 & -13l & 0 & -3l^2 & 0 & 0 & 0 & 8l^2 & 0 & 13l & 0 & -3l^2 & 0 & 0 & 0 & 0 & 0 \\ 0 & 0 & 0 & 0 & 0 & -13l & 0 & -3l^2 & 0 & 0 & 0 & 8l^2 & 0 & 13l & 0 & -3l^2 & 0 & 0 & 0 & 0 \\ 0 & 0 & 0 & 0 & 0 & 0 & 0 & 0 & 54 & 0 & 13l & 0 & 312 & 0 & 0 & 0 & 54 & 0 & -13l & 0 \\ 0 & 0 & 0 & 0 & 0 & 0 & 0 & 0 & 0 & 54 & 0 & 13l & 0 & 312 & 0 & 0 & 0 & 54 & 0 & -13l \\ 0 & 0 & 0 & 0 & 0 & 0 & 0 & 0 & -13l & 0 & -3l^2 & 0 & 0 & 0 & 8l^2 & 0 & 13l & 0 & -3l^2 & 0 \\ 0 & 0 & 0 & 0 & 0 & 0 & 0 & 0 & 0 & -13l & 0 & -3l^2 & 0 & 0 & 0 & 8l^2 & 0 & 13l & 0 & -3l^2 \\ 0 & 0 & 0 & 0 & 0 & 0 & 0 & 0 & 0 & 0 & 0 & 0 & 54 & 0 & 13l & 0 & 156 & 0 & -22l & 0 \\ 0 & 0 & 0 & 0 & 0 & 0 & 0 & 0 & 0 & 0 & 0 & 0 & 0 & 54 & 0 & 13l & 0 & 156 & 0 & -22l \\ 0 & 0 & 0 & 0 & 0 & 0 & 0 & 0 & 0 & 0 & 0 & 0 & -13l & 0 & -3l^2 & 0 & -22l & 0 & 4l^2 & 0 \\ 0 & 0 & 0 & 0 & 0 & 0 & 0 & 0 & 0 & 0 & 0 & 0 & 0 & -13l & 0 & -3l^2 & 0 & -22l & 0 & 4l^2 \end{bmatrix} \quad (2.72)$$

[illegible]

also, the reduced force vector will be expressed as follows:

$$\bar{\mathbf{F}} = \frac{-l}{20} \begin{bmatrix} F_{y_{22}} & (20f_{0y_2} + 20l m_e \ddot{\beta}) \\ F_{z_{22}} & (20f_{0z_2} + m_e \ddot{\alpha} l (10 \cos \beta + 10)) \\ M_{\omega_2} & \frac{4m_e l^2 \ddot{\beta}}{3} \\ M_{\vartheta_2} & \frac{l^2 m_e \ddot{\alpha}}{3} (5 \cos \beta - 1) \\ F_{y_{23}} & (20f_{0y_2} + 40l m_e \ddot{\beta}) \\ F_{z_{23}} & (20f_{0z_2} + m_e \ddot{\alpha} l (30 \cos \beta + 10)) \\ M_{\omega_3} & \frac{4m_e l^2 \ddot{\beta}}{3} \\ M_{\vartheta_3} & \frac{l^2 m_e \ddot{\alpha}}{3} (5 \cos \beta - 1) \\ F_{y_{24}} & (20f_{0y_2} + 60l m_e \ddot{\beta}) \\ F_{z_{24}} & (20f_{0z_2} + m_e \ddot{\alpha} l (50 \cos \beta + 10)) \\ M_{\omega_4} & \frac{4m_e l^2 \ddot{\beta}}{3} \\ M_{\vartheta_4} & \frac{l^2 m_e \ddot{\alpha}}{3} (5 \cos \beta - 1) \\ F_{y_{25}} & (20f_{0y_2} + 80l m_e \ddot{\beta}) \\ F_{z_{25}} & (20f_{0z_2} + m_e \ddot{\alpha} l (70 \cos \beta + 10)) \\ M_{\omega_5} & \frac{4m_e l^2 \ddot{\beta}}{3} \\ M_{\vartheta_5} & \frac{l^2 m_e \ddot{\alpha}}{3} (5 \cos \beta - 1) \\ F_{y_{26}} & T_{y2} \\ F_{z_{26}} & T_{z2} \\ M_{\omega_6} & 0 \\ M_{\vartheta_6} & 0 \end{bmatrix} \quad (2.74)$$

## 2.6 Derivation of the operating point

The operating point of the payload variables  $(\theta, \psi, L_2, \beta)$  is considered to be equal to  $(0, 0, L_{2_0}, \beta_0)$ , with  $\beta = \rho + \delta$  where  $\rho$  is the luff angle, thus  $\beta_0 = \rho_0$ , and the wind forces  $p_x = p_y = p_z = 0$ .

The elastic translational and rotational displacements vector  $\mathbf{q}_0$  can be computed from Eq. (2.67) by setting  $\ddot{\boldsymbol{\theta}}$  and the time dependent terms in  $\bar{\mathbf{F}}$  equal to zero, i.e.

$$\mathbf{q}_0 = \bar{\mathbf{K}}^{-1} \bar{\mathbf{F}}_0 \quad (2.75)$$

where,

$$\mathbf{q}_0 = [w_{2_0} \quad v_{2_0} \quad \gamma_{2_0} \quad \phi_{2_0} \quad \dots \quad w_{6_0} \quad v_{6_0} \quad \gamma_{6_0} \quad \phi_{6_0}]^T \quad (2.76)$$

and

$$\bar{\mathbf{F}}_0 = \frac{-l}{20} \begin{bmatrix} 20m_e g \cos \rho_0 \\ 0 \\ 0 \\ 0 \\ 20m_e g \cos \rho_0 \\ 0 \\ 0 \\ 0 \\ 20m_e g \cos \rho_0 \\ 0 \\ 0 \\ 0 \\ 20m_e g \cos \rho_0 \\ 0 \\ 0 \\ 0 \\ -\frac{20}{l} m_p g \cos \rho_0 \\ 0 \\ 0 \\ 0 \end{bmatrix} \quad (2.77)$$

In view of equation(2.75), one obtains:

$$\mathbf{q}_0 = \begin{bmatrix} -1/3 l^3 g \cos \rho_0 (13 m_e l + 7 m_p)/E I \\ 0 \\ -1/2 l^2 g \cos \rho_0 (16 m_e l + 9 m_p)/E I \\ 0 \\ -1/6 l^3 g \cos \rho_0 (89 m_e l + 52 m_p)/E I \\ 0 \\ -1/2 l^2 g \cos \rho_0 (25 m_e l + 16 m_p)/E I \\ 0 \\ -3/2 l^3 g \cos \rho_0 (19 m_e l + 12 m_p)/E I \\ 0 \\ -1/2 l^2 g \cos \rho_0 (29 m_e l + 21 m_p)/E I \\ 0 \\ -2/3 l^3 g \cos \rho_0 (65 m_e l + 44 m_p)/E I \\ 0 \\ -3 l^2 g \cos \rho_0 (5 m_e l + 4 m_p)/E I \\ 0 \\ -25/3 l^3 g \cos \rho_0 (7 m_e l + 5 m_p)/E I \\ 0 \\ -5/2 l^2 g \cos \rho_0 (6 m_e l + 5 m_p)/E I \\ 0 \end{bmatrix} \begin{matrix} w_{20} \\ v_{20} \\ \gamma_{20} \\ \phi_{20} \\ w_{30} \\ v_{30} \\ \gamma_{30} \\ \phi_{30} \\ w_{40} \\ v_{40} \\ \gamma_{40} \\ \phi_{40} \\ w_{50} \\ v_{50} \\ \gamma_{50} \\ \phi_{50} \\ w_{60} \\ v_{60} \\ \gamma_{60} \\ \phi_{60} \end{matrix} \quad (2.78)$$

## 2.7 Expanding the model about the current operating point

In view of equations (2.21, 2.22 and 2.23) and applying Taylor series expansion to the payload nonlinear model equations (2.16 and 2.17) yields to the following linearized equations:

$$\begin{aligned}
& \Delta \ddot{w}_6(L_{20} m_p)(-\sin \alpha_0 \sin \rho_0) + \Delta \ddot{v}_6(L_{20} m_p)(\cos \alpha_0) + \Delta \ddot{\theta} m_p L_{20}^2 \\
& + (g m_p L_{20} - P_y L_{20}) \Delta \theta \\
& = P_z L_{20} - \Delta \ddot{\alpha} (L_{20} m_p) (L_1 \cos \alpha_0 \cos \rho_0 - w_{60} \cos \alpha_0 \sin \rho_0) \\
& - \Delta \ddot{\rho} (L_{20} m_p) (-L_1 \sin \alpha_0 \sin \rho_0 - w_{60} \sin \alpha_0 \cos \rho_0) \\
& - \Delta \ddot{z}_{0A} (L_{20} m_p) + P_z \Delta L_2 \\
& - \Delta \ddot{\delta} (L_{20} m_p) (-L_1 \sin \alpha_0 \sin \rho_0 - w_{60} \sin \alpha_0 \cos \rho_0)
\end{aligned} \tag{2.79}$$

$$\begin{aligned}
& \Delta \ddot{w}_6 m_p L_{20} (-\cos \alpha_0 \sin \rho_0) + \Delta \ddot{v}_6 m_p L_{20} (-\sin \alpha_0) + \Delta \ddot{\psi} m_p L_{20}^2 \\
& + (m_p g L_{20} - p_y L_{20}) \Delta \psi \\
& = p_x L_{20} \\
& - \Delta \ddot{\alpha} L_{20} m_p (-L_1 \sin \alpha_0 \cos \rho_0 + w_{60} \sin \alpha_0 \sin \rho_0) \\
& - \Delta \ddot{\rho} L_{20} m_p (-L_1 \cos \alpha_0 \sin \rho_0 - w_{60} \cos \alpha_0 \cos \rho_0) \\
& - \Delta \ddot{x}_{0A} m_p L_{20} \\
& - \Delta \ddot{\delta} m_p L_{20} (-L_1 \cos \alpha_0 \sin \rho_0 - w_{60} \cos \alpha_0 \cos \rho_0) \\
& + p_x \Delta L_{20}
\end{aligned} \tag{2.80}$$

Similarly, in view of equations (2.21, 2.22, and 2.23), the forces acting on node 6 ( $T_{y2}$ ,  $T_{z2}$ ) described by equations (2.69 and 2.70) can be linearized to:

$$\begin{aligned}
T_{y2} = & \frac{-20}{l} \Delta \ddot{y}_{0A} m_p \cos \rho_0 \\
& - \frac{20}{l} m_p \Delta \ddot{\rho} (L_1 \cos^2 \rho_0 - w_{60} \sin \rho_0 \cos \rho_0) \\
& - \frac{20}{l} \Delta \ddot{\delta} m_p (L_1 \cos^2 \rho_0 - w_{60} \sin \rho_0 \cos \rho_0) \\
& - \frac{20}{l} m_p \Delta \ddot{w}_6 (\cos^2 \rho_0) + \frac{20}{l} m_p \Delta \ddot{L}_2 \cos \rho_0 \\
& - \frac{20}{l} m_p g \cos \rho_0 \\
& - \frac{20}{l} \Delta \psi (p_x \cos \rho_0 + m_p g \sin \rho_0 \cos \alpha_0 \\
& - p_y \sin \rho_0 \cos \alpha_0) \\
& - \frac{20}{l} \Delta \theta (m_p g \sin \alpha_0 \sin \rho_0 \\
& + p_z \cos \rho - p_y \sin \alpha_0 \sin \rho_0) \\
& + \frac{20}{l} p_y \cos \rho_0 - \frac{20}{l} \Delta \rho (-m_p g \sin \rho + p_y \sin \rho) \\
& - \frac{20}{l} \Delta \delta (-m_p g \sin \rho + p_y \sin \rho)
\end{aligned} \tag{2.81}$$

$$\begin{aligned}
T_{z2} = & \frac{-20}{l} [\Delta \psi (m_p g \sin \alpha_0 - p_y \sin \alpha_0) \\
& + \Delta \theta (-m_p g \cos \alpha_0 + p_y \cos \alpha_0)]
\end{aligned} \tag{2.82}$$

Therefore, the total mass matrix  $[\bar{\mathbf{M}}]$  becomes:

$$\begin{aligned}
& \frac{m_e l}{420} \begin{bmatrix}
\omega_2 & \vartheta_2 & \gamma_2 & \phi_2 & \omega_3 & \vartheta_3 & \gamma_3 & \phi_3 & \omega_4 & \vartheta_4 & \gamma_4 & \phi_4 & \omega_5 & \vartheta_5 & \gamma_5 & \phi_5 & \omega_6 & \vartheta_6 & \gamma_6 & \phi_6 & \theta & \varphi \\
\omega_2 & 312 & 0 & 0 & 0 & 54 & 0 & -13l & 0 & 0 & 0 & 0 & 0 & 0 & 0 & 0 & 0 & 0 & 0 & 0 & 0 & 0 \\
\vartheta_2 & 0 & 312 & 0 & 0 & 0 & 54 & 0 & -13l & 0 & 0 & 0 & 0 & 0 & 0 & 0 & 0 & 0 & 0 & 0 & 0 & 0 \\
\gamma_2 & 0 & 0 & 8l^2 & 0 & 13l & 0 & -3l^2 & 0 & 0 & 0 & 0 & 0 & 0 & 0 & 0 & 0 & 0 & 0 & 0 & 0 & 0 \\
\phi_2 & 0 & 0 & 0 & 8l^2 & 0 & 13l & 0 & -3l^2 & 0 & 0 & 0 & 0 & 0 & 0 & 0 & 0 & 0 & 0 & 0 & 0 & 0 \\
\omega_3 & 54 & 0 & 13l & 0 & 312 & 0 & 0 & 0 & 54 & 0 & -13l & 0 & 0 & 0 & 0 & 0 & 0 & 0 & 0 & 0 & 0 \\
\vartheta_3 & 0 & 54 & 0 & 13l & 0 & 312 & 0 & 0 & 0 & 54 & 0 & -13l & 0 & 0 & 0 & 0 & 0 & 0 & 0 & 0 & 0 \\
\gamma_3 & -13l & 0 & -3l^2 & 0 & 0 & 0 & 8l^2 & 0 & 13l & 0 & -3l^2 & 0 & 0 & 0 & 0 & 0 & 0 & 0 & 0 & 0 & 0 \\
\phi_3 & 0 & -13l & 0 & -3l^2 & 0 & 0 & 0 & 8l^2 & 0 & 13l & 0 & -3l^2 & 0 & 0 & 0 & 0 & 0 & 0 & 0 & 0 & 0 \\
\omega_4 & 0 & 0 & 0 & 0 & 54 & 0 & 13l & 0 & 312 & 0 & 0 & 0 & 54 & 0 & -13l & 0 & 0 & 0 & 0 & 0 & 0 \\
\vartheta_4 & 0 & 0 & 0 & 0 & 0 & 54 & 0 & 13l & 0 & 312 & 0 & 0 & 0 & 54 & 0 & -13l & 0 & 0 & 0 & 0 & 0 \\
\gamma_4 & 0 & 0 & 0 & 0 & -13l & 0 & -3l^2 & 0 & 0 & 0 & 8l^2 & 0 & 13l & 0 & -3l^2 & 0 & 0 & 0 & 0 & 0 & 0 \\
\phi_4 & 0 & 0 & 0 & 0 & 0 & -13l & 0 & -3l^2 & 0 & 0 & 0 & 8l^2 & 0 & 13l & 0 & -3l^2 & 0 & 0 & 0 & 0 & 0 \\
\omega_5 & 0 & 0 & 0 & 0 & 0 & 0 & 0 & 0 & 54 & 0 & 13l & 0 & 312 & 0 & 0 & 0 & 54 & 0 & -13l & 0 & 0 \\
\vartheta_5 & 0 & 0 & 0 & 0 & 0 & 0 & 0 & 0 & 0 & 54 & 0 & 13l & 0 & 312 & 0 & 0 & 0 & 0 & -13l & 0 & 0 \\
\gamma_5 & 0 & 0 & 0 & 0 & 0 & 0 & 0 & 0 & -13l & 0 & -3l^2 & 0 & 0 & 0 & 8l^2 & 0 & 13l & 0 & -3l^2 & 0 & 0 \\
\phi_5 & 0 & 0 & 0 & 0 & 0 & 0 & 0 & 0 & 0 & -13l & 0 & -3l^2 & 0 & 0 & 0 & 8l^2 & 0 & 13l & 0 & -3l^2 & 0 \\
\omega_6 & 0 & 0 & 0 & 0 & 0 & 0 & 0 & 0 & 0 & 0 & 0 & 0 & 54 & 0 & 13l & 0 & 0 & 0 & 0 & 0 & 0 \\
\vartheta_6 & 0 & 0 & 0 & 0 & 0 & 0 & 0 & 0 & 0 & 0 & 0 & 0 & 0 & 54 & 0 & 13l & 0 & 0 & 0 & 0 & 0 \\
\gamma_6 & 0 & 0 & 0 & 0 & 0 & 0 & 0 & 0 & 0 & 0 & 0 & 0 & 0 & 0 & -13l & 0 & -3l^2 & 0 & 0 & 0 & 0 \\
\phi_6 & 0 & 0 & 0 & 0 & 0 & 0 & 0 & 0 & 0 & 0 & 0 & 0 & 0 & 0 & 0 & -13l & 0 & -3l^2 & 0 & 0 & 0 \\
\theta & 0 \\
\varphi & 0
\end{bmatrix} \begin{bmatrix}
\Delta \dot{\omega}_2 \\
\Delta \dot{\vartheta}_2 \\
\Delta \dot{\gamma}_2 \\
\Delta \dot{\phi}_2 \\
\Delta \dot{\omega}_3 \\
\Delta \dot{\vartheta}_3 \\
\Delta \dot{\gamma}_3 \\
\Delta \dot{\phi}_3 \\
\Delta \dot{\omega}_4 \\
\Delta \dot{\vartheta}_4 \\
\Delta \dot{\gamma}_4 \\
\Delta \dot{\phi}_4 \\
\Delta \dot{\omega}_5 \\
\Delta \dot{\vartheta}_5 \\
\Delta \dot{\gamma}_5 \\
\Delta \dot{\phi}_5 \\
\Delta \dot{\omega}_6 \\
\Delta \dot{\vartheta}_6 \\
\Delta \dot{\gamma}_6 \\
\Delta \dot{\phi}_6 \\
\Delta \dot{\theta} \\
\Delta \dot{\varphi}
\end{bmatrix} \tag{2.83}
\end{aligned}$$

and the stiffness matrix  $[\bar{\mathbf{K}}]$  becomes:



(2.84)

With force vector  $\bar{F}$ :

(2.85)

Now the linear equations of motion of the crane can be expressed as:

(2.86)

Where

(2.87)

denotes the  $22 \times 1$  generalized displacement vector, and

$$\mathbf{d} = [\Delta x_{0A} \quad \Delta y_{0A} \quad \Delta z_{0A} \quad \Delta \delta]^T \quad (2.88)$$

denotes the 4×1 generalized measured disturbance vector, and

$$\mathbf{u} = [\Delta \rho \quad \Delta \alpha \quad \Delta L_2]^T \quad (2.89)$$

denotes the 3×1 generalized the control input vector, and

$$\mathbf{p} = [\Delta p_x \quad \Delta p_y \quad \Delta p_z]^T \quad (2.90)$$

denotes the 3×1 generalized wind force vector, and

$\bar{\mathbf{M}}_0$  and  $\bar{\mathbf{K}}_0$  are the total mass and stiffness matrices respectively of order 22×22,  $\mathbf{B}_1$  and  $\mathbf{B}_2$  are disturbance matrices of order 22×4,

$$\mathbf{B}_1 = \frac{-l}{20} \begin{bmatrix} 0 & 0 & 0 & -20m_e g \sin \rho_0 \\ 0 & 0 & 0 & 0 \\ 0 & 0 & 0 & 0 \\ 0 & 0 & 0 & 0 \\ 0 & 0 & 0 & -20m_e g \sin \rho_0 \\ 0 & 0 & 0 & 0 \\ 0 & 0 & 0 & 0 \\ 0 & 0 & 0 & 0 \\ 0 & 0 & 0 & -20m_e g \sin \rho_0 \\ 0 & 0 & 0 & 0 \\ 0 & 0 & 0 & 0 \\ 0 & 0 & 0 & -20m_e g \sin \rho_0 \\ 0 & 0 & 0 & 0 \\ 0 & 0 & 0 & 0 \\ 0 & 0 & 0 & 0 \\ 0 & 0 & 0 & \frac{-20}{l} (p_y \sin \rho_0 - m_p g \sin \rho_0) \\ 0 & 0 & 0 & 0 \\ 0 & 0 & 0 & 0 \\ 0 & 0 & 0 & 0 \\ 0 & 0 & 0 & 0 \\ 0 & 0 & 0 & 0 \\ 0 & 0 & 0 & 0 \end{bmatrix} \quad (2.91)$$

$$\mathbf{B}_2 = \frac{-l}{20} \begin{bmatrix}
(-20 \ m_e \cos \alpha_0 \sin \rho_0) & (20 \ m_e \cos \rho_0) & (-20 \ m_e \sin \alpha_0 \cos \rho_0) & 20l \ m_e \\
-20 \ \Delta \dot{x}_{0A} m_e \sin \alpha_0 & 0 & 20 \ m_e \cos \alpha_0 & 0 \\
0 & 0 & 0 & \frac{4m_e l^2}{3} \\
0 & 0 & 0 & 0 \\
(-20 \ m_e \cos \alpha_0 \sin \rho_0) & (20 \ m_e \cos \rho_0) & (-20 \ m_e \sin \alpha_0 \cos \rho_0) & 40l \ m_e \\
-20 \ m_e \sin \alpha_0 & 0 & 20 \ m_e \cos \alpha_0 & 0 \\
0 & 0 & 0 & \frac{4m_e l^2}{3} \\
0 & 0 & 0 & 0 \\
(-20 \ m_e \cos \alpha_0 \sin \rho_0) & (20 \ m_e \cos \rho_0) & (-20 \ m_e \sin \alpha_0 \cos \rho_0) & 60l \ m_e \\
-20 \ m_e \sin \alpha_0 & 0 & 20 \ m_e \cos \alpha_0 & 0 \\
0 & 0 & 0 & \frac{4m_e l^2}{3} \\
0 & 0 & 0 & 0 \\
(-20 \ m_e \cos \alpha_0 \sin \rho_0) & (20 \ m_e \cos \rho_0) & (-20 \ m_e \sin \alpha_0 \cos \rho_0) & 80l \ m_e \\
-20 \ m_e \sin \alpha_0 & 0 & 20 \ m_e \cos \alpha_0 & 0 \\
0 & 0 & 0 & \frac{4m_e l^2}{3} \\
0 & 0 & 0 & 0 \\
0 & \left( \frac{-20}{l} m_p \cos \rho_0 \right) & 0 & \left( \frac{-20}{l} L_1 m_p \cos^2 \rho_0 + \frac{20}{l} \omega_{6_0} m_p \sin \rho_0 \cos \rho_0 \right) \\
0 & 0 & 0 & 0 \\
0 & 0 & 0 & 0 \\
0 & 0 & 0 & 0 \\
0 & 0 & \frac{20}{l} (L_{2_0} m_p) & \frac{20}{l} (L_{2_0} m_p) (-L_1 \sin \alpha_0 \sin \rho_0 - \omega_{6_0} \sin \alpha_0 \cos \rho_0) \\
\frac{20}{l} m_p L_{2_0} & 0 & 0 & \frac{20}{l} m_p L_{2_0} (-L_1 \cos \alpha_0 \sin \rho_0 - \omega_{6_0} \cos \alpha_0 \cos \rho_0)
\end{bmatrix} \quad (2.92)$$

$\mathbf{B}_3$  and  $\mathbf{B}_4$  are input matrices of order  $22 \times 3$ ,

$$\mathbf{B}_3 = \frac{-l}{20} \begin{bmatrix}
-20m_e g \sin \rho_0 & 0 & 0 \\
0 & 0 & 0 \\
0 & 0 & 0 \\
0 & 0 & 0 \\
-20m_e g \sin \rho_0 & 0 & 0 \\
0 & 0 & 0 \\
0 & 0 & 0 \\
0 & 0 & 0 \\
-20m_e g \sin \rho_0 & 0 & 0 \\
0 & 0 & 0 \\
0 & 0 & 0 \\
0 & 0 & 0 \\
0 & 0 & 0 \\
\frac{-20}{l} (p_y \sin \rho_0 - m_p g \sin \rho_0) & 0 & 0 \\
0 & 0 & 0 \\
0 & 0 & 0 \\
0 & 0 & 0 \\
0 & 0 & 0 \\
0 & \frac{-20}{l} p_z & 0 \\
0 & \frac{-20}{l} p_z & 0
\end{bmatrix} \quad (2.93)$$

$$B_4 = \frac{-l}{20} \begin{bmatrix} 20l m_e & 0 & 0 \\ 0 & m_e l(10 \cos \rho_0 + 10) & 0 \\ \frac{4m_e l^2}{3} & 0 & 0 \\ 0 & \frac{l^2 m_e}{3} (5 \cos \rho_0 - 1) & 0 \\ 40l m_e & 0 & 0 \\ 0 & m_e l(30 \cos \rho_0 + 10) & 0 \\ \frac{4m_e l^2}{3} & 0 & 0 \\ 0 & \frac{l^2 m_e}{3} (5 \cos \rho_0 - 1) & 0 \\ 60l m_e & 0 & 0 \\ 0 & m_e l(50 \cos \rho_0 + 10) & 0 \\ \frac{4m_e l^2}{3} & 0 & 0 \\ 0 & \frac{l^2 m_e}{3} (5 \cos \rho_0 - 1) & 0 \\ 80l m_e & 0 & 0 \\ 0 & m_e l(70 \cos \rho_0 + 10) & 0 \\ \frac{4m_e l^2}{3} & 0 & 0 \\ 0 & \frac{l^2 m_e}{3} (5 \cos \rho_0 - 1) & 0 \\ \left( \frac{-20}{l} L_1 m_p \cos^2 \rho_0 + \frac{20}{l} \omega_{60} m_p \sin \rho_0 \cos \rho_0 \right) & 0 & \frac{20}{l} m_p \cos \rho_0 \\ 0 & 0 & 0 \\ 0 & 0 & 0 \\ 0 & 0 & 0 \\ \frac{20}{l} (L_{20} m_p) (-L_1 \sin \alpha_0 \sin \rho_0 - w_{60} \sin \alpha_0 \cos \rho_0) & \frac{20}{l} (L_{20} m_p) (L_1 \cos \alpha_0 \cos \rho_0 - w_{60} \cos \alpha_0 \sin \rho_0) & 0 \\ \frac{20}{l} L_{20} m_p (-L_1 \cos \alpha_0 \sin \rho_0 - w_{60} \cos \alpha_0 \cos \rho_0) & \frac{20}{l} L_{20} m_p (-L_1 \sin \alpha_0 \cos \rho_0 + w_{60} \sin \alpha_0 \sin \rho_0) & 0 \end{bmatrix} \quad (2.94)$$

and  $\mathbf{B}_5$  is the wind disturbance matrix,

$$\mathbf{B}_5 = \frac{-l}{20} \begin{bmatrix} 0 & 0 & 0 \\ 0 & 0 & 0 \\ 0 & 0 & 0 \\ 0 & 0 & 0 \\ 0 & 0 & 0 \\ 0 & 0 & 0 \\ 0 & 0 & 0 \\ 0 & 0 & 0 \\ 0 & 0 & 0 \\ 0 & 0 & 0 \\ 0 & 0 & 0 \\ 0 & 0 & 0 \\ 0 & 0 & 0 \\ 0 & 0 & 0 \\ 0 & 0 & 0 \\ 0 & 0 & 0 \\ 0 & 0 & 0 \\ 0 & 0 & 0 \\ 0 & \frac{20}{l} \cos \rho_0 & 0 \\ 0 & 0 & 0 \\ 0 & 0 & 0 \\ 0 & 0 & 0 \\ 0 & 0 & \frac{-20}{l} L_{20} \\ \frac{-20}{l} L_{20} & 0 & 0 \end{bmatrix} \quad (2.95)$$

The measurement vector  $\mathbf{y}_m$  and the interested outputs  $\mathbf{y}$  are specified as

$$\begin{aligned} \mathbf{y}_m &= [\Delta w_6 \quad \Delta v_6 \quad \theta \quad \psi]^T \\ &= \mathbf{C}_1 \mathbf{q} \end{aligned} \quad (2.96)$$

where  $\mathbf{C}_1$  is the measurement matrix of order  $4 \times 22$ ; it describes the position of the sensors on the crane.

$$\mathbf{C}_1 = \begin{bmatrix} \Delta w_2 & \dots & \Delta w_6 & \Delta v_6 & \theta & \psi \\ 0 & \dots & 1 & 0 & 0 & 0 \\ 0 & \dots & 0 & 1 & 0 & 0 \\ 0 & \dots & 0 & 0 & 1 & 0 \\ 0 & \dots & 0 & 0 & 0 & 1 \end{bmatrix}$$

## 3 Control system design

### 3.1 Introduction

This chapter presents the observer and controller design in order to minimize the pendulation of the payload which can be induced from ship rolling or from any other disturbance that can act on the crane during the cargo transfer operation. When the frequency of the ship rolling is close to the eigenfrequency of the crane for a period of time, resonance will occur and the pendulation of the payload can grow to a dangerous level even with small amplitude of the disturbing motion. This means that, if no control is used, the operation of the crane should be suspended. This control problem is explained in detail in this chapter.

### 3.2 State space representation

The linear equations of motion of the elastic boom and the payload, obtained in Eq. (2.86), can be rewritten as

$$\bar{\mathbf{M}}_0 \ddot{\mathbf{q}} + \bar{\mathbf{K}}_0 \mathbf{q} = \mathbf{B}_1 \mathbf{d} + \mathbf{B}_2 \ddot{\mathbf{d}} + \mathbf{B}_3 \mathbf{u} + \mathbf{B}_4 \ddot{\mathbf{u}} + \mathbf{B}_5 \mathbf{p}. \quad (3.1)$$

To obtain the state space model for the above equation, let

$$\mathbf{z}_1 = \bar{\mathbf{M}}_0 \mathbf{q} - \mathbf{B}_2 \mathbf{d} - \mathbf{B}_4 \mathbf{u} \quad (3.2)$$

$$\mathbf{z}_2 = \bar{\mathbf{M}}_0 \dot{\mathbf{q}} - \mathbf{B}_2 \dot{\mathbf{d}} - \mathbf{B}_4 \dot{\mathbf{u}} \quad (3.3)$$

Then from Eq. (3.2)

$$\mathbf{q} = \bar{\mathbf{M}}_0^{-1} (\mathbf{z}_1 + \mathbf{B}_2 \mathbf{d} + \mathbf{B}_4 \mathbf{u}) . \quad (3.4)$$

Thus the state space equations, corresponding to the current operating point, can be expressed in vector form as

$$\dot{\mathbf{z}} = \mathbf{A}\mathbf{z} + \mathbf{B}\mathbf{u} + \mathbf{E}\mathbf{d} + \mathbf{N}\mathbf{p} \quad (3.5)$$

where

$$\mathbf{z} = [\mathbf{z}_1 \quad \mathbf{z}_2]^T \quad (3.6)$$

denotes the state vector of order  $44 \times 1$ , and

$$A = \begin{bmatrix} \mathbf{0} & I \\ -\bar{K}_0 \bar{M}_0^{-1} & \mathbf{0} \end{bmatrix}, \quad (3.7)$$

$$B = \begin{bmatrix} \mathbf{0} \\ -\bar{K}_0 \bar{M}_0^{-1} B_4 + B_3 \end{bmatrix}, \quad (3.8)$$

represent the corresponding system and input matrices respectively, and

$$E = \begin{bmatrix} \mathbf{0} \\ -\bar{K}_0 \bar{M}_0^{-1} B_2 + B_1 \end{bmatrix}, \quad (3.9)$$

$$N = \begin{bmatrix} \mathbf{0} \\ B_5 \end{bmatrix}, \quad (3.10)$$

represent the disturbance matrices due to ship rolling and disturbance force acting on the payload respectively. Here  $\bar{M}_0$  is assumed to be non-singular.

In view of Eqs. (3.2, 3.3), the initial conditions of the states can be expressed as

$$z_0 = \begin{bmatrix} \bar{M}_0 & \mathbf{0} \\ \mathbf{0} & \bar{M}_0 \end{bmatrix} \begin{bmatrix} q_0 \\ \dot{q}_0 \end{bmatrix} - \begin{bmatrix} B_4 & \mathbf{0} \\ \mathbf{0} & B_4 \end{bmatrix} \begin{bmatrix} u_0 \\ \dot{u}_0 \end{bmatrix} - \begin{bmatrix} B_2 & \mathbf{0} \\ \mathbf{0} & B_2 \end{bmatrix} \begin{bmatrix} d_0 \\ \dot{d}_0 \end{bmatrix}. \quad (3.11)$$

The displacement vector  $q$  from Eq. (3.3) can be rewritten as

$$q = [\bar{M}_0^{-1} \quad \mathbf{0}]z + \bar{M}_0^{-1} B_2 d + \bar{M}_0^{-1} B_4 u \quad (3.12)$$

Therefore, the measurements  $y_m$ , given by Eq. (2.96), can be written as

$$y_m = Cz + Du + Fd, \quad (3.13)$$

where

$$C = [C_1 \bar{M}_0^{-1} \quad \mathbf{0}] \quad (3.14)$$

denotes the output matrix, and

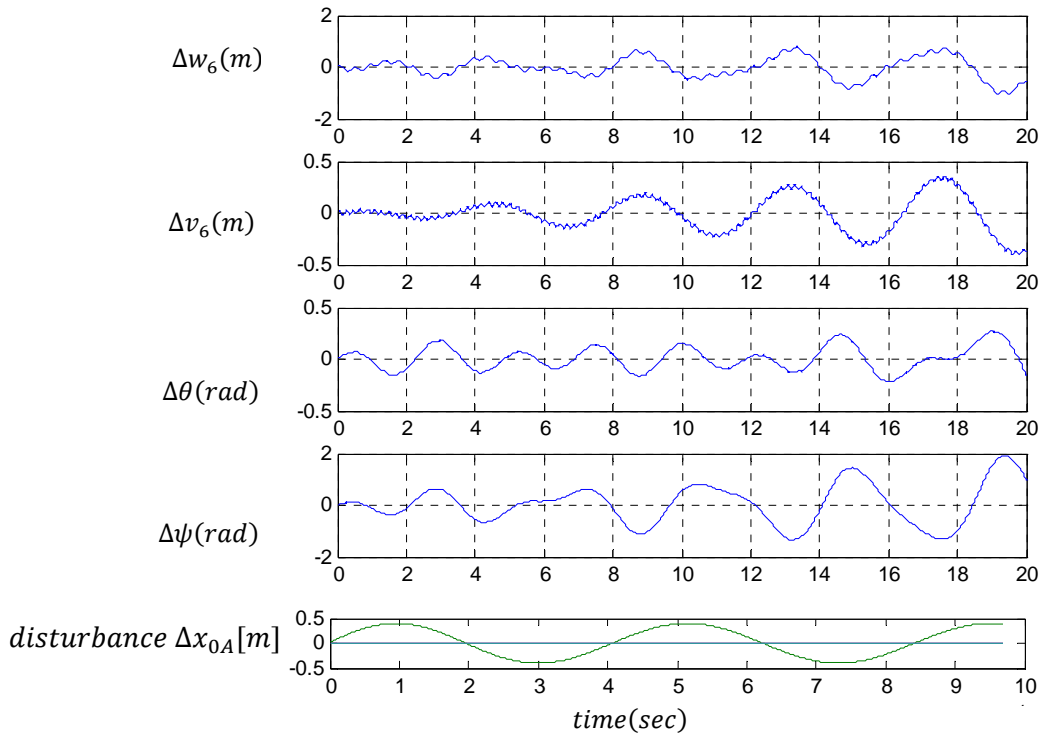
$$D = [C_1 \bar{M}_0^{-1} B_4], \quad (3.15)$$

$$F = [C_1 \quad \bar{M}_0^{-1} B_2] \quad (3.16)$$

represent the input and disturbance direct transmission matrices respectively. Here the rolling motion of the ship  $\Delta\delta(t)$  in addition to the displacements  $(\Delta x_0, \Delta y_0, \Delta z_0)$  are assumed to be measured.

### 3.3 Simulation results

In order to find the effect of the disturbances  $(\Delta x_{0A}, \Delta y_{0A}, \Delta z_{0A}, \Delta \rho_{0A})$ . The simulation was done to the state space model, applying the minimum eigenvalue of the system matrix  $\mathbf{A}$  as the frequency of the sinusoidal disturbance acting on the system, the result of the simulation was as follows:



Numerical values of the crane parameters:

$$\Delta \rho_0 = 45^\circ, \Delta \alpha_0 = 20^\circ$$

$$L_{20} = 4 \text{ m}, m_p = 100 \text{ kg}$$

Figure 3.1: The effect of  $\Delta x_{0A}$  on the crane .



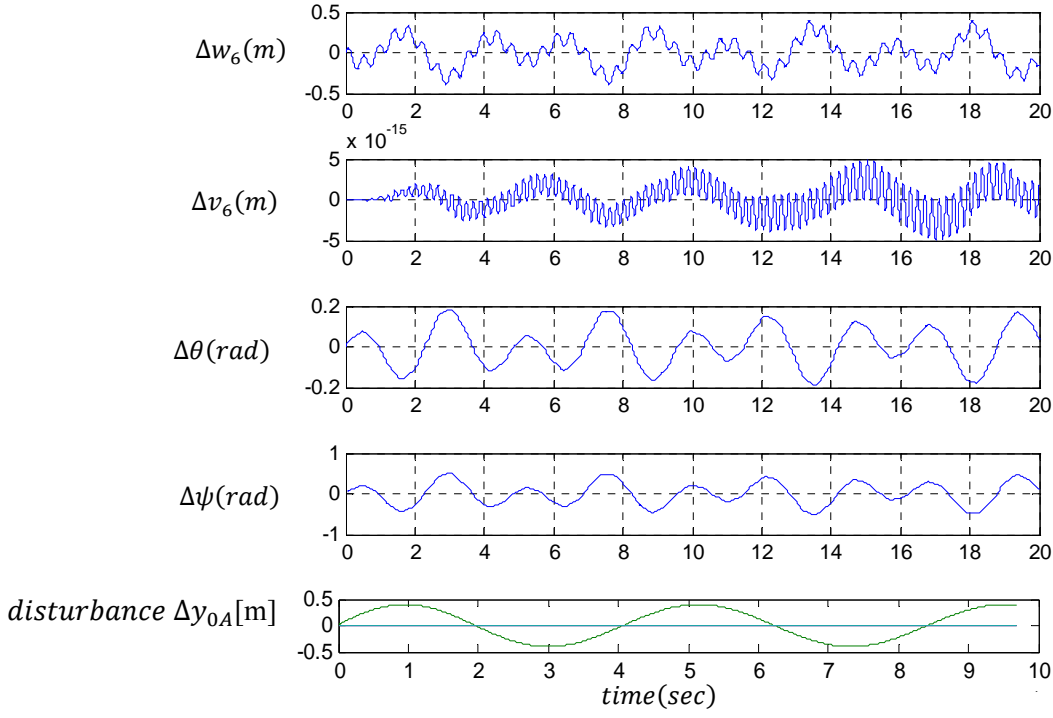


Figure 3.2: The effect of  $\Delta y_{0A}$  on the crane .

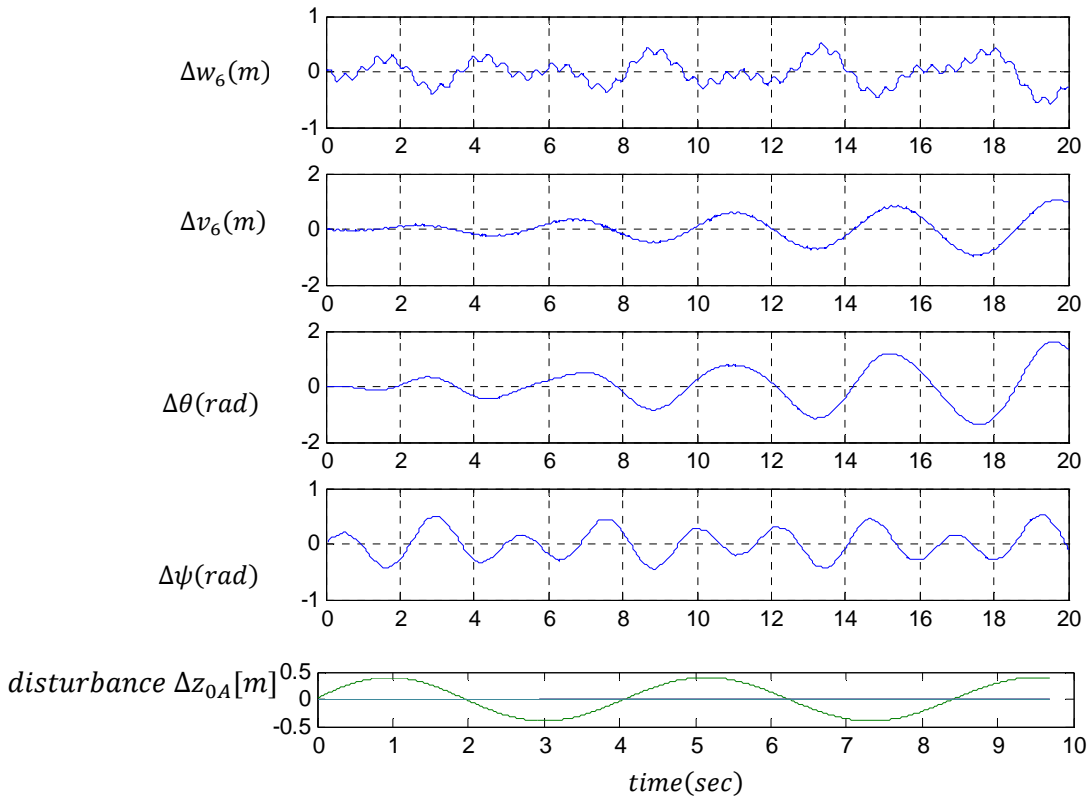
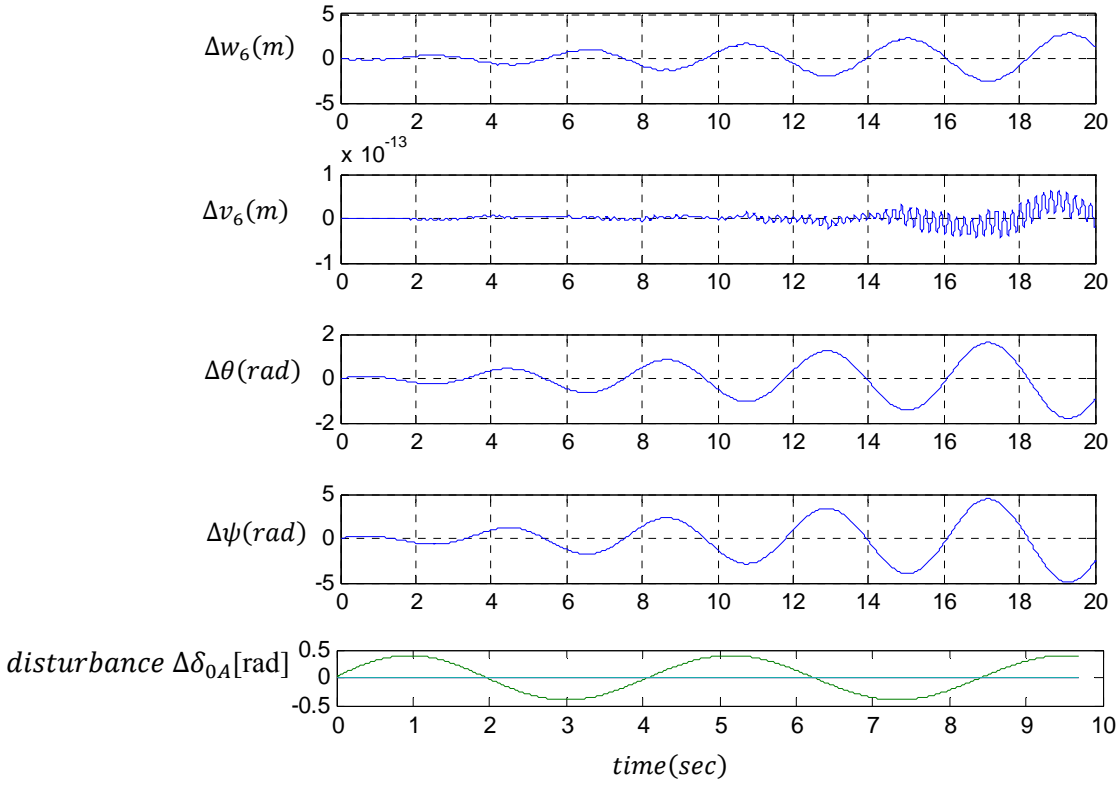


Figure 3.3: The effect of  $\Delta z_{0A}$  on the crane .

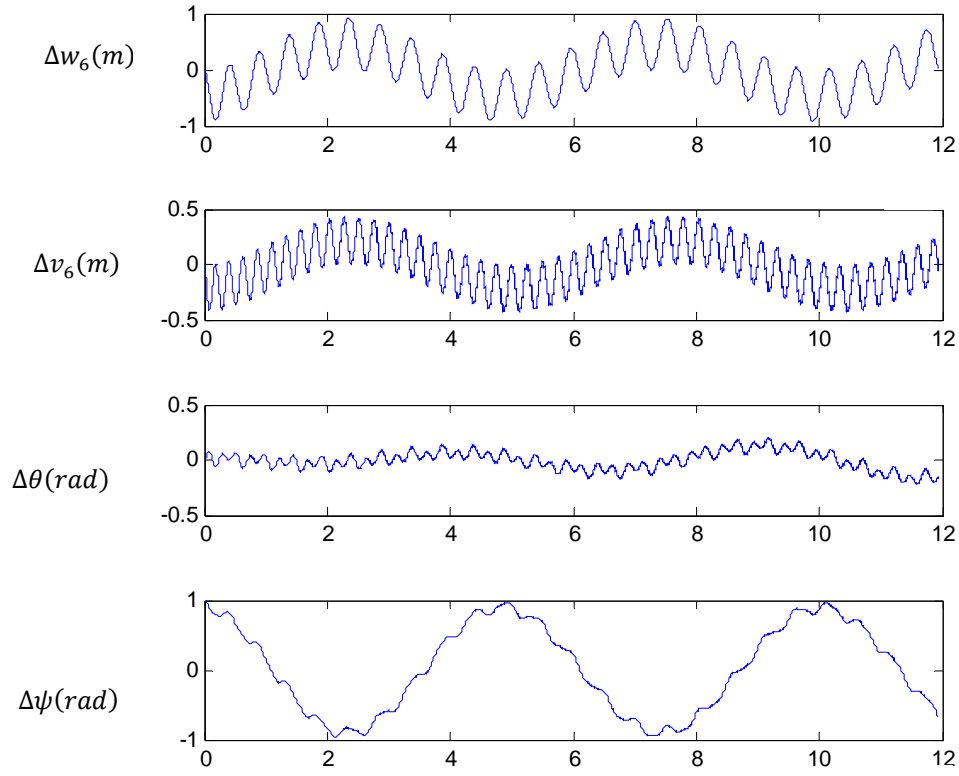


Numerical values of the crane parameters:  
 $\Delta \rho_0 = 45^\circ, \Delta \alpha_0 = 20^\circ$   
 $L_{20} = 4 \text{ m}, m_p = 100 \text{ kg}$

Figure 3.4: The effect of  $\Delta \delta_{0A}$  on the crane .

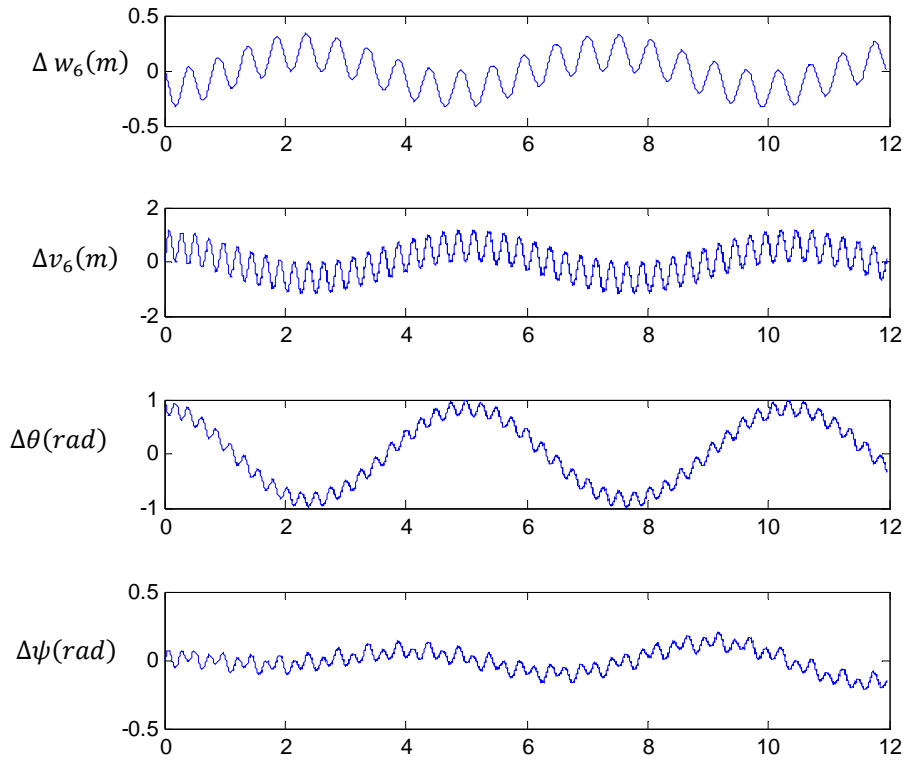
We can conclude from the figures above that amplitude of vibration grows without limit due to disturbances that have a frequency matching the fundamental eigenvalue of the system, and this is the problem that to be solved by building a suitable controller.

Also, simulation results for different initial conditions of the payload cable ( $\theta$  and  $\psi$ ), are shown in figures (3.5,6,7), it is clear that any non zero initial condition of the payload cable results in periodic oscillation. This is reasonable because the internal damping is neglected.



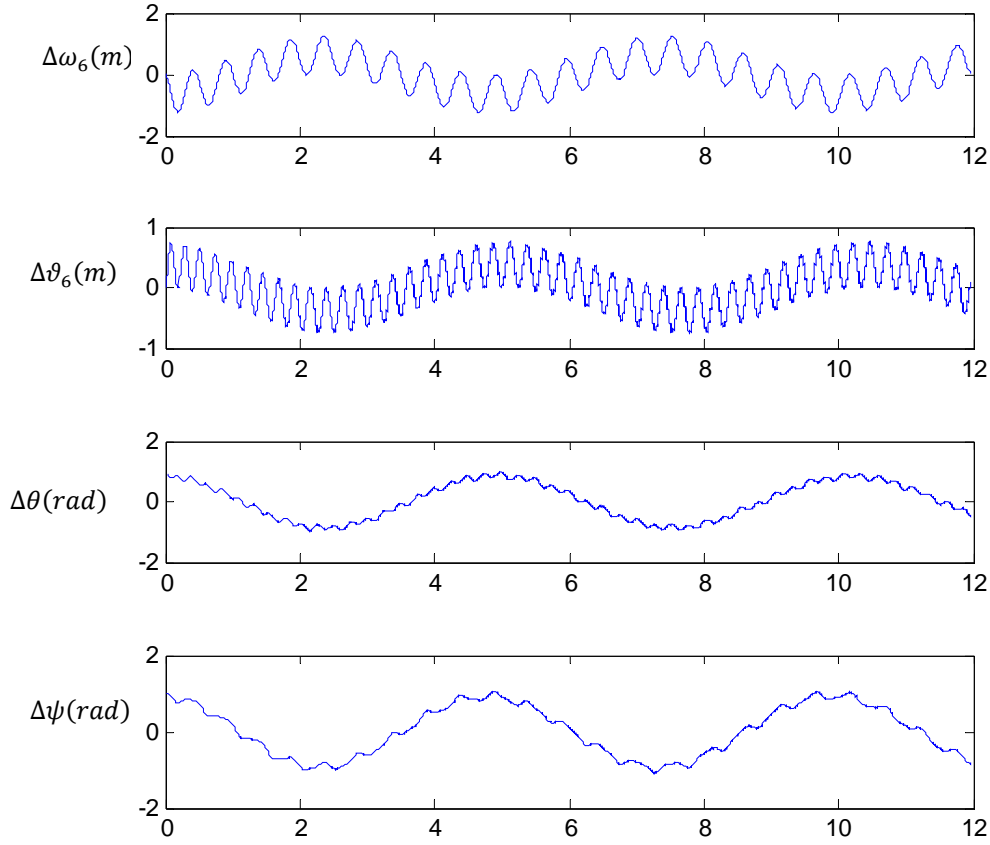
Numerical values of the crane parameters:  
 $\Delta\rho_0 = 45^\circ, \Delta\alpha_0 = 20^\circ$   
 $L_{20} = 4 \text{ m}, m_p = 100 \text{ kg}$

Figure 3.5: The effect of initial condition of  $\Delta\psi = 1 \text{ rad}$ ,  $\Delta\theta = 0 \text{ rad}$  on the crane .



Numerical values of the crane parameters:  
 $\Delta\rho_0 = 45^\circ, \Delta\alpha_0 = 20^\circ$   
 $L_{20} = 4 \text{ m}, m_p = 100 \text{ kg}$

Figure 3.6: The effect of initial condition of  $\Delta\psi = 0 \text{ rad}$ ,  $\Delta\theta = 1 \text{ rad}$  on the crane .



Numerical values of the crane parameters:  
 $\Delta\rho_0 = 45^\circ, \Delta\alpha_0 = 20^\circ$   
 $L_{20} = 4\text{ m}, m_p = 100\text{ kg}$

Figure 3.7: The effect of initial condition of  $\Delta\psi = 1\text{ rad}$ ,  $\Delta\theta = 1\text{ rad}$  on the crane .

### 3.4 State and disturbance estimation

In order to design an optimal state feedback controller, all state variables must be achievable. In most cases, as it is seen in the ship crane under consideration, not all the state variables are measured since the required sensors are not available due to economic or practical reasons. Only 4 out of 44 states can be easily measured which are  $[\Delta\omega_6 \quad \Delta\theta_6 \quad \theta \quad \psi]$ . In order to reconstruct the entire state vector  $\mathbf{z}$ , a suitable observer can be designed as a first step to realize optimal state controller design if the related conditions for applications are fulfilled. Since the state space model of the crane contains the unknown disturbance forces  $\mathbf{p}$ , the state variables and the unknown disturbance can be estimated by using a special observer design able to reconstruct system states in presence of additional unknown effects acting on the system. Here a extendable observer [7, 9, 10, 11] could be used. The structure of this observer is shown in Fig. 3.8. The estimated states are represented by the equations

$$\hat{\dot{\mathbf{z}}} = \mathbf{A}\hat{\mathbf{z}} + \mathbf{B}\mathbf{u} + \mathbf{E}\mathbf{d} + \mathbf{N}\hat{\mathbf{p}} + \mathbf{L}_1(\mathbf{y}_m - \hat{\mathbf{y}}_m) \quad (3.17)$$

and the unknown disturbance is reconstructed by

$$\hat{\mathbf{p}} = \mathbf{L}_2(\mathbf{y}_m - \hat{\mathbf{y}}_m) \quad (3.18)$$

where  $\hat{\mathbf{y}}_m$  is the output of the observer,  $\mathbf{L}_1$  and  $\mathbf{L}_2$  are the observer gain matrices of appropriate dimensions. Due to the difficulty of finding a simple linear model that can adequately describe the unknown disturbance, which is principally unknown, a suitable design procedure is necessary. Since any continuous signal can be approximated by a series of step functions, a practical choice for the linear model corresponding to the estimate of  $\mathbf{p}$  is a stepwise-constant approximation. If the signal is fast, then the observer dynamics should be also fast for the approximation to hold. Since the main expected cause of  $\mathbf{p}$  is the wind force, which usually has a low frequency, the disturbance can be estimated adequately without the need to use a relatively high gain approach. Therefore, the modified extended model can be written as

$$\underbrace{\begin{bmatrix} \hat{\dot{\mathbf{z}}} \\ \hat{\dot{\mathbf{p}}} \end{bmatrix}}_{\hat{\dot{\mathbf{z}}}_e} = \underbrace{\begin{bmatrix} \mathbf{A} & \mathbf{N} \\ \mathbf{0} & \mathbf{0} \end{bmatrix}}_{\mathbf{A}_e} \underbrace{\begin{bmatrix} \hat{\mathbf{z}} \\ \hat{\mathbf{p}} \end{bmatrix}}_{\hat{\mathbf{z}}_e} + \underbrace{\begin{bmatrix} \mathbf{B} \\ \mathbf{0} \end{bmatrix}}_{\mathbf{B}_e} \mathbf{u} + \underbrace{\begin{bmatrix} \mathbf{E} \\ \mathbf{0} \end{bmatrix}}_{\mathbf{E}_e} \mathbf{d} + \underbrace{\begin{bmatrix} \mathbf{L}_1 \\ \mathbf{L}_2 \end{bmatrix}}_{\mathbf{L}_e} (\mathbf{y}_m - \hat{\mathbf{y}}_m) \quad (3.19)$$

with

$$\hat{\mathbf{y}}_m = \underbrace{[\mathbf{C} \quad \mathbf{0}]}_{\mathbf{C}_e} \underbrace{\begin{bmatrix} \hat{\mathbf{z}} \\ \hat{\mathbf{p}} \end{bmatrix}}_{\hat{\mathbf{z}}_e} + \mathbf{D}\mathbf{u} + \mathbf{F}\mathbf{d} \quad (3.20)$$

This model gives the base for the observer development [7, 10, 12, 13]. It is necessary that the extended system is observable, i.e.,

$$\text{rank} \begin{bmatrix} \lambda_i I - \mathbf{A}_e \\ \mathbf{C}_e \end{bmatrix} = \dim(\mathbf{z}) + \dim(\mathbf{p}) \quad (3.20)$$

is satisfied for all eigenvalues  $\lambda_i$  of the system.

Now consider the real system represented by Eq. 3.5 it can be written in another form as follows:

$$\begin{aligned}\dot{\mathbf{z}} &= \mathbf{A}\mathbf{z} + \mathbf{B}\mathbf{u} + \mathbf{E}\mathbf{d} + \mathbf{N}\mathbf{p} \\ \dot{\mathbf{p}} &= \dot{\mathbf{p}}\end{aligned}\tag{3.22}$$

Now, we can write the above two equations can be written in compact form as:

$$\begin{bmatrix} \dot{\mathbf{z}} \\ \dot{\mathbf{p}} \end{bmatrix} = \begin{bmatrix} \mathbf{A} & \mathbf{N} \\ \mathbf{0} & \mathbf{0} \end{bmatrix} \begin{bmatrix} \mathbf{z} \\ \mathbf{p} \end{bmatrix} + \begin{bmatrix} \mathbf{B} \\ \mathbf{0} \end{bmatrix} \mathbf{u} + \begin{bmatrix} \mathbf{E} \\ \mathbf{0} \end{bmatrix} \mathbf{d} + \underbrace{\begin{bmatrix} \mathbf{0} \\ \mathbf{I} \end{bmatrix}}_J \dot{\mathbf{p}}\tag{3.23}$$

By subtracting Eq. 3.23 from Eq.3.19, the error dynamics of the extended observer can be expressed by:

$$\dot{\mathbf{e}} = \mathbf{A}_e \mathbf{e} - \mathbf{L}_e (\mathbf{y}_m - \hat{\mathbf{y}}_m) + \mathbf{J} \dot{\mathbf{p}}\tag{3.24}$$

where

$$\mathbf{e} = \begin{bmatrix} \mathbf{z} \\ \mathbf{p} \end{bmatrix} - \begin{bmatrix} \hat{\mathbf{z}} \\ \hat{\mathbf{p}} \end{bmatrix}\tag{3.25}$$

denotes the error vector of the extended observer, and

$$\mathbf{J} = \begin{bmatrix} \mathbf{0} \\ \mathbf{I} \end{bmatrix}\tag{3.26}$$

represents an input matrix to the error equation. Here the gain matrix of the observer  $\mathbf{L}_e$  is found by minimizing a linear quadratic performance index, which leads to solving the algebraic Riccati equation:

$$\mathbf{A}_e \mathbf{P} + \mathbf{P} \mathbf{A}_e^T + \mathbf{Q}_e - \mathbf{P} \mathbf{C}_e^T \mathbf{R}_e^{-1} \mathbf{C}_e \mathbf{P} = \mathbf{0}.\tag{3.27}$$

Here, this equation is solved using the built in matlab function *lqr* such that:

$$\mathbf{l}_e = \text{lqr}(\mathbf{A}_e^T, \mathbf{C}_e^T, \mathbf{Q}_e, \mathbf{R}_e)\tag{3.28}$$

$$\mathbf{L}_e = \mathbf{l}_e^T\tag{3.29}$$

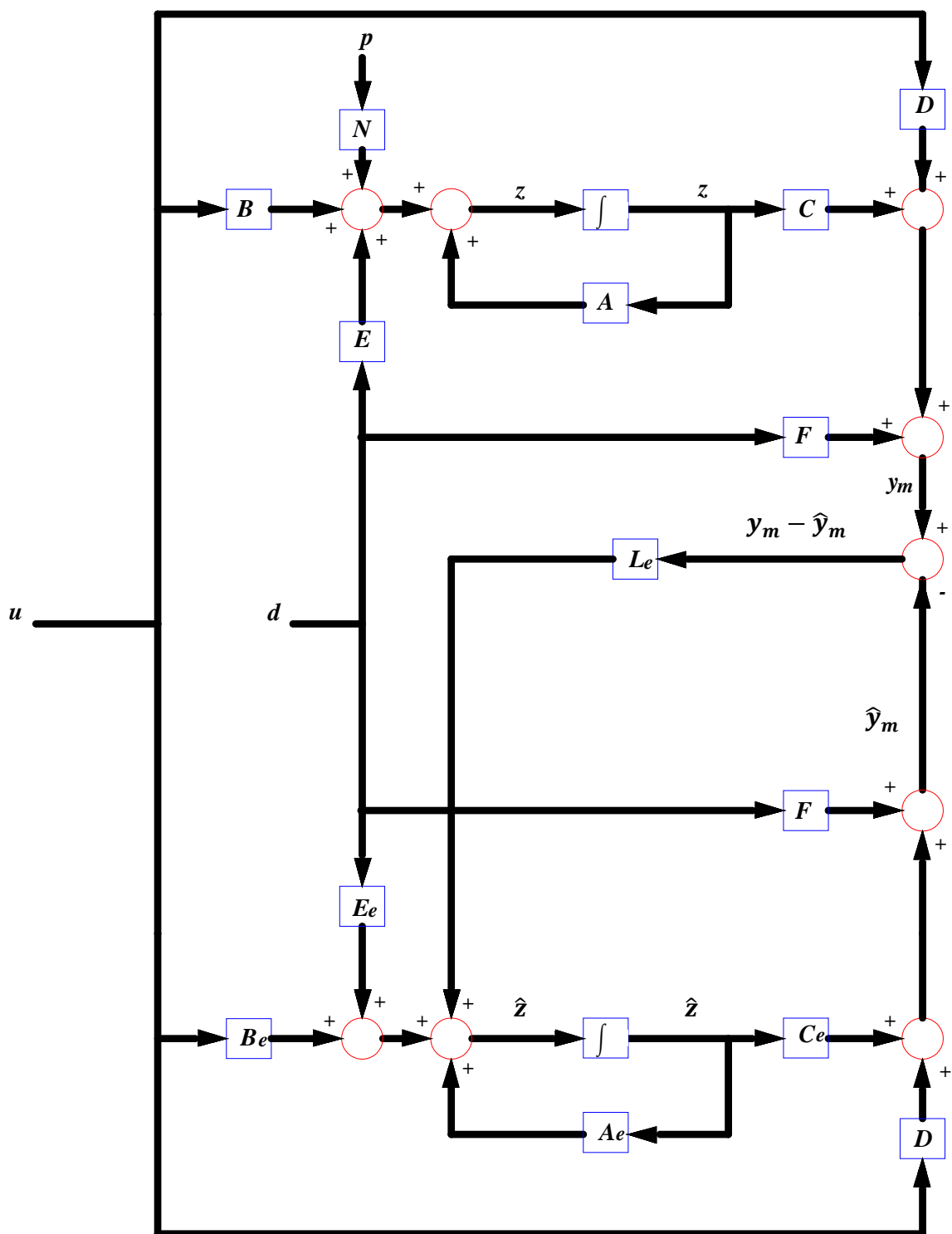


Figure 3.8: Structure of the extended observer .

where  $\mathbf{A}_e^T$  represents the transpose of the extended system matrix with dimension 47 by 47 and  $\mathbf{C}_e^T$  is the transpose of the extended system measurement matrix with dimension  $4 \times 47$ ,  $\mathbf{Q}_e$   $47 \times 47$  and  $\mathbf{R}_e$   $4 \times 4$  are symmetric positive definite weighting matrices for the extended states and the measurements respectively .

One important point to be mentioned here is that the estimation error corresponding to the last three states of the wind forces  $\mathbf{p} = [p_x \ p_y \ p_z]^T$  in  $\mathbf{A}_e$  matrix have to be weighted much more than the other 44 states, i.e., the observer eigenvalue corresponding to last state should be far to the left of the other eigenvalues in the complex plane, we can accomplish this by setting the last entities in  $\mathbf{Q}_e$  corresponding to the wind forces very big weight. All other eigenvalues are weighted such that the observer is asymptotically stable and sufficiently faster than the real passive system. This guarantees that the observer error converges to zero in real time, which means that the estimates converge to their real values in real time and are ready for the implementation of an optimal state feedback controller; this strategy is successfully used for fault diagnosis of large systems [7, 10] and other engineering applications [7, 11, 13].

Simulation result for an actual wind forces signal  $\mathbf{p}$  and their estimated values from the observer are shown in Fig. 3.9. All the simulation result are based on the following crane parameters:

$$L_{20} = 3m, m_p = 100kg, \rho_0 = 45^\circ, \alpha_0 = 20^\circ$$

$p_x = p_y = p_z = 5[N]$  are the actual values of the wind forces.

The simulation results in figures (3.9, 10, 11) were done under the effect of rolling disturbance  $\Delta\delta$  with frequency close to the fundamental eigenvalue of the system.

As you can see from Fig.3.8 the observer estimated the wind forces with dynamic error approached zero.



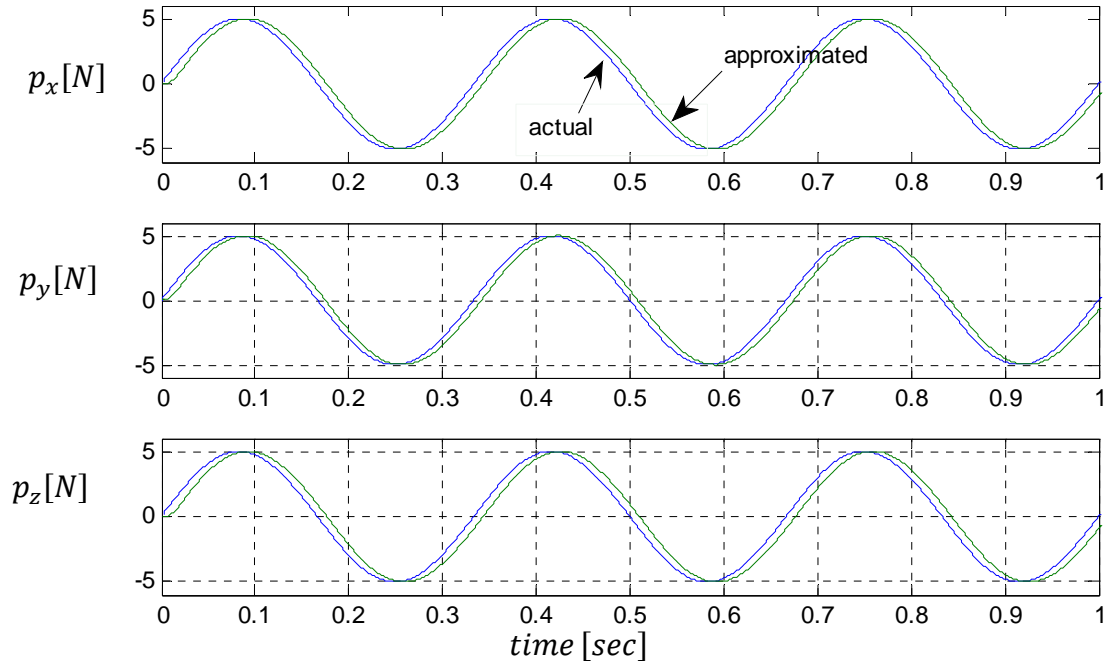
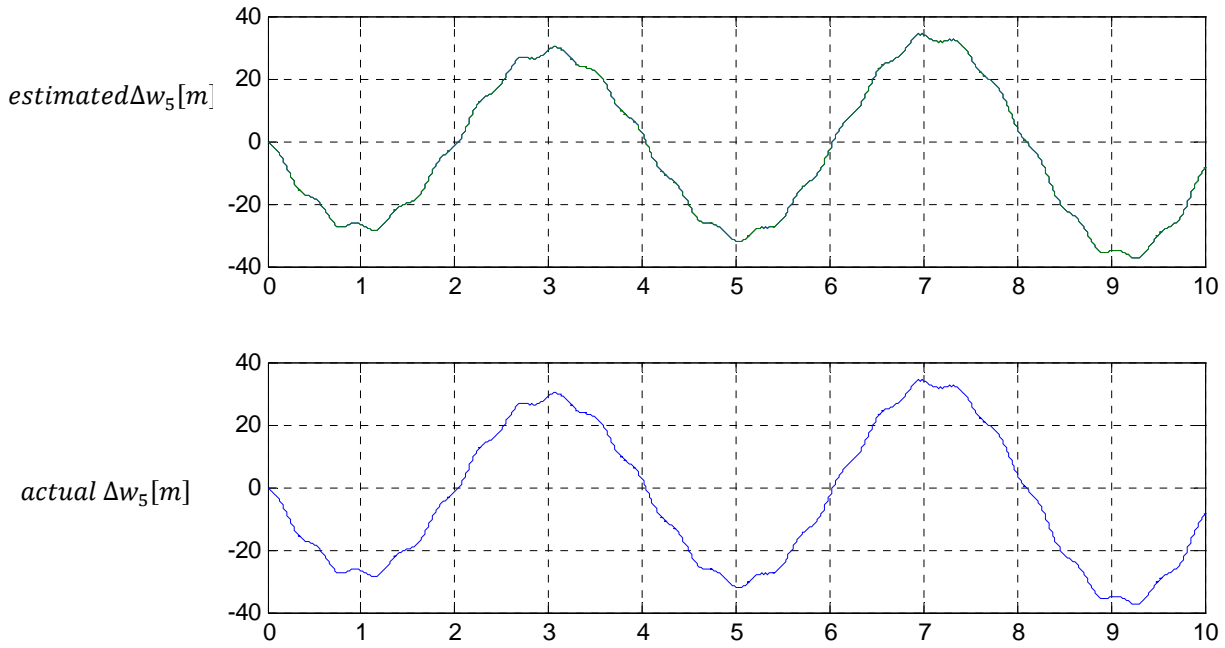


Figure 3.9: The actual and the estimated signals of the wind forces.

The simulation result for the unmeasured displacements and their time derivatives  $[\Delta w_5 \quad \Delta v_5 \quad \dot{\Delta w}_5 \quad \dot{\Delta v}_5]$  are shown together with their estimation values in Fig.3.9 and Fig 3.10 respectively.



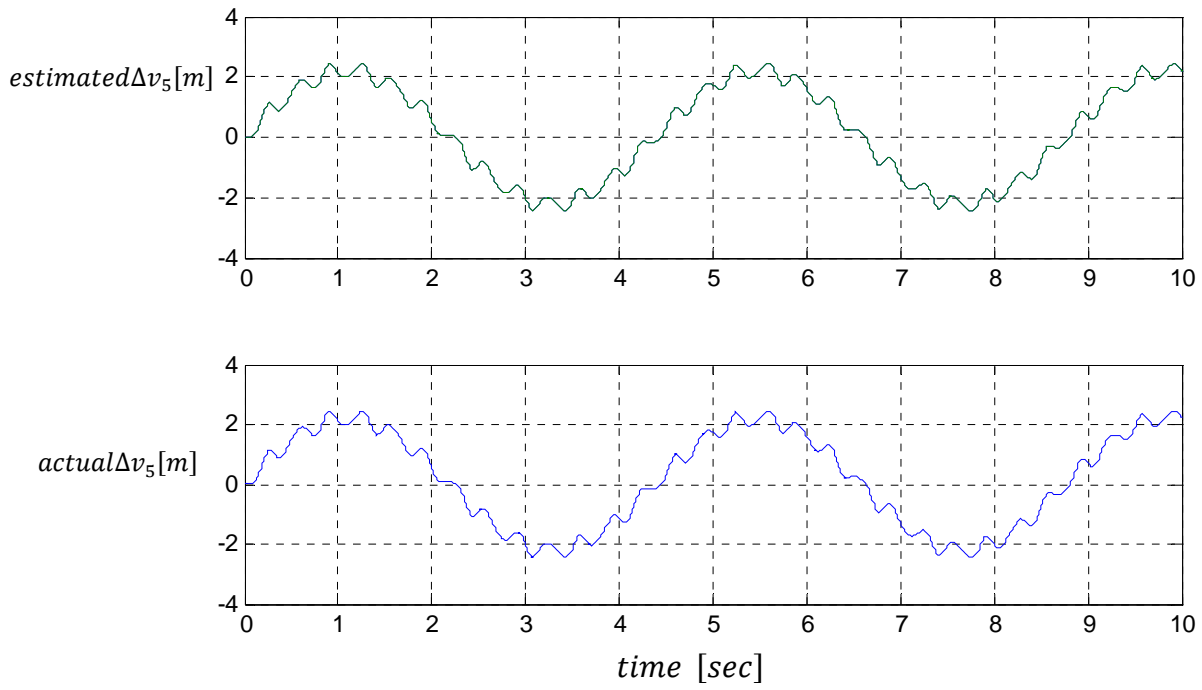
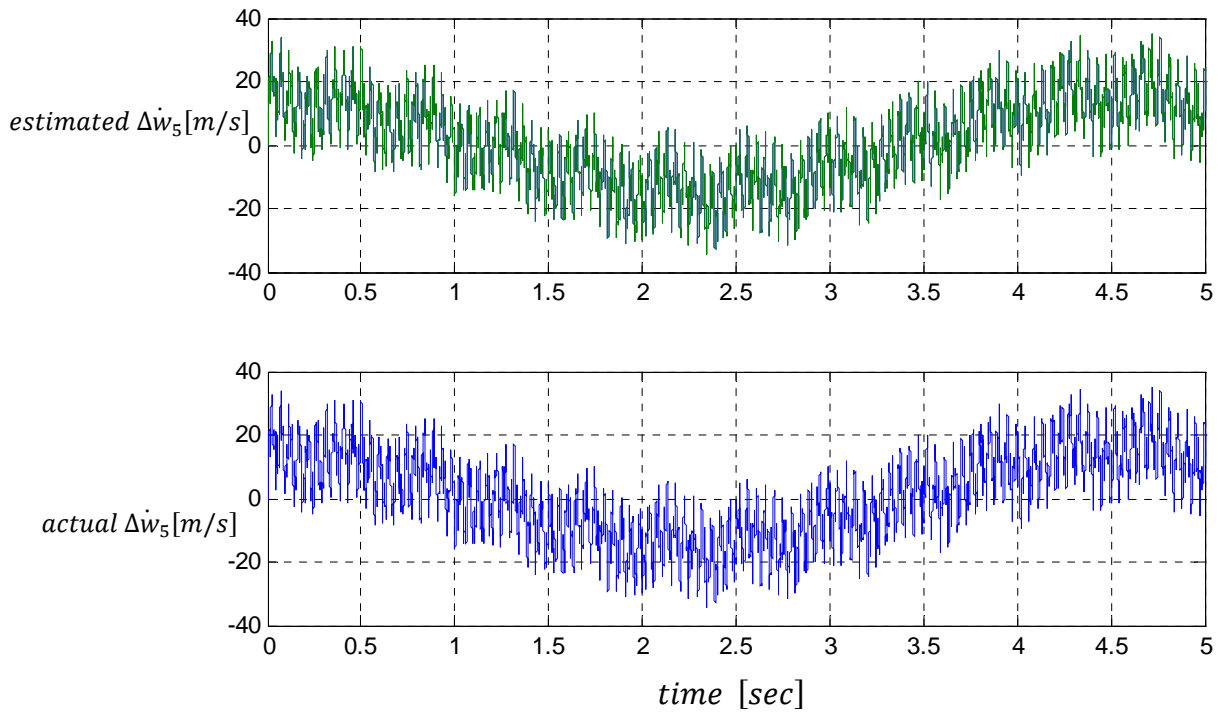


Figure 3.10: The actual and estimated signals of  $[\Delta w_5 \quad \Delta v_5]$ .



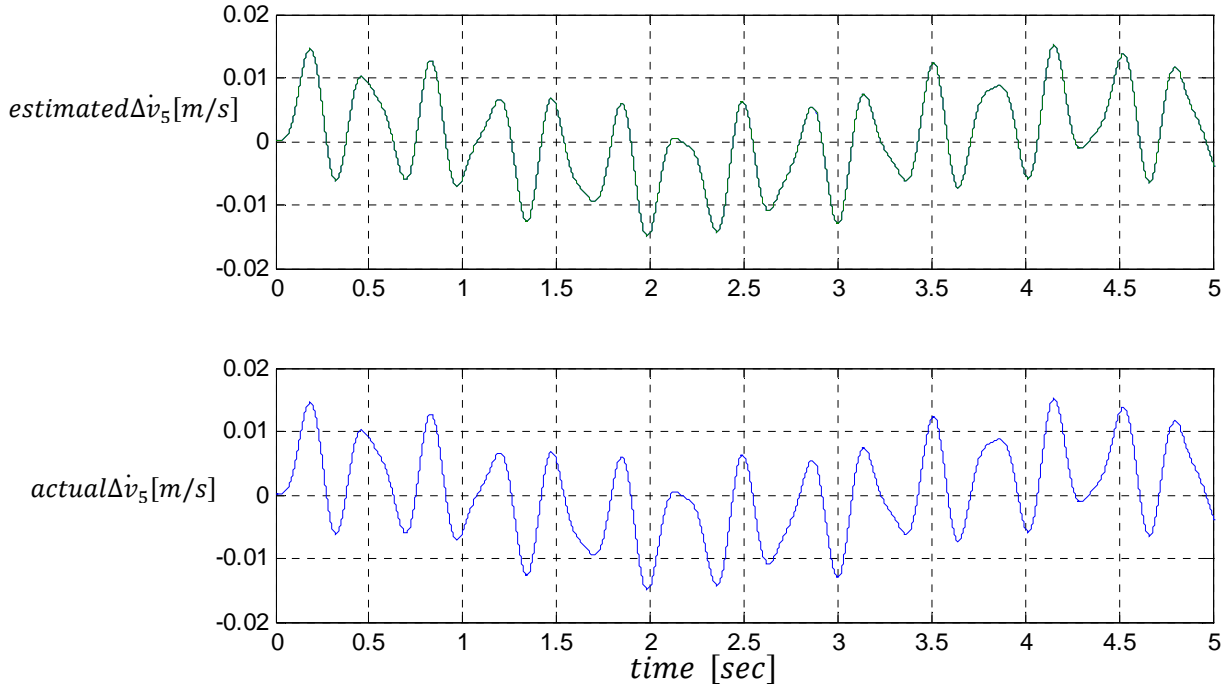


Figure 3.11: The actual and estimated signals of  $[\Delta \dot{w}_5 \quad \Delta \dot{v}_5]$ .

All the above simulation results are done under the effect of sinusoidal measured disturbance  $\ddot{x}_{0A}$ . As we can see from Fig. 3.10 and Fig. 3.11 the observer estimates the unmeasured states with a dynamic error equal to zero.

As you can see from Fig. 3.12 when the initial conditions of the observer are set to zero and the actual initial condition vector of the original system is characterized by  $\theta = \psi = \frac{\pi}{4}$ . Note that the error of the observer due to the difference in the initial conditions disappears in the first second, and the observer estimates the wind forces very well.

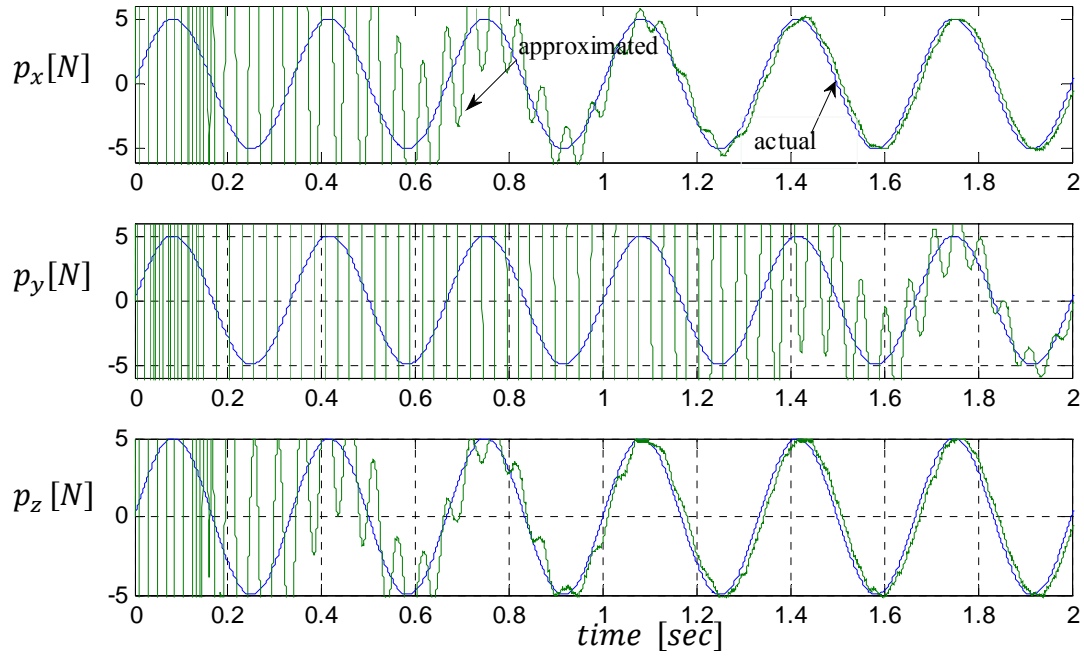


Figure 3.12: The actual and the estimated signals of the wind forces under the effect of the initial conditions of original system.

It is clear from Eqs.3.23 that the observer gain matrix  $\mathbf{L}_e$  depends directly on the extended system matrix  $\mathbf{A}_e$  in addition to the measurement matrix  $\mathbf{C}_e$ . Also, the matrix  $\mathbf{A}_e$  depends on the system matrix  $\mathbf{A}$  which is governed by the mass matrix  $\bar{\mathbf{M}}_0$  and the stiffness matrix  $\bar{\mathbf{K}}_0$ . Since  $\bar{\mathbf{M}}_0$  and  $\bar{\mathbf{K}}_0$  are calculated at the current operating point, which varies with the length of the payload cable  $L_{02}$ , the boom luff angle  $\rho_0$  and the slew angle  $\alpha_0$ , the observer gain matrix  $\mathbf{L}_e$  must be updated according to the current operating point. This leads to the concept of developing a variable-gain extended observer which can cover all possible operating points of the crane.

To design such an observer, the length of the payload cable  $L_{02}$  is divided into three ranges with an increment of  $2m$ , the luff angle  $\rho_0$  is divided into three ranges with an increment of  $20^\circ$  and the slew angle  $\alpha_0$  is divided into 12 ranges with an increment of  $30^\circ$  as shown in figure 3.13 which means that the operating of the crane is covered by  $3 \times 3 \times 12 = 108$  region, each region is characterized by an integer number  $i$  that governs the calculation of the corresponding gain matrix  $\mathbf{L}_e$ . This yields that, the operation of the crane is covered by different observer gain matrices  $(\mathbf{L}_e)_i$ . The

switching between these gains takes place automatically according to the output ( $i$ ) of the region finder (Fig. 3.13), which uses the measurements of the luff angle, the length of the cable and the slew angle to detect the current operating region.

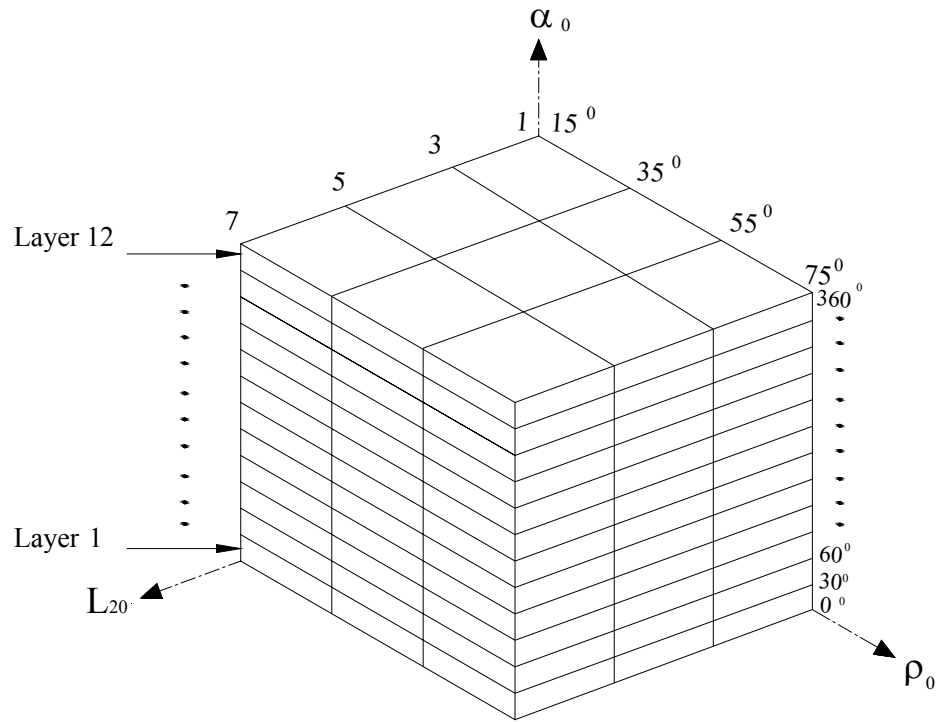


Figure 3.13: The operating regions of the crane.

### 3.5 Controller design

The extended observer discussed in section 3.4 reconstructs the states and the unknown wind forces  $\mathbf{p}$ , now one can design a state feedback controller for the model given by Eqs. (3.5) and (3.13), in order to reduce the effect of the disturbances and to ensure safe cargo transfer of the cane.

### 3.5.1 Optimal state feedback control

Using the extended state observer described in section 3.3, an optimal linear state feedback controller can be designed if the system is completely state controllable (the system is said to be controllable if an input to a system can be found that takes every state variable from desired initial state to desired final state) if the eigenvalue are distinct. State controllability can be confirmed by transformation the state space model given by Eq. (3.5) into a diagonal conical form or (Jordan canonical form);

Let

$$\begin{aligned} x &= VZ \\ \dot{x} &= V\dot{Z} \end{aligned} \quad (3.30)$$

where

$V$  columns are the eigenvectors of the system matrix  $A$

so the transformed model will be as

$$\dot{x} = \underbrace{V^{-1}AV}_{A_c} x + \underbrace{V^{-1}B}_{B_c} u + V^{-1}Ed + V^{-1}Np \quad (3.31)$$

the matrix  $A_c$  represents the modal canonical system matrix form in which its diagonal represents the eigenvalues of the system, so to ensure the state controllability, the input matrix  $B_c$  must have no rows with zeros for all values of payload cable  $L_2$ , the rolling angle  $\rho$  and the slew angle  $\alpha$  under consideration [7, 14].

In order to design a closed loop state feedback controller, all the state variables are fed back to the control input  $u$  vector through again matrix  $-K_f$  so the input vector  $u$  can be written as:

$$u = -K_f z \quad (3.32)$$

By inserting Eq. (3.32) into Eq. (3.5) gives

$$\dot{\mathbf{z}} = \underbrace{(\mathbf{A} - \mathbf{BK}_f)}_{\mathbf{A}_f} \mathbf{z} + \mathbf{Ed} + \mathbf{Np} \quad (3.33)$$

The new system matrix  $\mathbf{A}_f$  matrix depends on the original system matrix  $\mathbf{A}$ , the original input matrix  $\mathbf{B}$  and the gain closed loop state feedback control  $-\mathbf{K}_f$ . Now by changing the gain matrix we can change the place of the eigenvalues of the system to reduce the effect of the disturbances that act on the crane and to ensure safe cargo transfer of the crane.

The state feedback matrix  $\mathbf{K}_f$  can be calculated as

$$\mathbf{K}_f = \mathbf{R}^{-1} \mathbf{B}^T \mathbf{P} \quad (3.34)$$

where  $\mathbf{P}$  represents the solution of the algebraic Riccati equation [7, 15, 16]

$$\mathbf{A}^T \mathbf{P} + \mathbf{PA} + \mathbf{Q} - \mathbf{PBR}^{-1} \mathbf{B}^T \mathbf{P} = \mathbf{0}. \quad (3.35)$$

Here  $\mathbf{Q}$  and  $\mathbf{R}$  are symmetric positive definite weighting matrices of the states and inputs respectively [7, 17]. According to the numerical structure of these matrices, the eigenvalues of the controlled crane system can be altered to get the required behavior of the dynamic response. In reality, the estimated states are used in the feedback loop instead of their real values. Therefore, to guarantee the operation of the controller, the observer must be faster than the real system. Therefore, the eigenvalues of the observer are placed enough to the left of the eigenvalues of the controlled crane; this can be done by tuning the numerical structure of the corresponding weight matrices. It is also important to mention here, that the numerical values of the controller gain  $\mathbf{K}_f$  must be updated according to the current operating, which is governed by the current length of the rope  $L_{02}$ , the current luff angles  $\rho_0$  and the slew angle  $\alpha_0$  is determined by the region finder as discussed before in section 3.4. A block diagram representation of the proposed control strategy is shown in Fig. 3.14.

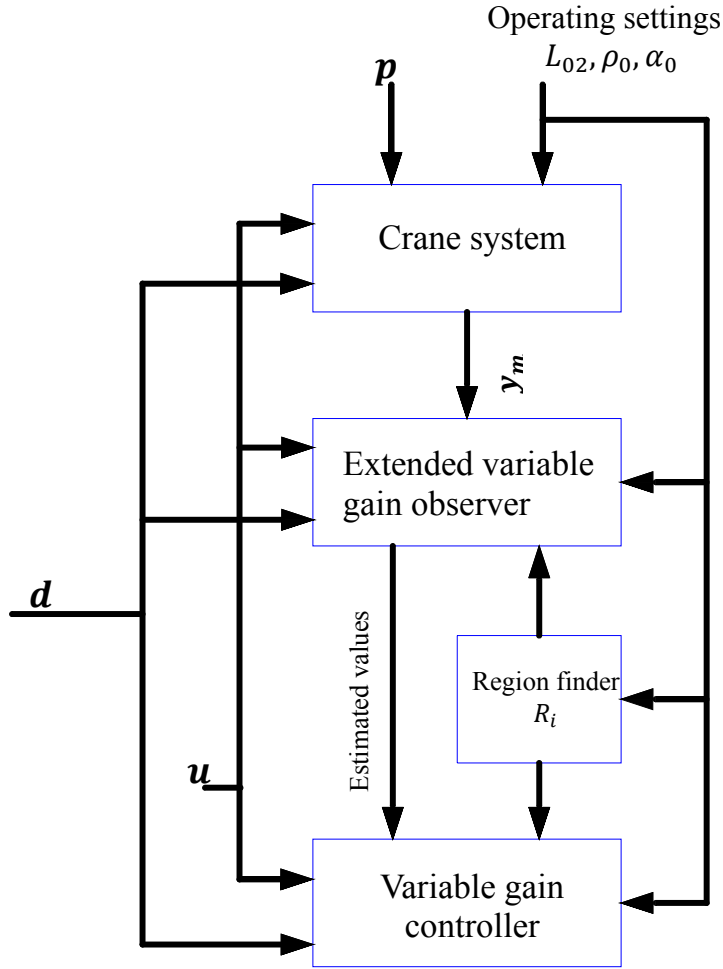


Figure 3.14: Block diagram of the control system.

### 3.6 Robustness

Stability and performance robustness must be taken into consideration in designing feedback control systems. A stable closed loop feedback control system is said to be robust with respect to stability if it remains stable after some changes have been made in the physical or control parameters of the system. In addition, if the system still fulfills a given level of acceptability of a specific performance criterion such as damping or settling time, then the system is said to be robust with respect to its performance [7, 18]. Here the parameters of the crane vary depending on the current operating point leading to a multi-model problem. Accordingly, the used control strategy is based on dividing the operating parameter space into 9 uniform regions for each layer (number of layers 12 ) shown in Fig 3.13 ; each region uses a different



controller/observer gain set. The size of the region is limited such that the stability and performance robustness of the closed loop control system are ensured over the region. There are many methods to check robustness over the operating region; in the crane under consideration, robustness is guaranteed such that, for all operating points inside each individual region, the dominant eigenvalues of the closed loop system remain in the neighborhood of their nominal values that correspond to the calculated gain of the controller.

To find the appropriate point inside the region at which the corresponding controller gain should be calculated, consider for example the region  $R_1$  in the first layer shown in Fig. 3.15, and assume, as a first trial, that the region is covered by a constant gain controller and a constant gain observer, and assume that the gain matrix is calculated at the center of the region, i.e., the observer gain matrix and the controller gain matrix are calculated at  $\rho_0 = (15^\circ + 35^\circ)/2$ ,  $L_{02} = (1\text{ m} + 3\text{ m})/2$  and  $\alpha_0 = 15^\circ$  these values represent the center of the operation region  $R_1$ . The weighting matrices  $\mathbf{Q}$  and  $\mathbf{R}$  for the controller are selected such that, sufficient damping is created in the crane.  $\mathbf{Q}_e$  and  $\mathbf{R}_e$  for the observer are selected such that the dominant eigenvalues of the observer to be placed far enough to the left of the dominant eigenvalues of the controller to make the observer faster than the controller to estimate the unmeasured states and wind forces to feed the controller with the estimated data. Since  $\mathbf{A}$  and  $\mathbf{B}$  vary with the current operating point  $(L_{02}, \rho_0, \alpha_0)$  inside the current region, the eigenvalues also vary consequently.

The plotting of the imaginary parts versus real parts of the three dominant eigenvalues of the closed loop system  $(\lambda_1, \lambda_2, \lambda_3)$  due to the variation in  $L_{02}$ ,  $\rho_0$  and  $\alpha_0$  inside the region  $R_1$ , are shown in Fig. 3.16. It can be easily recognized that as the operating point varies inside the considered region the eigenvalue  $\lambda_2$  get closer to the imaginary axis, which means that the crane will lose a considerable percentage of its relative stability with a reduction in the damping ratio.

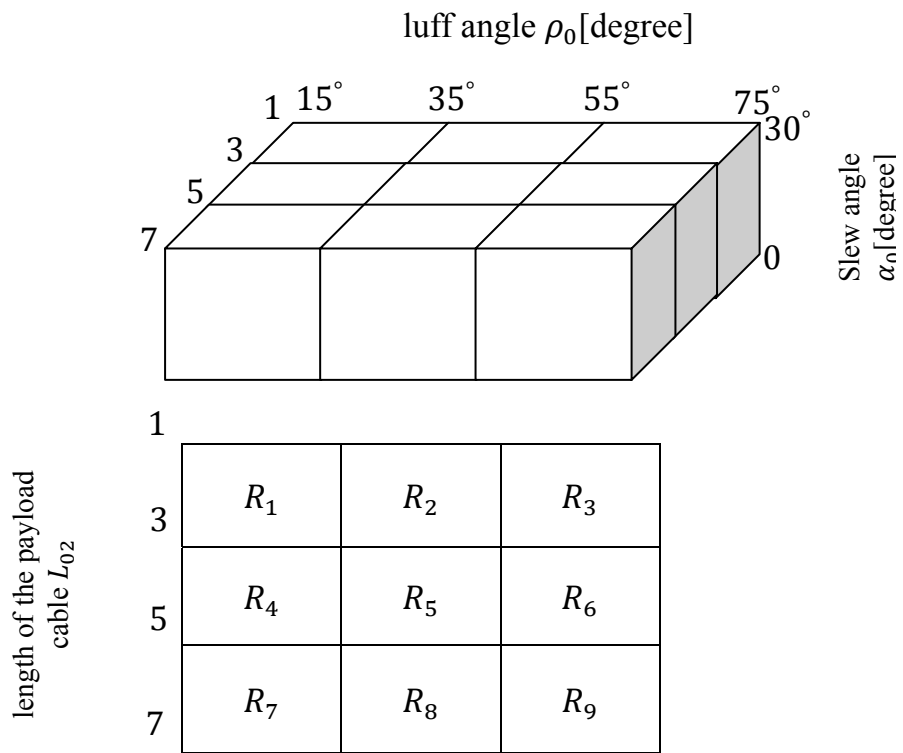


Figure 3.15: Operating regions ( $R_i$ ),  $i = 1, \dots, 108$

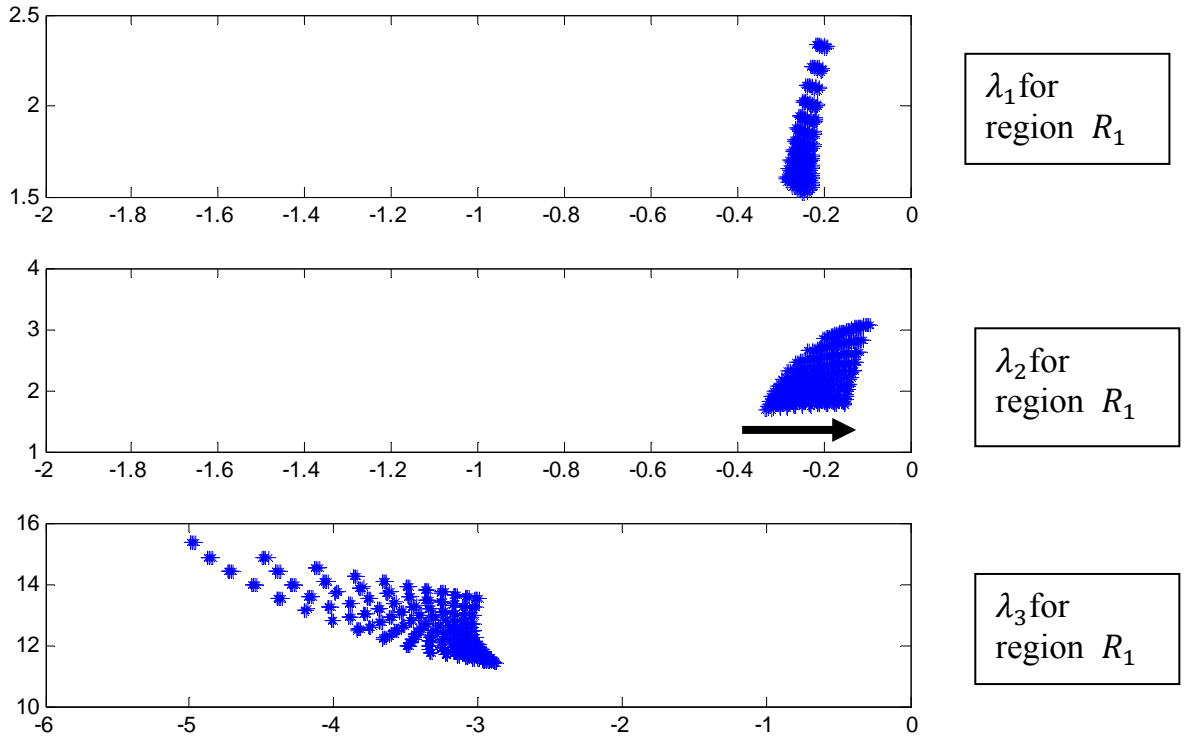


Figure 3.16 : The plotting of  $(\lambda_1, \lambda_2, \lambda_3)$  for  $R_1$ , the design point is the center point of the region.

To overcome this problem, the observer and the controller gains should be updated continuously inside the operating region according to the current value of  $(L_{02}, \rho_0, \alpha_0)$  to preserve the damping ratio and relative stability over the region. In this way, the gains are calculated at each individual corner of the considered region; the weight matrices are chosen to produce nearly the same relative stability and damping at each corner, and each corner gain should provide a stable operation of the crane for all possible operating points inside the region. The total value of the controller gain, corresponding to the current operating point, is described by the 3-D interpolation polynomial in Eq.3.36.

$$K_f(x, y, z) = \mathbf{a}_0 + \mathbf{a}_1x + \mathbf{a}_2y + \mathbf{a}_3z + \mathbf{a}_4xy + \mathbf{a}_5xz + \mathbf{a}_6yz + \mathbf{a}_7xyz \quad (3.36)$$

where  $x$  ,  $y$  and  $z$  denote the local normalized coordinate of the region as shown in Fig.3.17, ,  $a_0, \dots, a_7$  denote the polynomial coefficient matrices, the numerical values of the these coefficient matrices

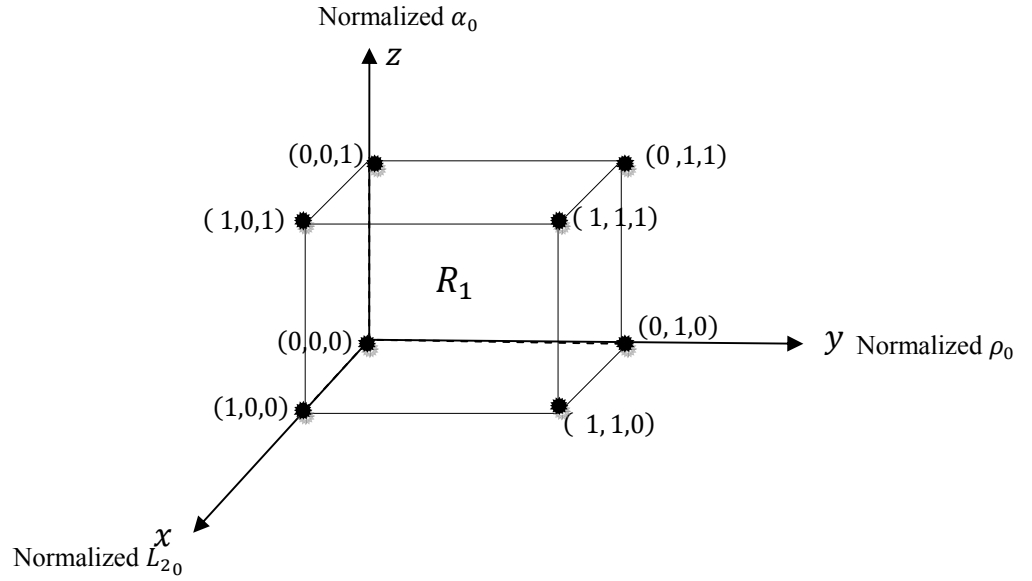


Figure 3.17: the local coordinates of region  $R_1$  .

depend on the gains associated with the corners of the region.

Each corner gain is assumed to satisfy the given interpolation polynomial; thus the following assumptions were made:

$$\begin{aligned}
 K_f(0,0,0) &= K_1 \\
 K_f(1,0,0) &= K_2 \\
 K_f(0,1,0) &= K_3 \\
 K_f(1,1,0) &= K_4 \\
 K_f(0,0,1) &= K_5 \\
 K_f(1,0,1) &= K_6 \\
 K_f(0,1,1) &= K_7 \\
 K_f(1,1,1) &= K_8
 \end{aligned} \tag{3.37}$$

therefore, the coefficients of this polynomial can be calculated from Eq. (3.36) and Eq.(3.37) to get

$$\begin{aligned}
 a_0 &= K_1 \\
 a_1 &= K_2 - K_1 \\
 a_2 &= K_3 - K_1 \\
 a_3 &= K_5 - K_1 \\
 a_4 &= K_4 - K_3 - K_2 + K_1 \\
 a_5 &= K_6 - K_5 - K_2 + K_1
 \end{aligned} \tag{3.38}$$

$$\begin{aligned}
a_6 &= K_7 - K_5 - K_3 + K_1 \\
a_7 &= K_8 - K_7 - K_6 + K_5 - K_4 + K_3 + K_2 - K_1
\end{aligned}$$

Substituting Eq. (3.38) into Eq. (3.36) gives

$$\begin{aligned}
\mathbf{K}_f &= \mathbf{K}_1(1 - x - y - z + xy + xz + yz - xyz) + \mathbf{K}_2(x - xy - \\
& \quad xz + xyz) + \mathbf{K}_3(y - xy - yz + xyz) + \mathbf{K}_4(xy - xyz) + \\
& \quad \mathbf{K}_5(z - xz - yz + xyz) + \mathbf{K}_6(xz - xyz) + \mathbf{K}_7(yz - xyz) + \mathbf{K}_8xyz
\end{aligned} \tag{3.39}$$

Similarly, the corresponding value of the extended observer gain matrix can be expressed as

$$\begin{aligned}
\mathbf{L}_e &= \mathbf{L}_{e1}(1 - x - y - z + xy + xz + yz - xyz) \\
& \quad + \mathbf{L}_{e2}(x - xy - xz + xyz) + \mathbf{L}_{e3}(y - xy - yz + xyz) \\
& \quad + \mathbf{L}_{e4}(xy - xyz) + \mathbf{L}_{e5}(z - xz - yz + xyz) \\
& \quad + \mathbf{L}_{e6}(xz - xyz) + \mathbf{L}_{e7}(yz - xyz) + \mathbf{L}_{e8}xyz
\end{aligned} \tag{3.40}$$

This includes that the gains can be updated continuously according to the local  $x$ -,  $y$ - and  $z$ -coordinates of the current operating point. The distribution of the dominant eigenvalues corresponding to  $R_1$  (i.e.,  $x \in [1;0]$ ,  $y \in [1;0]$ ,  $z \in [1;0]$ ) are shown in figure 3.18. Note that the regions of the dominant eigenvalues are considerably contracted. Therefore, the relative stability and the damping property are preserved for all operating points inside the region.

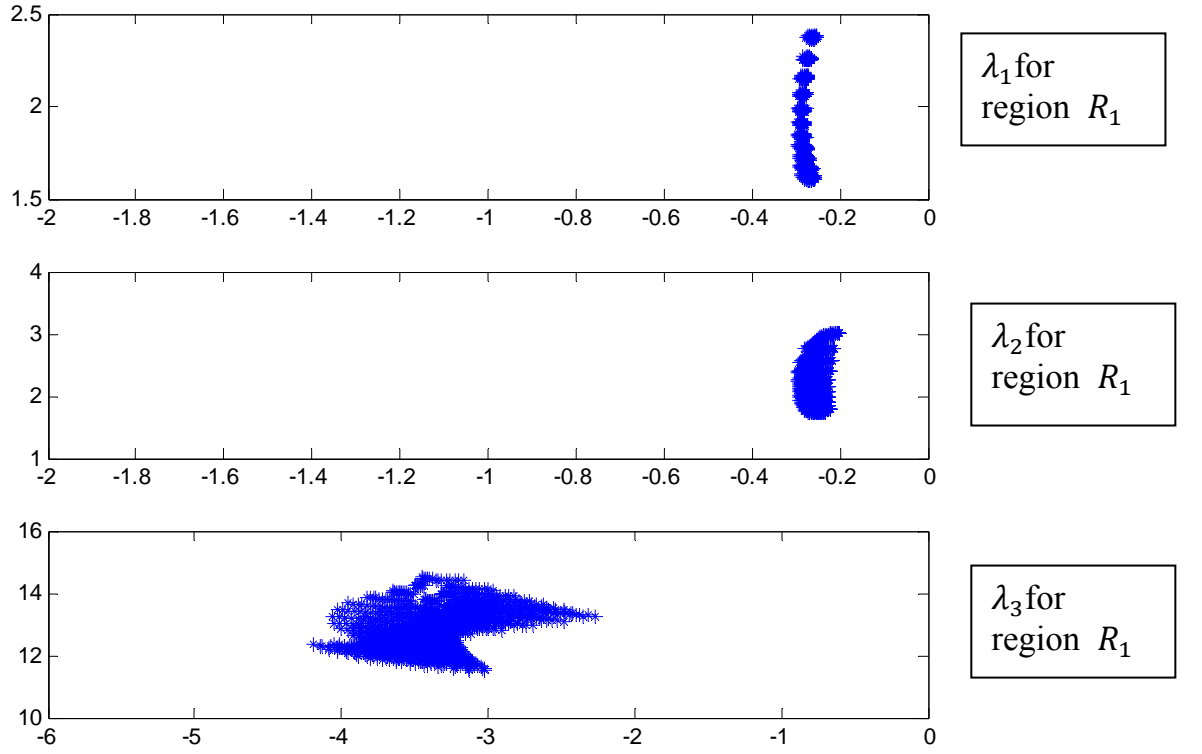


Figure 3.18 : The plotting of  $(\lambda_1, \lambda_2, \lambda_3)$  for  $R_1$  , after the updating of gains for each operating point.

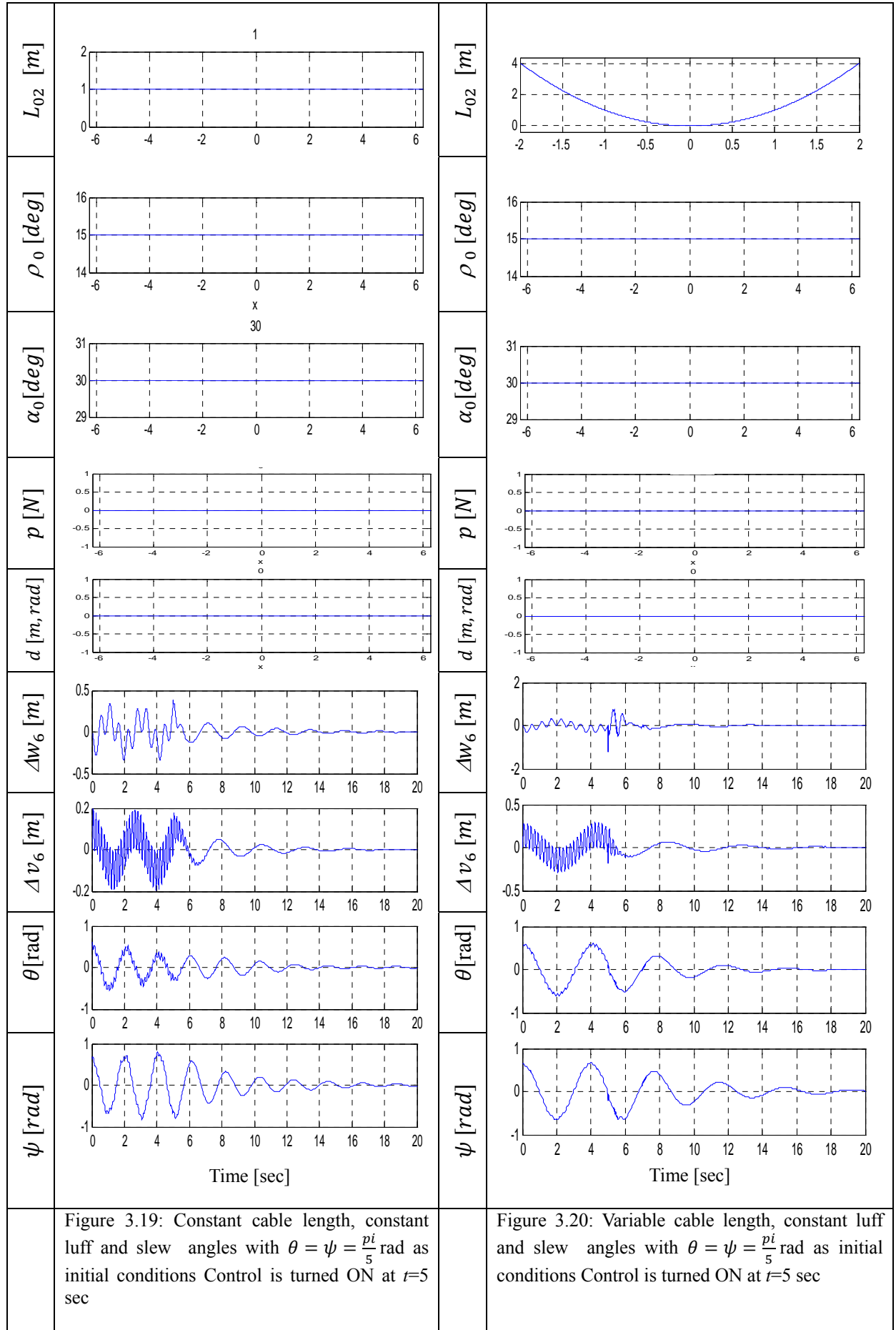
Another significant advantage acquired using this interpolation method is that, the problem which may appear due to a stepwise change of the controller gain between two different regions is avoided.

### 3.7 Simulation results

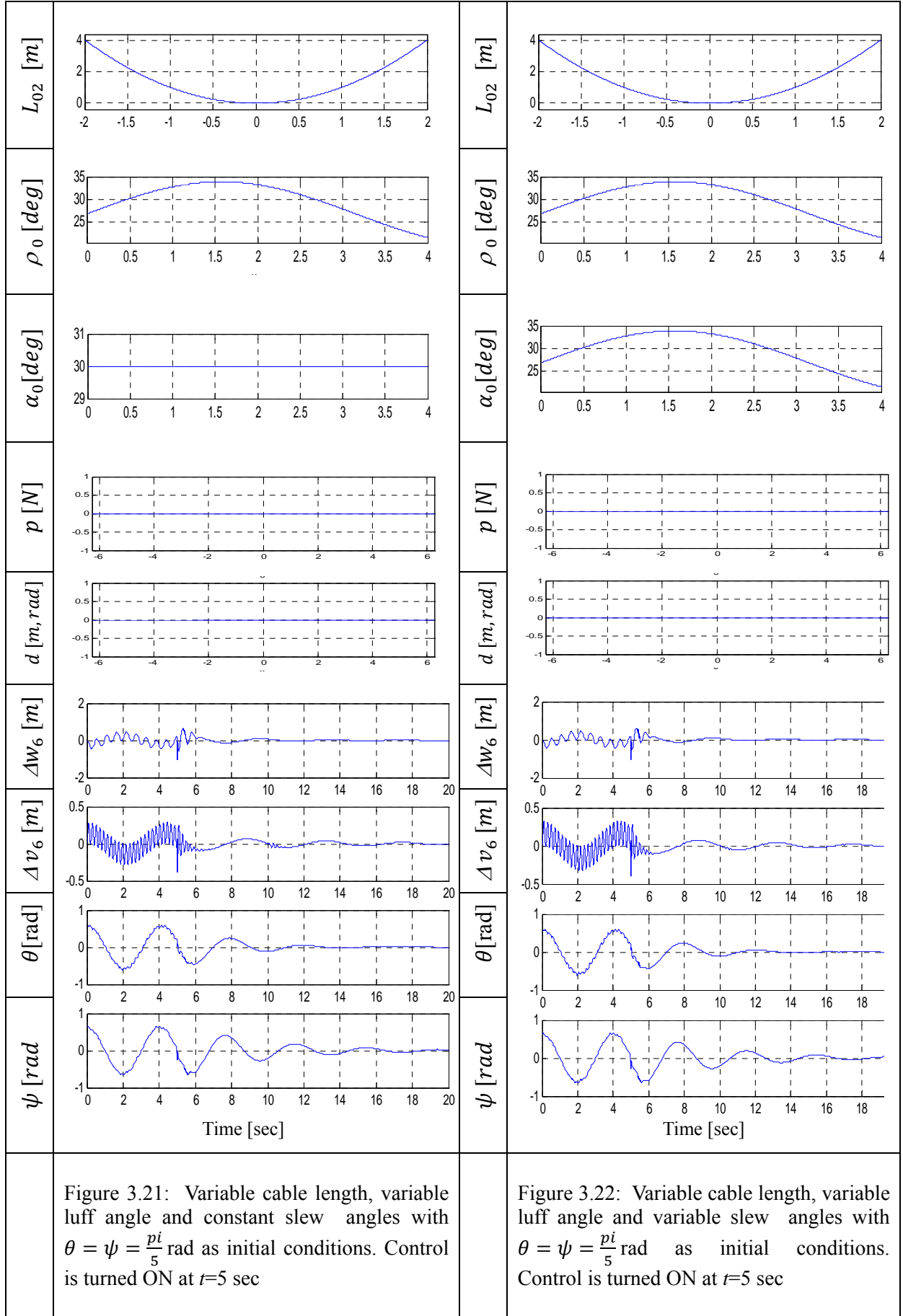
Simulation results for different operating conditions, based on the developed continuous gain method, are shown in Figs. (3.19-3.26). In Figs. (3.19-3.22) the payload is subjected to the initial condition  $\theta = \psi = \pi/5$  rad with different operating conditions in terms of the luff  $\rho_0$ , slew  $\alpha_0$  angles and payload cable length  $L_{02}$ . Here the crane is allowed to vibrate for the first 5seconds, and then the controller is turned ON at  $t=5$  seconds to check the operation of the controller and its ability to suppress the vibrations of the crane. The simulation was conducted with the following

assumptions of the crane geometry, the payload mass  $m_p = 100kg$  the elastic boom length  $L_1 = 5m$  and the circular cross section of the elastic boom has outer diameter  $D_o = .12m$  and inner diameter  $D_i = .1m$ .

In Fig. 3.23 the ship is subjected to sinusoidal rolling disturbance  $\Delta\delta$  with a variable frequency. The response for a sinusoidal rolling close to the average value of the first eigenfrequency of the crane and payload is given in Fig. 3.23. And the effect of a nonzero initial condition in addition to the rolling disturbance is shown in Fig. 3.25. In all cases the observer has no knowledge about the initial condition of the crane. i.e., the initial condition of the observer is set to be zero. In Fig. 3.26, a nonzero disturbance force acting directly on the payload is included. For all of the above mentioned cases, it can be recognized that the controller performs very well and the oscillations are reduced significantly without any noticeable abnormal secondary effect or chattering in the response due to changing the operating region of the crane.







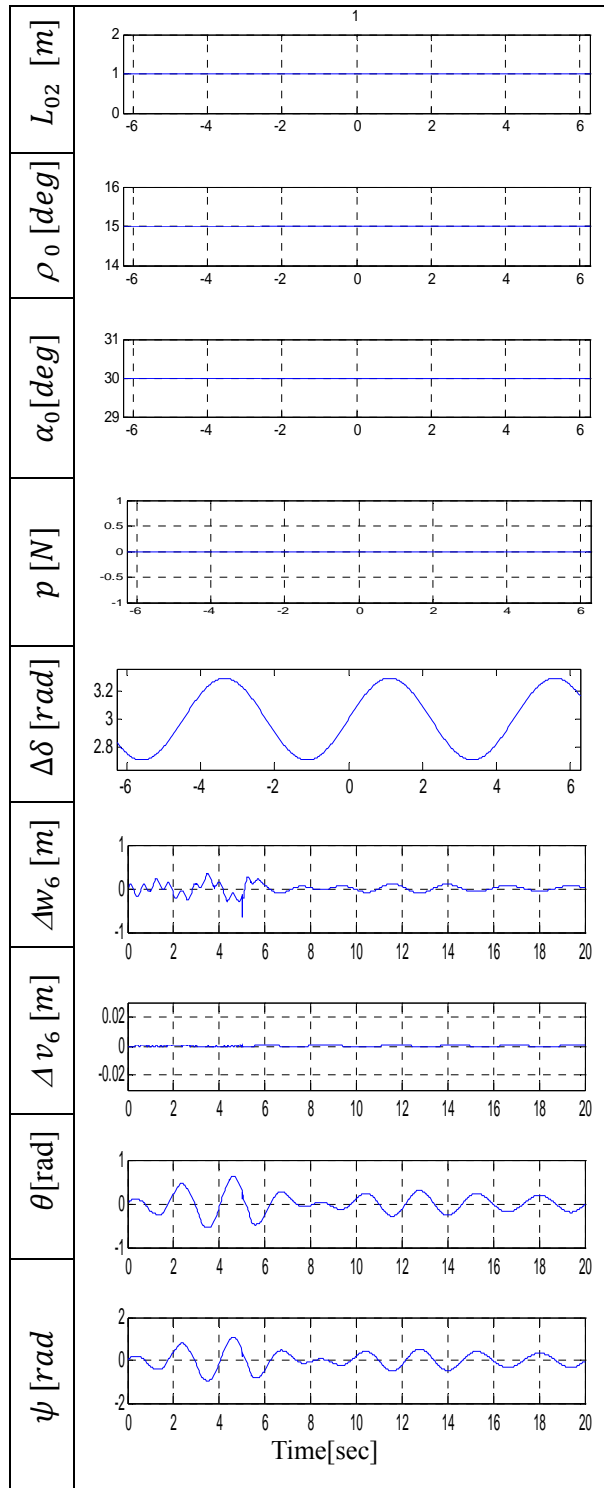


Figure 3.23: Constant cable length, constant luff and slew angles with sinusoidal rolling at the average value of the first eigenfrequency. Control is turned ON at  $t=5$  sec.

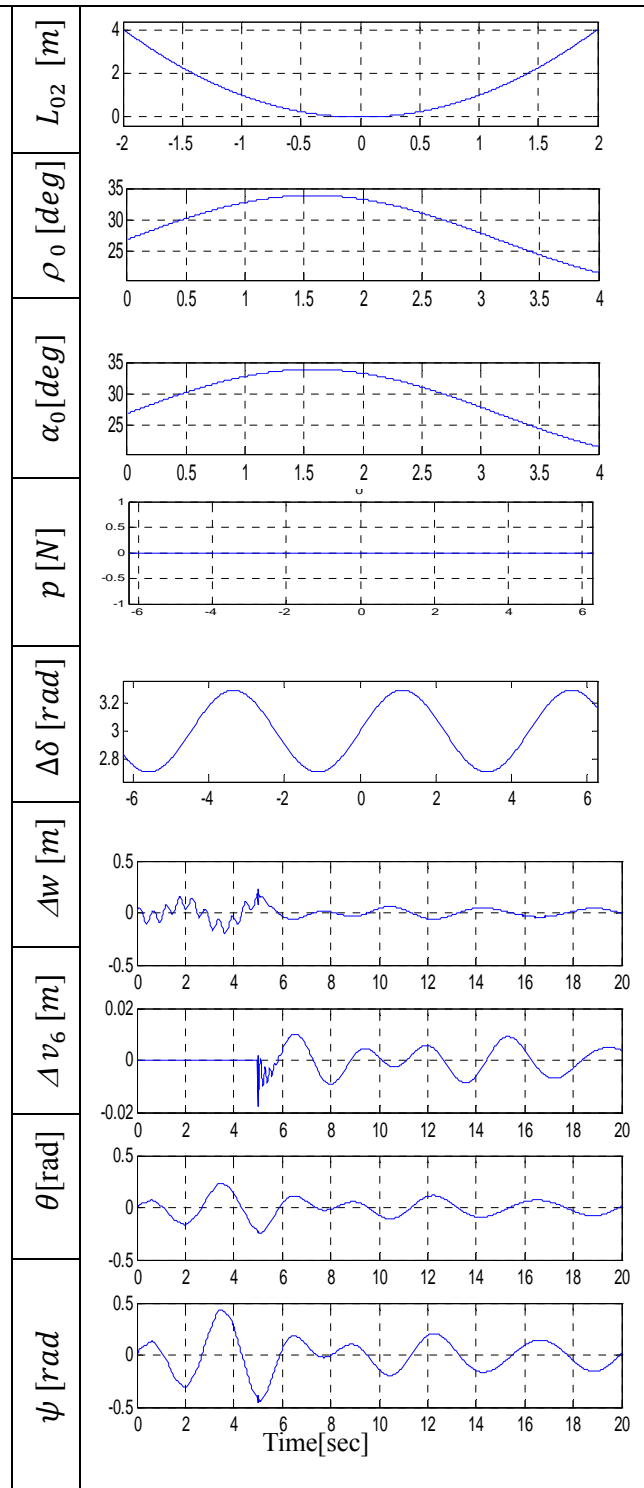
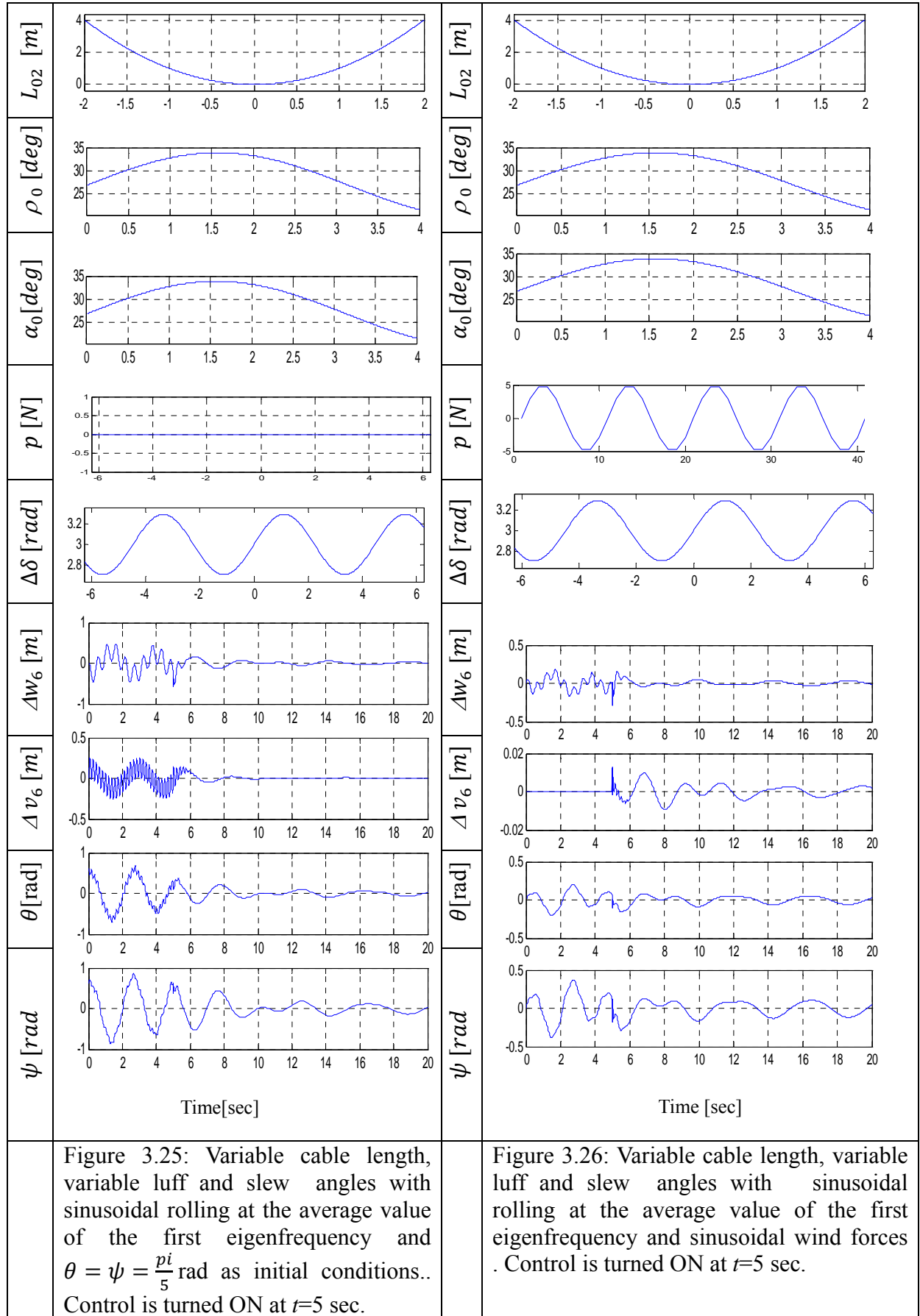


Figure 3.24: : Variable cable length, variable luff and slew angles with sinusoidal rolling at the average value of the first eigenfrequency. Control is turned ON at  $t=5$  sec.



Also, the control system is simulated for a chaotic rolling disturbance . Here the chaotic rolling motion is generated with frequency close to the first eigenvalue of the system using the Chua's equations set which is one of the popular tools for producing such signal. A general dimensionless state equation for a Chua's Oscillator is given as [7, 19]

$$\begin{aligned}\dot{\mathcal{G}}_1 &= k\alpha(\mathcal{G}_2 - \mathcal{G}_1 - f(\mathcal{G})) \\ \dot{\mathcal{G}}_2 &= k(\mathcal{G}_1 - \mathcal{G}_2 + \mathcal{G}_3) \\ \dot{\mathcal{G}}_3 &= k(-\sigma\mathcal{G}_2 - \gamma\mathcal{G}_3)\end{aligned}\tag{3.41}$$

with

$$f(\mathcal{G}) = b\mathcal{G}_1 + \frac{1}{2}(a-b)\{|\mathcal{G}_1 + 1| - |\mathcal{G}_1 - 1|\},\tag{3.42}$$

where  $\alpha$ ,  $\sigma$ ,  $\gamma$ ,  $a$ ,  $b$ , and  $k$  are constant parameters. For the selection:  $\alpha = 15.6$ ,  $\sigma = 28.58$ ,  $\gamma = 0$ ,  $a = -1.14286$ ,  $b = -0.714286$ ,  $k = 1$ , with the initial conditions  $\mathcal{G}_1(0) = 1.16346$ ,  $\mathcal{G}_2(0) = -0.4972335$ , and  $\mathcal{G}_3(0) = -0.905656$ , the solution of Chua's equations for  $\mathcal{G}_1(t)$  is chaotic. Therefore, the rolling excitation is chosen as

$$\Delta\delta(t) = m\mathcal{G}_1(t),\tag{3.43}$$

where  $m$  is constant; it's value determines the amplitude of the chaotic rolling. The numerical solution of the above three equations is displayed in Fig. 3.27 bellow.

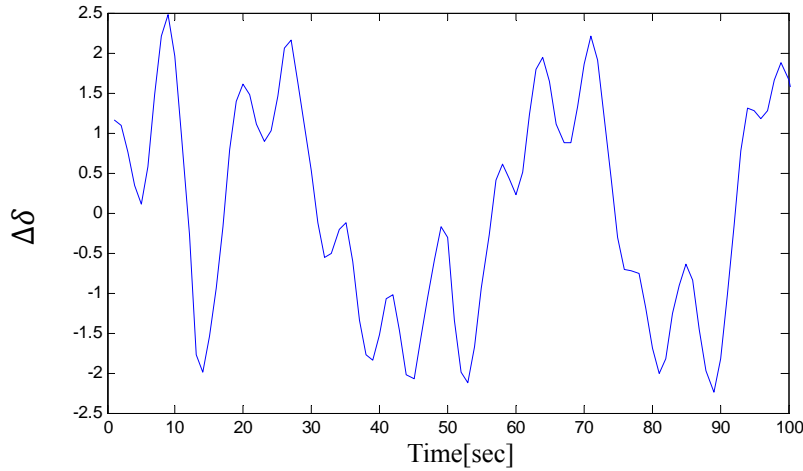
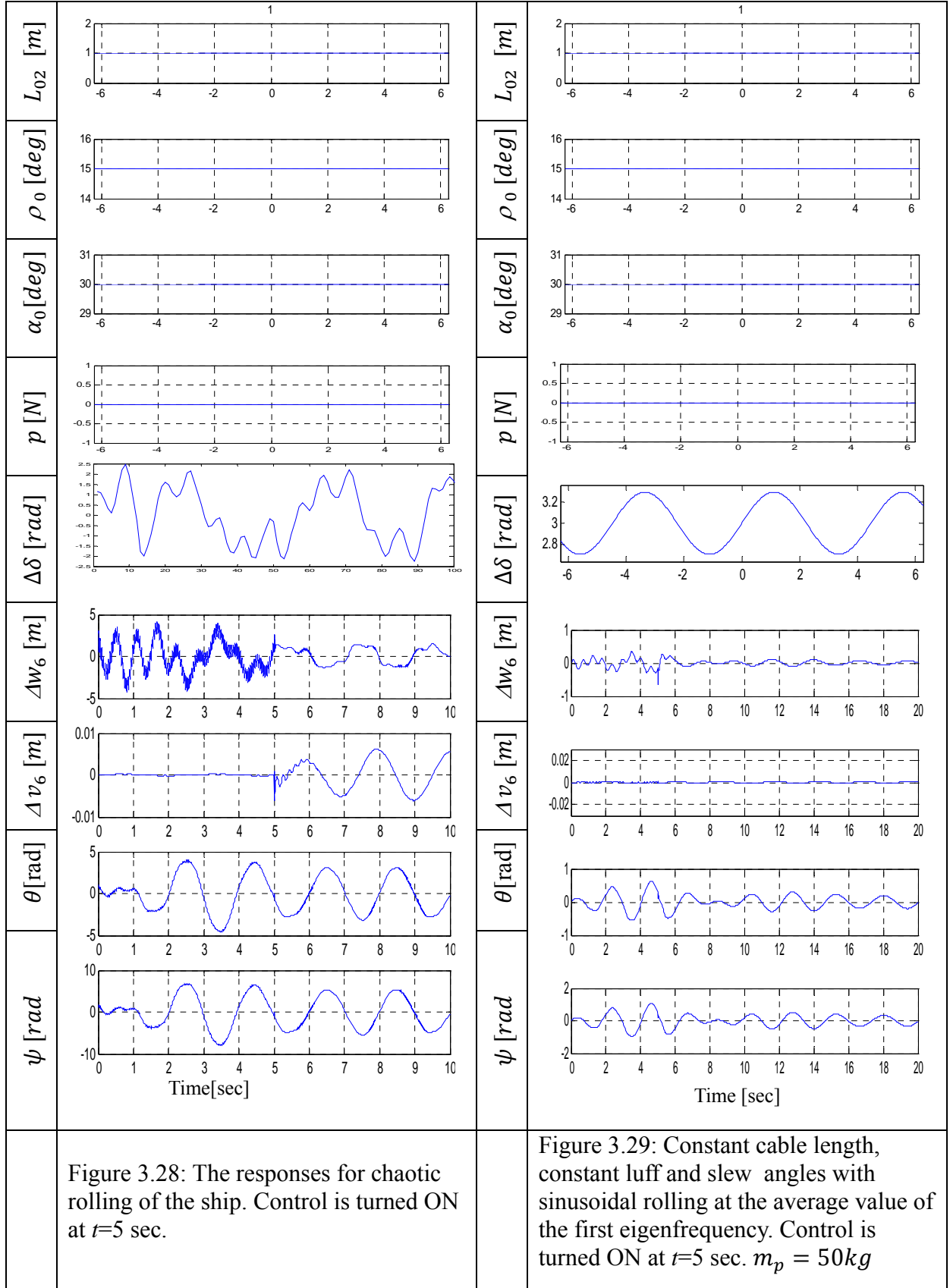


Figure 3.27: Chaotic rolling displacement.

The responses due to chaotic rolling excitation of the ship are shown in Fig. 3.28, it can be recognized that the measured oscillations can increase significantly if no control is used, and they are well suppressed when the controller is used. In Fig. 3.29 the crane is subjected to rolling disturbance with frequency closed to first eigenvalue frequency

of the system but in this time the payload mass was changed to 50 kg , it can be seen that that the controller performs very well despite the payload mass was reduced .



## 4 Summary, conclusions, and recommendations

### 4.1 Summary and conclusions

The full nonlinear mathematical model of an elastic ship-mounted crane is derived. The obtained model describes the coupled dynamics of the elastic boom and the payload. Taylor series expansion method is utilized to expand the model about the current operating point, which varies with the length of the payload cable, the luff and the slew angles of the boom. The linear model is considered to design the variable gain model-based controller.

Since the model is linearized about the current operating point which is dependent on the operator commands (the cable length, the boom operate luff and slew angles), the dynamic of the crane is described using a multi model approach; each model is valid only for a specified operating point and therefore for a defined region in the neighborhood of the operating point.

The state space model was derived to the linear mathematical model, the simulation shows that, when the disturbances affecting the crane is close to any of the eigenvalue of the crane system, resonance occurs and the vibrations will grow up without limit. Also the state space model was tested under the effect of different initial conditions of the system.

Observability and controllability are guaranteed using four measurements and three control inputs. The states in addition to the disturbance force acting on the payload are reconstructed by designing an extended observer. An optimal state feedback controller was designed based on the states reconstructed by the extended observer; its duty is to create the necessary damping to suppress the vibrations due to disturbances and nonzero initial conditions acting on the payload, it is also responsible to suppress the vibrations caused by operator commands (hoisting and lowering the payload).

A variable gain observer and a variable-gain controller are designed to control the crane which represented by a multi-model problem; the numerical values of the gains are updated in real time according to (a) the current operating region, which is determined by the region finder, and (b) the location of the current operating point inside the current region. Each operating region has eight corners, and each corner has its own observer and controller gain set. The actual controller and observer gains at any point inside the region are calculated using 3D interpolation polynomial; this ensures a smooth operation of the controller and preserves the stability and performance robustness as demonstrated using the plotting of the distribution of the dominant eigenvalues of the controlled system . In addition, transition of the controller between different operating regions (leaving a certain operating region and entering a new region) takes place gradually and in a smooth manner because any two successive regions have a common edge of four common nodes. This guaranteed that no stepwise change in the gains occurred and therefore chattering in the response is avoided. Simulation results showed that the payload cable length and the luff angle have the dominant effect in determining the size of each region but the slew angle has very small effect.

Consequently, this work can be considered as a background for a new construction of ship mounted cranes of elastic booms which can carry out the cargo transfer faster than rigid boom cranes with less power consumption. This distinguishes the proposed crane design from the previous cranes which have rigid booms . Another important advantage which should be added here is that, the proposed crane can operate safely in the worst case scenario of sea motion excitations at the resonance frequencies. This is due to the controllability capability obtained by using the three inputs together.

## 4.2 Recommendations

For further studies and future works, we recommend the following:

1. Include the dynamics of the actuator in the model
2. Design a filter in the input side to contribute in damping out the oscillations coming from the operator command inputs.
3. Conducts experiments to validate the controller operation.
4. Extend the controller to include a tracking loop to guarantee smooth tracking of the operator command.



## References

- [1] Chin, C. and Nayfeh, A. H., 1996, "Nonlinear Dynamics of Crane Operation at Sea," in proceedings of the 37<sup>th</sup> structures, Structural Dynamics, and Materials Conference, Salt Lake City, UT, AIAA-96-1485.
- [2] Yuan, G. H., Hunt, B. R., Grebogi, C., Ott, E., Yorke, J. A., and Kostelich, E. J., 1997, "Design and control of shipboard cranes," *DETC 97 Proceedings of the ASME Design Engineering Technical Conference*, Sacramento, CA, DETC97/VIB-4095.
- [3] Kimiaghalam, B., Homaifar, A., and Bikdash, M., 1999, "Pendulation suppression of a shipboard crane using fuzzy controller," *Proceedings of the American Control Conference*, San Diego, CA, Vol. 1, pp. 586-590.
- [4] Dadone, P. and Van Landingham, H. F., 1999, "The use of Fuzzy logic for controlling Coulomb friction in crane swing alleviation," *Intelligent Engineering Systems through Artificial Neural Networks* **9**, 751-756.
- [5] Kimiaghalam, B., Homaifar, A., and Bikdash, M., 2000, "Feedback and Feedforward Control Law for a Ship Crane with Maryland Rigging System," *Proceedings of the American Control Conference*, Chicago, IL, Vol. 2, pp. 1047-1051.
- [6] Al-Sweiti, Y., Söffker, D., "Planar cargo control of elastic ship cranes with the Maryland Rigging system," *Journal of Vibration and Control*, Vol. 13, No. 3, 241-267 (2007).
- [7] Yousef M. Al-Sweiti, "Modeling and Control of an Elastic Ship Mounted Crane Using Variable-Gain Model-Based Controller." PH.D. Von der Fakultät für Ingenieurwissenschaften, Abteilun. Maschinenbau der Duisburg-Essen University. Proceedings of t

- [8] Meirovitch, L. 1986, “*Elements of Vibration Analysis*,” 2<sup>nd</sup> ed. McGraw-Hill Book Company, New York, Chap. 8, pp. 300-346.
- [9] Müller, P. C., 1998, “Control of nonlinear systems by applying disturbance rejection control techniques”. In Proceedings IEE Int. Conference CONTROL 88, Institution of Electrical Engineers, London, pp. 734-737.
- [10] Söffker, D., Bajkowski, J. and Müller, P.C., 1993, “Detection of Cracks in Turbo Rotors – a New Observer Based Method”. ASME Journal of Dynamic Systems, Measurements and Control 3, pp. 518-524.
- [11] Söffker, D., Yu, T. J., Müller, P. C., 1995, “State Estimation of Dynamical Systems with Nonlinearities by using Proportional-Integral Observer”. International Journal of System Science, Vol. **26** (9), pp. 1571-1582.
- [12] Krajcin, I., Söffker, D., 2005, “Advanced Model-Based Disturbance Rejection Control Using Proportional-Integral-Observer,” *DETC 2005 ASME 20th Biennial Conference on Mechanical Vibration and Noise (VIB)*, Long Beach, California, DETC 2005-84997.
- [13] Krajcin, I., Söffker, D., 2005, “Diagnosis and Control of 3D Elastic Mechanical Structures”. In Precedings 12<sup>th</sup> international Symposium, Smart Structures and Materials: Smart Structures and Integrated Systems, San Diego, USA, 13 pages.
- [14] Lunze, 2002 “*Regelungstechnik2, Mehrgrößensysteme, Digital Regelung*” Springer Verlag, Berlin.
- [15] Katsuhiko Ogata. 2002, “*Modern Control Engineering*,” 4<sup>th</sup> ed. Prentice Hall, New Jersey.
- [16] Gene F. Franklin, J. David Powell, Abbas Emami-Naeini, 2002, “*Feedback Control of Dynamic Systems*,” 4<sup>th</sup> ed. Prentice Hall, New Jersey.

- [17] Müller, P. C., Lückel, J., 1997, "Zur Theorie der Störgrößenaufschaltung in linearen Mehrgrößenregelsystemen". *Regelungstechnik* **25**, pp. 54-59.
- [18] Daniel J. Inman. 1989, "*Vibration with Control, Measurement, and Stability*," Prentice-Hall International, Mexico, pp. 141-182.
- [19] Shahrokh Yadegari, 2003, "Chaotic Signal Synthesis with Real Time Control: Solving Differential Equations in PD, MAX/MSP, and JMAX," *Proceedings of the 6<sup>th</sup> Int. Conference on Digital Audio Effects (DAFx-03)*, London, UK.

# Appendix A

Matlab code

*The main program.*

```
clear all
format long

ro=8000;
syms w2 v2 gama2 phi2 w3 v3 gama3 phi3 w4 v4 gama4 phi4
syms w5 v5 gama5 phi5 w6 v6 gama6 phi6 theta opsi
l=1; %length of one element of the
elastic boom in(m)
mp=100 ; %weight of the payload in (kg)
row0=45*pi/180; % luff angle in (degrees)
L2 =4 ; %length of the payload cable
in (m)
alph0= 20*pi/180; %outplanar motion of the
elastic boom (degrees)
Ee=207*10^9 ; % modulus of elasticity in
(pascal)
Do=0.12; % radius of the cross section of
the elastic boom in(m)
Di=0.1;
I=(1/64)* pi*(Do^4-Di^4); %I:-moment of inertia
(m^4)
vol=(pi/4)*(Do^2-Di^2)*l;
me= ro*vol;
Py=5;Px=5;Pz=5; %wind step forces in (N)
g=9.81; %gravity acceleration in (m/s^2)
L1=5*l; % total length of the elastic
boom in (m)

%%%%%%%%%%%%%%%%%%%%%%%%%%%%%%%%%%%%%%%%%%%%%%%%%%%%%%%%%%%%%%%%%%%%%%%%
%%%%%%%%%%%%%%%%%%%%%%%%%%%%%%%%%%%%%%%%%%%%%%%%%%%%%%%%%%%%%%%%%%%%%%%%
%---Total mass matrix u=[w2; v2; gama2; phi2; w3; v3; gama3 ;phi3; w4
;v4;gama4; phi4;w5 ;v5 ;gama5; phi5; w6 ;v6; gama6; phi6;theta;opsi];
mtotal = (( me*l)/420) ...
* [312, 0, 0, 0, 54, 0, -13*l, 0, 0,
0, 0, 0, 0, 0, 0, 0, 0, 0,
0,0 ,0;
0, 312, 0, 0, 0, 54, 0, -13*l, 0,
0, 0, 0, 0, 0, 0, 0, 0, 0,
0,0 ,0;
0, 0, 8*l^2, 0, 13*l, 0, -3*l^2, 0, 0,
0, 0, 0, 0, 0, 0, 0, 0, 0,
0,0,0;
0, 0, 0, 8*l^2, 0, 13*l, 0, -3*l^2, 0,
0, 0, 0, 0, 0, 0, 0, 0, 0,
0,0,0;
54, 0, 13*l, 0, 312, 0, 0, 0, 54,
0, -13*l, 0, 0, 0, 0, 0, 0, 0,
0,0,0;
0, 54, 0, 13*l, 0, 312, 0, 0, 0,
54, 0, -13*l, 0, 0, 0, 0, 0, 0,
0,0,0;
```





```

B1_distur_disp=(-1/20)*[0,0,0,-20*me*g*sin(row0);
0,0,0,0;
0,0,0,0;
0,0,0,0;
0,0,0,-20*me*g*sin(row0);
0,0,0,0;
0,0,0,0;
0,0,0,0;
0,0,0,-20*me*g*sin(row0);
0,0,0,0;
0,0,0,0;
0,0,0,0;
0,0,0,-20*me*g*sin(row0);
0,0,0,0;
0,0,0,0;
0,0,0,0;
0,0,0,0;
0,0,0,(-20/l)*(Py*sin(row0-mp*g*sin(row0)));
0,0,0,0;
0,0,0,0;
0,0,0,0;
0,0,0,0;
0,0,0,0;
0,0,0,0];%(-20/l)*(-Py*sin(row0+mp*g*sin(row0)))
%%%%%%%%%%%%%%%%%%%%%%%%%%%%%%%%%%%%%%%%%%%%%%%%%%%%%%%%%%%%%%%%%%%%%%%%
%%%%%%%%%%%%%%%%%%%%%%%%%%%%%%%%%%%%%%%%%%%%%%%%%%%%%%%%%%%%%%%%%%%%%%%%
%-----Acceleration of disturbances [x0A;y0A;z0A;dleta]
B2distur_acce=(-1/20)*[ -20*me*cos(alph0)*sin(row0), 20*me*cos(row0), -
20*me*sin(alph0)*cos(row0),20*l*me;
-20*me*sin(row0),0,20*me*cos(alph0),0;
0,0,0,(4*me*l^2)/3;
0,0,0,0;
-20*me*cos(alph0)*sin(row0), 20*me*cos(row0),-
20*me*sin(alph0)*cos(row0),40*l*me;...
-20*me*sin(row0),0,20*me*cos(alph0),0;
0,0,0,(4*me*l^2)/3;
0,0,0,0;
-20*me*cos(alph0)*sin(row0), 20*me*cos(row0),-
20*me*sin(alph0)*cos(row0),60*l*me;
-20*me*sin(row0),0,20*me*cos(alph0),0;
0,0,0,(4*me*l^2)/3;
0,0,0,0;
-20*me*cos(alph0)*sin(row0), 20*me*cos(row0),-
20*me*sin(alph0)*cos(row0),80*l*me;
-20*me*sin(row0),0,20*me*cos(alph0),0;
0,0,0,(4*me*l^2)/3;
0,0,0,0;
0,(-20*mp*cos(row0))/l,0,((-20*L1*mp*cos(row0)*cos(row0))/l)+((20*(-
25/3*l^3*g*cos(row0)*(7*l*me+5*mp)/Ee/I)*mp*sin(row0)*cos(row0))/l);
0,0,0,0;
0,0,0,0;
0,0,0,0;
0,0,(20*L2*mp)/l,(20*L2*mp*(-L1*sin(alph0)*sin(row0))-((-
25/3*l^3*g*cos(row0)*(7*l*me+5*mp)/Ee/I)*sin(alph0)*cos(row0)))/l;
(20*L2*mp)/l,0,0,(20*L2*mp*(-L1*cos(alph0)*sin(row0))-((-
25/3*l^3*g*cos(row0)*(7*l*me+5*mp)/Ee/I)*cos(alph0)*cos(row0)))/l];
%%%%%%%%%%%%%%%%%%%%%%%%%%%%%%%%%%%%%%%%%%%%%%%%%%%%%%%%%%%%%%%%%%%%%%%%
%%%%%%%%%%%%%%%%%%%%%%%%%%%%%%%%%%%%%%%%%%%%%%%%%%%%%%%%%%%%%%%%%%%%%%%%
%-----input dispalcement [row;alpha;L2]

```

```

B3_input_disp=(-1/20)*[-20*me*g*sin(row0),0,0;
    0,0,0;
    0,0,0;
    0,0,0;
    -20*me*g*sin(row0),0,0;
    0,0,0;
    0,0,0;
    0,0,0;
    -20*me*g*sin(row0),0,0;
    0,0,0;
    0,0,0;
    0,0,0;
    -20*me*g*sin(row0),0,0;
    0,0,0;
    0,0,0;
    0,0,0;
    (-20/l)*(Py*sin(row0-mp*g*sin(row0))),0,0;
    0,0,0;
    0,0,0;
    0,0,0;
    0,0,(-20*Pz)/l;
    0,0,(-20*Pz)/l];%(-20/l)*(-Py*sin(row0+mp*g*sin(row0)))

%%%%%%%%%%%%%%%%%%%%%%%%%%%%%%%%%%%%%%%%%%%%%%%%%%%%%%%%%%%%%%%%%%%%%%%%
%-----Acceleration of input variables[row;alpha;L2]
B4_input_acc= (-1/20)*[20*l*me,0,0;
    0,me*l*(10*cos(row0)+10),0;
    (4*me*l^2)/3,0,0;
    0,(l^2*me*(5*cos(row0)-1))/3,0;
    40*l*me,0,0;
    0,me*l*(30*cos(row0)+10),0;
    (4*me*l^2)/3,0,0;
    0,(l^2*me*(5*cos(row0)-1))/3,0;
    60*l*me,0,0;
    0,me*l*(50*cos(row0)+10),0;
    (4*me*l^2)/3,0,0;
    0,(l^2*me*(5*cos(row0)-1))/3,0;
    80*l*me,0,0;
    0,me*l*(70*cos(row0)+10),0;
    (4*me*l^2)/3,0,0;
    0,(l^2*me*(5*cos(row0)-1))/3,0;
    ((-20*L1*mp*cos(row0)*cos(row0))/l)+((20*(-
25/3*l^3*g*cos(row0)*(7*l*me+5*mp)/Ee/I)*mp*sin(row0)*cos(row0))/l),0,(-
20*mp*cos(row0))/l;
    0,0,0;
    0,0,0;
    0,0,0;
    (20*L2*mp*((-L1*sin(alph0)*sin(row0))-((-
25/3*l^3*g*cos(row0)*(7*l*me+5*mp)/Ee/I)*sin(alph0)*cos(row0)))/l,(20*L2*m
p*((-L1*cos(alph0)*cos(row0))-((-
25/3*l^3*g*cos(row0)*(7*l*me+5*mp)/Ee/I)*cos(alph0)*sin(row0)))/l,0;
    (20*L2*mp*((-L1*cos(alph0)*sin(row0))-((-
25/3*l^3*g*cos(row0)*(7*l*me+5*mp)/Ee/I)*cos(alph0)*cos(row0)))/l,(20*L2*m
p*((-L1*sin(alph0)*cos(row0))-((-
25/3*l^3*g*cos(row0)*(7*l*me+5*mp)/Ee/I)*sin(alph0)*sin(row0)))/l,0];

%%%%%%%%%%%%%%%%%%%%%%%%%%%%%%%%%%%%%%%%%%%%%%%%%%%%%%%%%%%%%%%%%%%%%%%%
%%%%%%%%%%%%%%%%%%%%%%%%%%%%%%%%%%%%%%%%%%%%%%%%%%%%%%%%%%%%%%%%%%%%%%%%

```



```

%%%%%%%%%%%%%%%%%%%%%%%%%%%%%%%%%%%%%%%%%%%%%%%%%%%%%%%%%%%%%%%%%%%%%%%%%%%%%%
%%
%-----wind force [px;py;pz]
B5wind=(-1/20)*[0,0,0;
    0,0,0;
    0,0,0;
    0,0,0;
    0,0,0;
    0,0,0;
    0,0,0;
    0,0,0;
    0,0,0;
    0,0,0;
    0,0,0;
    0,0,0;
    0,0,0;
    0,0,0;
    0,0,0;
    0,(-20*cos(row0))/1,0;
    0,0,0;
    0,0,0;
    0,0,0;
    0,0,(-20*L2)/1;
    (-20*L2)/1,0,0];

%%%%%%%%%%%%%%%%%%%%%%%%%%%%%%%%%%%%%%%%%%%%%%%%%%%%%%%%%%%%%%%%%%%%%%%%%%%%%%
%%
% deriving the state space model
c1=zeros(4,22);
c1(1,17)=1; %to measure w6
c1(2,18)=1; %to measure v6
c1(3,21)=1; %to measure theta
c1(4,22)=1; %to measure opsi
u=[w2; v2; gama2; phi2; w3; v3; gama3 ;phi3; w4 ;v4; gama4; phi4;...
    w5 ;v5 ;gama5; phi5; w6 ;v6; gama6; phi6;theta;opsi;zeros(22,1)];
A=[zeros(22,22), eye(22);-
ktotal*inv(mtotal),zeros(22,22)];%%%%%%%%%%%%%%%%%%%%%%%%%%%%%%%%%%%%%%%%%%%%%%%%%%%%%%%%%%%%%%%%%%%%%%%%
size(A);
B=[zeros(22,3);(-ktotal*inv(mtotal)*B4_input_acc)+B3_input_disp];
size(B);
C=[c1*inv(mtotal) zeros(4,22)];
size(C);
D=[c1*inv(mtotal)*B4_input_acc];
F=[c1*inv(mtotal)*B2distur_acce];
size(F);
N=[zeros(22,3);B5wind];
E=[zeros(22,4);(-ktotal*inv(mtotal)*B2distur_acce)+B1_distur_disp];
size(E);
% sys=ss(A,B,C,D)
% %q0=[(-1/3*1^3*g*cos(row0)*(13*1*me+7*mp)/Ee/I);
%      0;
%      (-1/2*1^2*g*cos(row0)*(16*1*me+9*mp)/Ee/I);
%      0;
%      -1/6*1^3*g*cos(row0)*(89*1*me+52*mp)/Ee/I;
%      0;
%      -1/2*1^2*g*cos(row0)*(25*1*me+16*mp)/Ee/I;
%      0;
%      -3/2*1^3*g*cos(row0)*(19*1*me+12*mp)/Ee/I;
%      0;

```



```
%=====Design observer
```

```
Ae=[A N;zeros(3,47)];
sizeAe=size(Ae);
Be=[B;zeros(3,3)];
sizeBe=size(Be);
Ee=[E;zeros(3,4)];
sizeEe=size(Ee);
Ce=[C zeros(4,3)];
sizeCe=size(Ce);
Qe=10000*eye(47);
Qe(45,45)=1e15;
Qe(46,46)=1e15;
Qe(47,47)=1e15;
Re=.0001*eye(4,4);
le=lqr(Ae',Ce',Qe,Re);
Le=le';
sizeLe=size(Le);
eigA=eig(A);
He=zeros(47,3);
He(45,1)=1;He(46,2)=1;He(47,3)=1;

file='LeatowdimR1.mat';
Le0=Le;
save(file,'Le0');
load 'LeatowdimR1.mat';
eigobserver=sort(eig(Ae-Le0*Ce),'descend');

for i=1:size(eigcontroller)
    if eigobserver(i,1) < eigcontroller(i,1)
        x(1,i)=1;
    else
        x(1,i)=0;
    end
end
x
```

### ***Matlab code to calculate the zero operating point***

```
syms me beta g E l I mp
syms w2 v2 gama2 phi2 w3 v3 gama3 phi3 w4 v4 gama4 phi4
syms w5 v5 gama5 phi5 w6 v6 gama6 phi6
F0=(-
1/20)*[20*me*g*cos(beta);0;0;0;20*me*g*cos(beta);0;0;0;20*me*g*cos(beta);..
.
0;0;0;20*me*g*cos(beta);0;0;0; (20/l)*mp*g*cos(beta) ;...
0;0;0];
ktotalinvers=(E*I/l^3)*[
24, 0, 0, 0, -12, 0, 6*l,
0, 0, 0, 0, 0, 0, 0,
0, 0;
0, 24, 0, 0, 0, -12, 0, 6*l, 0, 0,
0, 0, 0, 0, 0, 0, 0, 0, 0;
0, 0, 8*l^2, 0, -6*l, 0, 2*l^2, 0, 0, 0,
0, 0, 0, 0, 0, 0, 0, 0, 0;
0, 0, 0, 8*l^2, 0, -6*l, 0, 2*l^2, 0, 0,
0, 0, 0, 0, 0, 0, 0, 0, 0;
```

```

-12, 0, -6*1, 0, 24, 0, 0, 0, -12, 0,
6*1, 0, 0, 0, 0, 0, 0, 0, 0, 0;
0, -12, 0, -6*1, 0, 24, 0, 0, 0, -12,
0, 6*1, 0, 0, 0, 0, 0, 0, 0, 0;
6*1, 0, 2*1^2, 0, 0, 0, 8*1^2, 0, -6*1, 0,
2*1^2, 0, 0, 0, 0, 0, 0, 0, 0, 0;
0, 6*1, 0, 2*1^2, 0, 0, 0, 8*1^2, 0, -6*1,
0, 2*1^2, 0, 0, 0, 0, 0, 0, 0, 0;
0, 0, 0, 0, 0, -12, 0, -6*1, 0, 24, 0,
0, 0, -12, 0, 6*1, 0, 0, 0, 0, 0;
0, 0, 0, 0, 0, -12, 0, -6*1, 0, 24,
0, 0, 0, -12, 0, 6*1, 0, 0, 0, 0;
0, 0, 0, 0, 0, 6*1, 0, 2*1^2, 0, 0, 0,
8*1^2, 0, -6*1, 0, 2*1^2, 0, 0, 0, 0, 0;
0, 0, 0, 0, 0, 6*1, 0, 2*1^2, 0, 0, 0,
0, 8*1^2, 0, -6*1, 0, 2*1^2, 0, 0, 0, 0;
0, 0, 0, 0, 0, 0, 0, 0, -12, 0, -
6*1, 0, 24, 0, 0, 0, -12, 0, 6*1, 0;
0, 0, 0, 0, 0, 0, 0, 0, 0, 0, -12,
0, -6*1, 0, 24, 0, 0, 0, -12, 0, 6*1;
0, 0, 0, 0, 0, 0, 0, 0, 0, 6*1, 0,
2*1^2, 0, 0, 0, 8*1^2, 0, -6*1, 0, 2*1^2, 0;
0, 0, 0, 0, 0, 0, 0, 0, 0, 0, 6*1,
0, 2*1^2, 0, 0, 0, 8*1^2, 0, -6*1, 0, 2*1^2;
0, 0, 0, 0, 0, 0, 0, 0, 0, 0, 0,
0, 0, -12, 0, -6*1, 0, 12, 0, -6*1, 0;
0, 0, 0, 0, 0, 0, 0, 0, 0, 0, 0,
0, 0, 0, -12, 0, -6*1, 0, 12, 0, -6*1;
0, 0, 0, 0, 0, 0, 0, 0, 0, 0, 0,
0, 0, 6*1, 0, 2*1^2, 0, -6*1, 0, 4*1^2, 0;
0, 0, 0, 0, 0, 0, 0, 0, 0, 0, 0,
0, 0, 0, 6*1, 0, 2*1^2, 0, -6*1, 0, 4*1^2];
v00=inv(ktotalinvers)*F0;

v0=simple(v00)/(E*I/(l^3)))
u=[w2; v2; gama2; phi2; w3; v3; gama3; phi3; w4; v4; gama4; phi4;...
w5; v5; gama5; phi5; w6; v6; gama6; phi6];
ktotal_andu=simple(ktotalinvers*v0)

```

### ***Matlab code to calculate the tension and the position of the tip of the crane by axis transformation method***

```

%find x6 y6 z6 of point B and the tension T
syms alpha beta w6 v6 L1
Rx1_0=[cos(alpha) 0 -sin(alpha);0 1 0;sin(alpha) 0 cos(alpha)];
Rx2_x1=[cos(beta) -sin(beta) 0;sin(beta) cos(beta) 0;0 0 1];
Rx2_0=Rx1_0*Rx2_x1
position_ofB=[L1;w6;v6];%relative to x2y2z2 plane
posit_B= (Rx1_0*Rx2_x1)*position_ofB %relative to x0y0z0

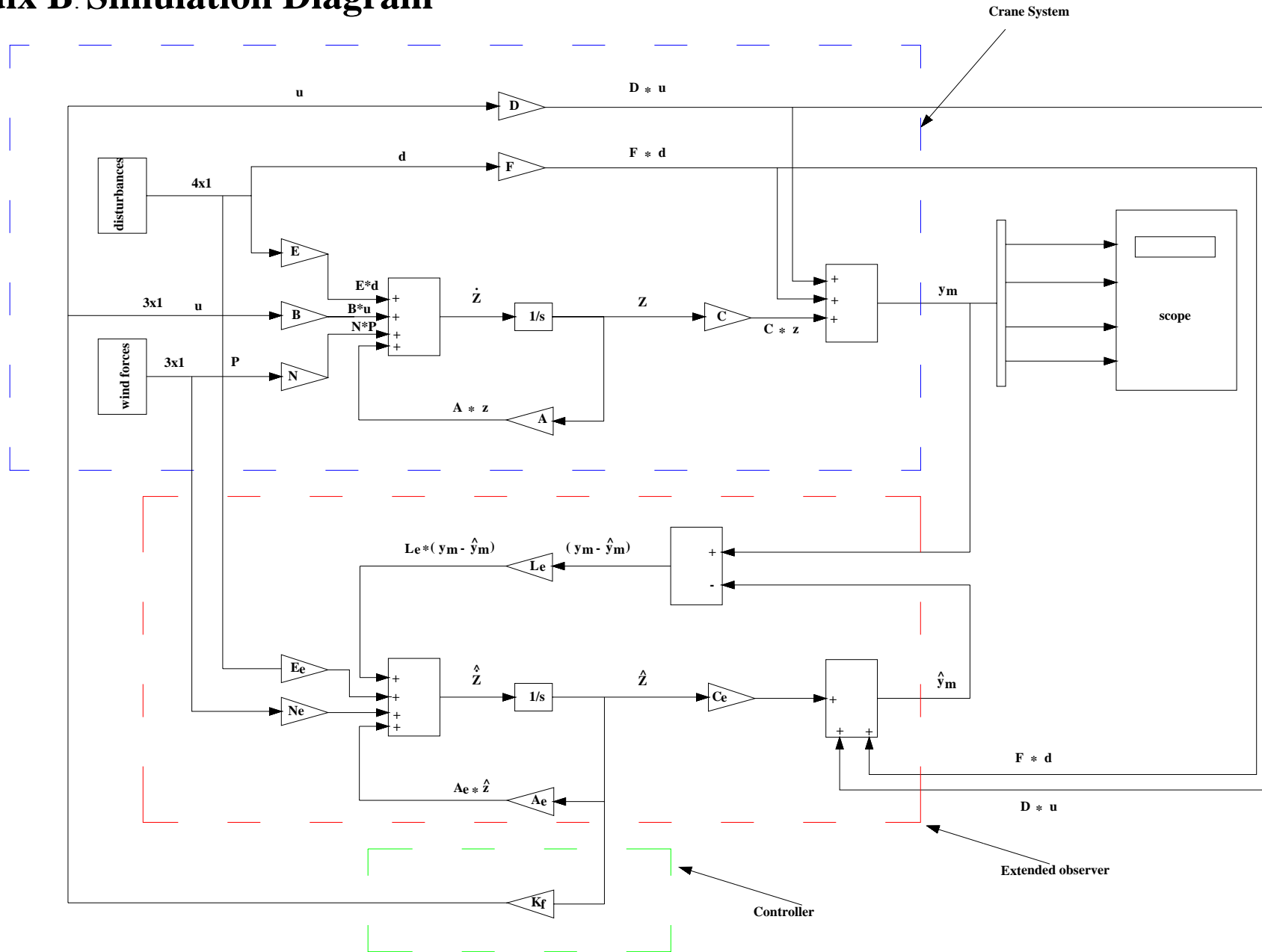
syms th ops T

Tx=T*cos(th)*sin(ops);
Ty=-T*cos(th)*cos(ops);
Tz=T*sin(th);
transRx2_0=[cos(alpha)*cos(beta), sin(beta),sin(alpha)*cos(beta);...
-cos(alpha)*sin(beta), cos(beta),-
sin(alpha)*sin(beta);...
-sin(alpha), 0 , cos(alpha)];
tension=transRx2_0 *[Tx;Ty;Tz] %relative to x2y2z2

```



# Appendix B: Simulation Diagram



## Appendix C: Derivation of the payload equation of motion using Lagrange.

The physical coordinates for the payload are  $(X_p, Y_p, Z_p)$ , the independent generalized coordinates which describe the full motion of the payload are the length of the hoisting cable  $L_2$ , the in-plane angle  $\theta$  and the out-of-plane angle  $\varphi$ .

The physical coordinates can be written as a function of the generalized coordinates as follows:

$$\begin{aligned} X_p &= X_p(L_2, \theta, \psi) \\ Y_p &= Y_p(L_2, \theta, \psi) \\ Z_p &= Z_p(L_2, \theta, \psi) \end{aligned} \tag{C1}$$

We can derive the virtual displacement (the change of the physical coordinates while the time is held constant) in the direction of the physical coordinates with respect to generalized coordinates using the following definition of the virtual displacement :

$$\delta r_i = \sum_{j=1}^m \frac{\partial r_i}{\partial q_j} \delta q_j \tag{C2}$$

where:

$\delta r_i$ : is the virtual displacement of the physical coordinates (  $i = 1, 2, \dots, N$ ), where  $N$  is the number of physical coordinates .

$q_j$ : is the generalized coordinates  $j = 1, 2, \dots, m$ , where  $m$  is number of generalized coordinates.

$\delta q_j$ : the virtual displacement of the generalized coordinates.

As follows:

$$\begin{aligned}
\delta X_P &= \frac{\partial X_P}{\partial L_2} \delta L_2 + \frac{\partial X_P}{\partial \theta} \delta \theta + \frac{\partial X_P}{\partial \varphi} \delta \psi \\
\delta Y_P &= \frac{\partial Y_P}{\partial L_2} \delta L_2 + \frac{\partial Y_P}{\partial \theta} \delta \theta + \frac{\partial Y_P}{\partial \varphi} \delta \psi \\
\delta Z_P &= \frac{\partial Z_P}{\partial L_2} \delta L_2 + \frac{\partial Z_P}{\partial \theta} \delta \theta + \frac{\partial Z_P}{\partial \varphi} \delta \psi
\end{aligned} \tag{C3}$$

Also we can write the applied wind forces  $(F_x, F_y, F_z)$  in the direction of the physical coordinates in terms of the generalized coordinates  $(L_2, \theta, \psi)$ , by using the principle of the virtual work which states that: the work performed by the applied forces through infinitesimal virtual displacement compatible with the system coordinates is zero in mathematical notation,

$$\delta \omega = \sum_{i=1}^N F_i \cdot \delta r_i = 0 \tag{C4}$$

By using Eq. C4 the virtual work performed by the applied wind forces will be given as:

$$\delta \omega = F_x \cdot \delta X_P + F_y \cdot \delta Y_P + F_z \cdot \delta Z_P = 0 \tag{C5}$$

Substitute Eq.C3 into Eq.C5

$$\begin{aligned}
\delta \omega &= \left( F_x \cdot \frac{\partial X_P}{\partial L_2} + F_y \cdot \frac{\partial Y_P}{\partial L_2} + F_z \cdot \frac{\partial Z_P}{\partial L_2} \right) \delta L_2 + \\
&\quad \left( F_x \cdot \frac{\partial X_P}{\partial \theta} + F_y \cdot \frac{\partial Y_P}{\partial \theta} + F_z \cdot \frac{\partial Z_P}{\partial \theta} \right) \delta \theta + \left( F_x \cdot \frac{\partial X_P}{\partial \varphi} + F_y \cdot \frac{\partial Y_P}{\partial \varphi} + F_z \cdot \frac{\partial Z_P}{\partial \varphi} \right) \delta \psi = 0
\end{aligned} \tag{C6}$$

Then the virtual work done in the direction of the virtual generalized coordinate  $\delta L_2$  is:

$$\delta \omega_{\delta L_2} = \left( F_x \cdot \frac{\partial X_P}{\partial L_2} + F_y \cdot \frac{\partial Y_P}{\partial L_2} + F_z \cdot \frac{\partial Z_P}{\partial L_2} \right) \delta L_2 = 0 \tag{C7}$$

and in the direction of generalized coordinate  $\delta \theta$  is:

$$\delta \omega_{\delta \theta} = \left( F_x \cdot \frac{\partial X_P}{\partial L_2} + F_y \cdot \frac{\partial Y_P}{\partial L_2} + F_z \cdot \frac{\partial Z_P}{\partial L_2} \right) \delta \theta = 0 \tag{C8}$$

and in the direction of generalized coordinate  $\delta \varphi$  is:

$$\delta \omega_{\delta \psi} = \left( F_x \cdot \frac{\partial X_P}{\partial L_2} + F_y \cdot \frac{\partial Y_P}{\partial L_2} + F_z \cdot \frac{\partial Z_P}{\partial L_2} \right) \delta \psi = 0 \tag{C9}$$



But the virtual work can be written in terms of generalized forces as:

$$\delta\omega = \sum_{k=1}^m Q_k \delta q_k \quad \text{C10}$$

where:

$Q_k$ : the generalized forces  $k = 1, 2, \dots, m$ , where  $m$  is the number of generalized coordinates.

$\delta q_k$ : the virtual displacement of the generalized coordinates.

Then we can conclude from Eq. C7, Eq. C8 and Eq. C9 that the generalized forces  $Q_k$  in the direction of the generalized coordinates  $(L_2, \theta, \psi)$  can be expressed as follows respectively:

$$Q_{L_2} = \left( F_x \cdot \frac{\partial X_P}{\partial L_2} + F_y \cdot \frac{\partial Y_P}{\partial L_2} + F_z \cdot \frac{\partial Z_P}{\partial L_2} \right) \quad \text{C11}$$

$$Q_{\theta} = \left( F_x \cdot \frac{\partial X_P}{\partial L_2} + F_y \cdot \frac{\partial Y_P}{\partial L_2} + F_z \cdot \frac{\partial Z_P}{\partial L_2} \right) \quad \text{C12}$$

$$Q_{\psi} = \left( F_x \cdot \frac{\partial X_P}{\partial L_2} + F_y \cdot \frac{\partial Y_P}{\partial L_2} + F_z \cdot \frac{\partial Z_P}{\partial L_2} \right) \quad \text{C13}$$

Now by applying the Lagrange for neoconservative forces which can be expressed as:

$$\frac{d}{dt} \left( \frac{\partial L}{\partial \dot{q}_k} \right) - \frac{\partial L}{\partial q_k} = Q_k \quad \text{C14}$$

Then the equations of motion of the payload are represented by equations 2.13, 2.14 and 2.15.

( Region finder)

-6

Linear )

( interpolation

-7

•

•

-1

( initial conditions)

•

•

•

-4

•

```
( observer
```

# Modeling & Control of an Elastic Ship-Mounted Crane

:

( slew angle)

( luff angle )

.

:

.

.

.

Taylor

.

.

.

.

.

(variable-gain extended observer)

( )

( variable-gain controller)

.

108

.